SOFTENING AND HARDENING TRANSITIONS IN FERROELECTRIC Pb(Zr,Ti)O₃ CERAMICS

THÈSE N^O 3368 (2005)

PRÉSENTÉE À LA FACULTÉ SCIENCES ET TECHNIQUES DE L'INGÉNIEUR

Institut des matériaux

SECTION DE SCIENCE ET GÉNIE DES MATÉRIAUX

ÉCOLE POLYTECHNIQUE FÉDÉRALE DE LAUSANNE

POUR L'OBTENTION DU GRADE DE DOCTEUR ÈS SCIENCES

PAR

Maxim MOROZOV

Maître ès Techniques et Technologies, Université Electrotechnique d'Etat de St. Pétersbourg, Russie
et de nationalité russe

acceptée sur proposition du jury:

Prof. N. Setter, directrice de thèse
Dr D. Damjanovic, rapporteur
Prof. J. Lemaître, rapporteur
Dr B. Malic, rapporteur
Prof. H. Tuller, rapporteur

Lausanne, EPFL
2005

Abstract

Hysteretic and nonlinear dielectric behaviour in ferroelectric ceramics has been of interest since 1950s, when these materials found application in various electronic devices. Presently, these phenomena concern with important areas of science, technology and engineering. In particular, nonlinearity and hysteresis are the key factors in performance, precision and accuracy of modern devices. Many theoretical and experimental studies have been aimed at understanding the origins of hysteresis and nonlinearity in ferroelectrics. Nowadays, there are several models that describe major contributions to nonlinearity and hysteresis on phenomenological, microscopical or statistical levels. These models have a limited area of applicability due to the complexity of physical processes occurring in real materials. Empirically, hysteresis and nonlinearity in ferroelectrics can be controlled by softening and hardening of the material. This is the case of most widely used ferroelectric, lead zirconate titanate (PZT). The soft compositions possess large electro-mechanical coefficients but also large hysteresis and nonlinearity while the opposite is true for the hard compositions. After fifty years since introduction of these materials, the mechanisms of softening and hardening remain poorly understood.

The present study is aimed at a better understanding of the processes leading to hardening and softening of $Pb(Zr,Ti)O_3$ ceramics in order to verify the key principles required for a more universal physical model of hysteresis and nonlinearity. Based on the present state of knowledge, such model should consider domain wall contribution to nonlinear and hysteretic polarization response and at the same time account for hardening and softening of the ferroelectric. For this purpose the well known lead zirconate titanate (PZT) ceramics doped with various concentrations of niobium (soft materials) or iron (hard materials) are chosen as a prototype of the ferroelectric system.

The starting hypothesis of the thesis' approach is that the softening and hardening are a result of electrostatic arrangement of charged defects in the ceramic bulk: the hard materials are characterized by the ordered and the soft by disordered defects. The thesis then develops in detail the idea that hardening-softening transitions in a ferroelectric system may occur under the influence of (i) dopants, depending on their type and concentration, (ii) a cyclically applied electric field, (iii) a thermal treatment, and (iv) time. The transition from microscopic order to microscopic disorder is confirmed experimentally using carefully

analyzed phenomenological parameters of the macroscopic hysteresis and nonlinearity. Among the nonlinear and hysteretic parameters characterizing the polarization response of a ferroelectric material, some (e.g., third harmonic of polarization) are shown to be particularly sensitive to the softness and hardness of ferroelectric system and thus may serve as the characteristics of ferroelectric hardening-softening transitions. Contribution of domain walls to hysteresis and nonlinearity is analyzed in terms of domain wall energy potential and degree of ordering of pinning centres. It is shown that two existing models characterizing hard (V-potential) and soft (random potential) materials are ideal, limiting cases and that some real materials are described by an intermediary case, which can evolve with time and under influence of external factors. The dielectric characterization performed at wide range of frequencies has revealed an increase of the apparent frequency dispersion of the dielectric permittivity with the transition from the hard to soft state in PZT ceramics. The investigation of dielectric response over a wide temperature range has revealed the profound presence of hopping conductivity in iron doped PZT ceramics below the Curie temperatures and its absence in niobium doped PZT ceramics. The role of hopping charged species in ferroelectric hardening – softening transitions is analyzed and discussed.

The thesis is organized in the following way. A brief introduction (Chapter 1) and a literature review of the theoretical description of domain wall contribution to dielectric nonlinearity and hysteresis in ferroelectrics (Chapter 2) is followed by the thesis outline and discussion of a unified model of hysteresis and nonlinearity in ferroelectrics with ordered and disordered states of domain wall pinning centres (Chapter 3). Processing of ceramics is described in Chapter 4 and mathematical and experimental background for the dielectric spectroscopy study in Chapter 5. The results and discussion of detailed experimental studies of polarization response in ferroelectric PZT ceramics under subswitching and switching conditions are given in Chapters 6 and 7. The summary of the main results and conclusions are given in the last thesis section.

Version Abrégé

Beaucoup d'intérêt a été porté au comportement diélectrique hystérétique et non-linéaire des matériaux ferroélectriques depuis les années 1950, lorsque des nombreuses applications dans des dispositifs électroniques. Présentement, ces comportements concernent d'importants domaines scientifiques, technologiques et d'ingénierie. En particulier, la non-linéarité et l'hystérèse sont les paramètres clefs pour la performance, la précision et l'exactitude des dispositifs modernes. De nombreuses études théoriques et expérimentales ont été destinées à comprendre les origines de l'hystérèse et de la non-linéarité dans les matériaux ferroélectriques. De nos jours, il existe de nombreux modèles qui décrivent les contributions principales à la non-linéarité et à l'hystérèse sur des niveaux phénoménologiques, microscopiques ou statistiques. Ces modèles ont des champs d'application limités à cause de la complexité des processus physiques se produisant dans les matériaux réels. Empiriquement, l'hystérèse et la non-linéarité dans les ferroélectriques peuvent être contrôlées par le *adoucissement* et le *durcissement* des matériaux. C'est le cas du matériau ferroélectrique le plus utilisé, le titanate zirconate de plomb (PZT). Les compositions douces possèdent de coefficients électromécaniques élevés, mais aussi une grande hystérèse et non-linéarité, alors que l'opposé est vrai pour les compositions de type *dur*. Cinquante ans après l'introduction de ces matériaux, les mécanismes de l'*adoucissement* et *du durcissement* sont toujours mal compris.

La présente étude a comme but la meilleure compréhension des processus menant au *durcissement* et au *adoucissement* des céramiques de Pb(Zr,Ti)O3 afin de vérifier des principes fondamentaux requis pour un modèle physique universel pour l'hystérèse et la non-linéarité. Basé sur les connaissances actuelles, un tel modèle devrait considérer la contribution des parois de domaine à la non-linéarité et l'hystérèse de la polarisation tout en considérant le *durcissement* et *adoucissement* des ferroélectriques. Dans ce but, les bien connues céramiques de titanate zirconate de plomb (PZT) dopées avec diverses concentrations de niobium (matériaux *doux*) ou de fer (matériaux *dur*) ont été choisies comme matériaux ferroélectriques prototypes.

La principale supposition de l'approche de cette thèse est que l'*adoucissement* et le *durcissement* sont le résultat de l'arrangement électrostatique des défauts chargés dans la céramique: les matériaux de type *dur* sont caractérisés par des défauts ordonnés alors que les *doux* par des défauts désordonnés. La thèse développe ensuite en détail l'idée que les transitions entre *durcissement* et *adoucissement* dans un système ferroélectrique a lieu sous l'influence de (i) dopants, dépendant de leur type et de leur concentration, (ii) d'un champ électrique cyclique appliqué, (iii) d'un traitement thermique et (iv) du temps. La transition

d'un ordre microscopique à un désordre microscopique est confirmée expérimentalement en utilisant des paramètres phénoménologiques de l'hystérèse macroscopique et de la non-linéarité soigneusement analysés. Parmi les paramètres hystérétiques et non-linéaires caractérisant la réponse de la polarisation d'un matériau ferroélectrique, quelques-uns (par exemple la troisième harmonique de la polarisation) sont montrés comme étant particulièrement sensibles au caractère *doux* ou *dur* du système ferroélectrique et ainsi pourraient servir comme caractéristiques des transitions ferroélectriques *durcissement – adoucissement*. La contribution des parois de domaine à l'hystérèse et à la non-linéarité est analysée en terme d'énergie potentielle des parois de domaines et du degré d'ordre des centres d'ancrage. Il est montré que deux modèles existant caractérisant les matériaux dur (potentiel en V) et doux (potentiel aléatoire) sont des cas limitant idéaux et que quelques matériaux réels sont décrits par un cas intermédiaire, qui peut évoluer dans le temps et sous l'influence de facteurs externes. La caractérisation diélectrique effectuée sur une large gamme de fréquences a révélé une augmentation de la dispersion en fréquence de la permittivité diélectrique avec la transition d'un état *dur* à un état *doux* dans les céramiques de PZT. L'investigation de la réponse diélectrique sur une grande gamme de températures a révélé une présence profonde de la conduction par sauts dans les céramiques dopées au fer en dessous de la température de Curie et son absence dans les céramiques de PZT dopées au niobium. Le rôle des espèces chargées se déplaçant par sauts dans les transitions ferroélectriques *durcissement - adoucissement* sont analysées et discutées.

Cette thèse est organisée de la manière suivante. Une brève introduction (chapitre 1) et une revue littéraire de la description théorique des contributions des parois de domaines à la non-linéarité et l'hystérèse diélectrique dans les matériaux ferroélectriques (chapitre 2) est suivie par le plan de thèse et une discussion d'un modèle unifié de l'hystérèse et la non-linéarité dans les ferroélectriques avec des états ordonnés et désordonnés des défauts de parois de domaines. La mise en œuvre des céramiques est décrite dans le chapitre 4 et les bases mathématiques et expérimentales pour la spectroscopie diélectrique dans le chapitre 5. Les résultats et la discussion d'études expérimentales détaillées de la réponse de la polarisation dans les céramiques ferroélectriques de PZT dans et en-dessous des conditions d'inversion de la polarisation sont donnés dans les chapitres 6 et 7. Le résumé des principaux résultats et les conclusions sont donnés dans la dernière section de la thèse.

Acknowledgements

Contents

Hysteresis loops come in all sizes and shapes, and, similar to a fingerprint, identify the material in a very special way

G. H., Haertling [1]

Chapter 1

Introduction

1.1. Nonlinear dielectric materials

Nonlinear dielectric materials are characterized by the field dependence of the dielectric permittivity on the external electric field strength. In most of the dielectrics, the dielectric permittivity is linear or weakly depends on the electric field up to the breakdown values. In contrast, the ferroelectric materials usually exhibit nonlinear dielectric response for quite a large range of applied electric fields. Dielectric nonlinearity as many other ferroelectric properties such as pyroelectric effect, piezoelectricity, electrostriction, electrooptic effect, conductivity and others are closely linked to the variation of spontaneous polarization under influence of external factors. The study of dielectric nonlinearity and related phenomena in this class of dielectric materials is of interest since they are used in many areas of technology, engineering, and science, often under conditions where nonlinearity can not be ignored.

1.2. Applications of nonlinear dielectrics

The applications of ferroelectrics are all-embracive and multifarious covering many areas of modern technologies from high-dielectric-constant capacitors to non-volatile memories and integrated optic devices. Ferroelectric materials are deeply involved into piezoelectric applications in ceramic form due to the discovery of the electrical poling process that aligns the internal polarization of the crystallites within the ceramic and causes the ceramic to act very similar to a single crystal. Ferroelectric ceramics, in general, are technologically simpler to manufacture than single crystal piezoelectrics and have greater capacity in technological variety of their formulations, form (bulk, films), and fabrication. A comprehensive review of ferroelectric ceramics applications is given in the recent papers of Haertling [1] and Waser [2]. Application of ferroelectric ceramics can be classified by form of realization (bulk or films) and by the functional effect responsible for the device operation.

The first area of ferroelectric ceramics application was capacitor engineering. Here, the direct dielectric effect is exploited. Most ceramic capacitors are, in reality, high-dielectric-constant ferroelectric compositions which have their ferroelectric properties (hysteresis loop) suppressed with suitable chemical dopants while retaining a high dielectric constant over a broad temperature range. Historically, the first composition used for such capacitors was $BaTiO_3$ and its modifications. Nowadays their number is enhanced by lead-containing relaxors and other compositions.

By far the largest majority of applications for electro-active materials occurs in the area of piezoelectric ceramics. In this category, the ceramics are usually poled once, and no polarization reorientation takes place after that during the life of the device. Depending on whether direct, converse piezoelectric effects or their combinations are employed, there are three categories of applications: (1) Charge or voltage generators (direct piezoelectric effect). This class of devices includes various sensors, such as microphones, phonograph cartridge, gas ignitors, accelerometers, photoflash actuators, pressure sensors, impact fuses etc. The operating characteristic varies from millivolts to kilovolts. (2) Displacement actuators (converse piezoelectric effect). This class contains various actuators – loud speakers, camera shutters, buzzers, ink jet printer, microrobots, relays, pumps and others. (3) High frequency transformers and resonant devices. In this class, there are ranging

transducers, sonar, ultrasonic cleaners, ultrasonic welders, filters, transformers, and delay lines, non-destructive testing. These devices operate at working frequencies from kilohertz to megahertz.

Transparent single crystals are traditionally used for electrooptic applications. Since late 1960s, when transparent Lead Lanthanum Zirconate Titanate (PLZT) ferroelectric materials were first developed, ferroelectric ceramics have been thoroughly researched, and their characteristics studied to the point that they have now taken their place alongside single crystals as legitimate candidates for certain electrooptic applications. The electrooptic properties of PLZT materials are intimately related to their ferroelectric properties. Consequently, varying the ferroelectric polarization with an electric field, such as in hysteresis loop, also produces a change in the optical properties of the ceramics. [3].

Applications of ferroelectric materials in a film form are growing due to the need for miniaturization and integration of electronic components, and due to development of microtechnologies, material fabrication and engineering. Aside from the obvious advantages, such as smaller size, less weight and easier integration to integrated circuit technology, ferroelectric films offer additional benefits, including lower operating voltage, higher speed, and the ability to fabricate unique micro-level structures. In addition, the sintering temperatures of the films are usually hundreds of degrees Celsius lower than that of the bulk, and this often can be the deciding factor in a successful design and applications [4-7]. Among the most common ferroelectric film applications are non-volatile memories, integrated optics, electrooptic displays, microactuators, microtransducers, and capacitors fabricated in a film form.

Other applications of ferroelectrics are exploiting the electrostrictive effect, positive temperature coefficient of resistivity, and stress-induced depoling.

1.3. Lead Zirconate Titanate ceramics and their "soft" and "hard" modifications

Lead Zirconate Titanate ($Pb(Zr,Ti)O_3$ or PZT) is the most widely used ferroelectric ceramics for piezoelectric application (transducers, actuators, sensors and others). This is because PZT compositions possess the advantageous combination of properties such as (1)

high electromechanical coupling coefficient; (2) relatively high Curie temperature (T_c), which permits operation at temperature up to 200 °C; (3) wide range of dielectric constants; (4) capability to form solid-solutions with many different compositions, thus allowing a wide range of properties modifications; (5) can be easily poled and (6) can be sintered at relatively low temperature [1].

PZT is especially attractive for material properties designing. Wide range of physical properties can be obtained by variation of Zr/Ti ratio, particularly in so-called morphotropic phase boundary (MPB) region. In addition, PZT ceramics are almost always used with a dopant or a modifier to improve and optimize their basic properties for specific applications [8-10].

The donors, such as Nb^{5+} replacing (Zr^{4+},Ti^{4+}), are compensated either by A-site vacancies or by electrons and can reduce the natural p-type conductivity of the PZT by as much as 3 orders of magnitude. The donors are usually compensated by A-site vacancies. These additives in combination with corresponding vacancies appear to enhance domain orientation with respect to undoped material. Ceramics produced with these additives are characterized by square hysteresis loops, high dielectric loss, high mechanical compliance, advanced piezoelectric properties, reduced ageing and easy depoling. This type of ceramics is called "Soft PZT" [8,11].

Acceptors, such as Fe^{3+} replacing (Zr^{4+},Ti^{4+}), are compensated by oxygen vacancies and usually have only limited solubility in the lattice. These additives lead to opposite effects to those of donors. Domain reorientation is limited, and, hence, ceramics with acceptor additives are characterized by poorly developed hysteresis loops, lower dielectric constant, low dielectric losses, low piezoelectric properties, low compliances, higher ageing rate, and ceramics are more difficult to depole. These ceramics are called "Hard PZT" [8].

Isovalent additives, such as Ba^{2+} or Sr^{2+} replacing Pb^{2+} or Sn^{4+} replacing Zr^{4+} or Ti^{4+}, in which the substituting ion is of the same valency and approximately the same size as the replaced ion, usually lead to inhibited domain orientation and poorly developed hysteresis loops. Other properties include lower dielectric loss, low compliance, and higher ageing rates. For some applications the isovalent modifiers are used to change Curie temperature, for example, the transition temperature of Sr-modified PZT ceramics decreases about 9.5 °C per each atomic percent of Sr concentration [12].

Chapter 2

Theoretical description of domain wall contribution to dielectric nonlinearity and hysteresis in ferroelectrics

In order to formulate the thesis goals with respect to the modern state of the art, the literature review of the results related to the dielectric nonlinearity and hysteresis phenomena is presented in this chapter. The main focus of the review is the domain wall contribution to the polarization response and phenomenological models describing this contribution in various contexts.

2.1. Dielectric nonlinearity and hysteresis phenomena in ferroelectrics

The term "dielectric nonlinearity" is used to describe the relationship between dielectric displacement $\mathbf{D}$ and electric field strength $\mathbf{E}$ in nonlinear materials. It can be expressed by the dependence $\varepsilon(\mathbf{E})$, where ε is the dielectric permittivity of the material. The dielectric nonlinearity is usually accompanied by the dielectric hysteresis. In general, dielectric hysteresis is the result of delay in polarization response of dielectric to an electric field change which is expressed by hysteretic field dependence of dielectric polarization $\mathbf{P(E)}$ and phase lag δ between the driving field and the response. The hysteresis and nonlinearity often have a common origin, although not necessarily always [13,14].

The nonlinearity and hysteresis have a profound influence on application of ferroelectric materials. Except in the memory applications, which are based on polarization switching and hysteresis by external electric field, the hysteresis is undesired in high precision sensor, actuator, and capacitor applications. In most of applications, nonlinearity is also undesired, and the devices based on nonlinear materials usually need calibration. However, there are applications based on the dielectric nonlinearity, such as tuneable filters, variconds and other microwave devices.

The origins of dielectric nonlinearity and hysteresis are complex and can be intrinsic and extrinsic. Intrinsic properties are usually defined in literature as the properties of the crystal lattice of pure material. Correspondingly, extrinsic origins are related to nonlattice contributions, such as movements of defects, grain boundary effects, displacement of interfaces (such as domain walls) and interphase boundaries. In most of ferroelectric materials, especially in ceramic and at weak fields, the extrinsic properties play a major role. Surfaces, boundaries, and interface effects may give significant contribution to the polarization nonlinearity in thin films, however, in general case, the dominant origin of extrinsic contributions to the dielectric, elastic, and piezoelectric properties of ferroelectric materials is displacement of domain walls [15].

2.2. Preisach approach to extrinsic contribution in material response.

One of the first formal approaches to model a material's hysteresis response was proposed by Preisach [16]. This approach was first used to interpret empirical Rayleigh relations [17] for magnetization hysteresis in ferromagnets. However, this approach is formal enough to describe hysteresis phenomena in general, and has been used by many authors to describe ferroelectric [18-29] and piezoelectric [14,29-36] nonlinearity and hysteresis.

Preisach approach assumes macroscopic hysteresis as a collection of the elementary contributions given by bistable units, representing the elementary hysteretic action in the system. The elementary bistable units representing contribution to polarization response is shown in Fig.2.1. Each unit is characterized by two parameters: a bias (or internal) field E_i

and a coercive field $\mathbf{E_c}$. Each state of unit is assumed to contribute to the total polarization response by the same amount $\pm\mathbf{P_0}$.
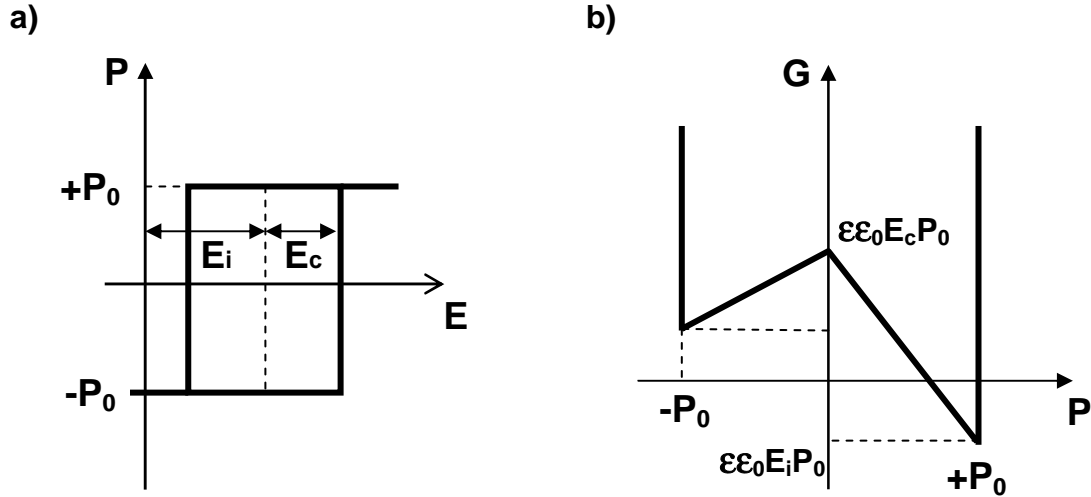
Figure 2.1. *Elementary bistable unit represented as square hysteresis (a) and as energy profile (b).*

The bias field can take any value $\mathbf{E_i} \in (-\infty; +\infty)$, while the coercive field is defined as nonnegative $\mathbf{E_c} \in [0; +\infty)$. The half plane of possible values for $\mathbf{E_i}$ and $\mathbf{E_c}$ is called the Preisach plane. In a given system, the bistable units exhibit a statistical distribution of these parameters which can be described by a distribution function $\mathbf{f(E_i, E_c)}$ defining the number of bistable units between $\mathbf{[F_i; F_i + dF_i]}$ and $\mathbf{[F_c; F_c + dF_c]}$ as $\mathbf{f(E_i, E_c)\ dE_i, dE_c}$. It must be normalized as

$$\int\limits_{0}^{\infty} \int\limits_{-\infty}^{\infty} \mathbf{f(F_i, F_c) dF_i dF_c = 1} \tag{2.1}$$

It has been proven that the agreement of a given experimental hysteretic system with this formalism is verified if and only if it exhibits two basic properties [37,38]:

(1) Wiping-out property: for a given field profile, the final state of the system depends only on the series of local extrema that are greater than any subsequent extremum, i.e.,

intermediate extrema between greater ones do not alter the final state of the system. In practice, this property means that when a field alternating between two defined values is applied to the system, the generated loop will be closed for any arbitrary profile of the field having these two values as extrema.

(2) Congruency property: stationary hysteresis loops between two defined fields extrema are geometrically superimposable independently of the history of the system.

The total polarization response is defined as the sum of all bistable unit contributions over the Preisach plane. The initial state of Preisach plane of the system unexposed to any external influence is shown in Fig.2.2. It can be divided into three regions:

(a) $E_i > E_c$, bistable units contribute by negative value (**-P$_0$**);

(b) $|E_i| < E_c$, states of bistable units are not defined or depend on the history;

(c) $E_i < -E_c$, bistable units contribute by positive value (**+P$_0$**);
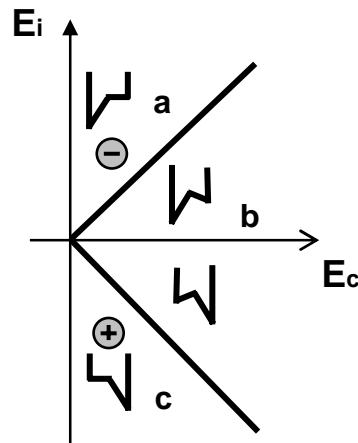
Figure 2.2. *State of bistable units as a function of their position on the Preisach plane at zero applied field (after Ref [39])*

When external field **E** is applied, it superposes with internal bias field E_i, and changes the conditions of the bistable unit states. The b-region cone, $E_i = E \pm E_c$, is thus moved upward or downward, and units crossing the region limits are switched to the stable state. The nonlinear and hysteretic polarization – field dependence **P(E)**, for alternating

electric field $E \in [-E_0; +E_0]$ can be obtained as field dependent integral of the distribution function over the growing regions on Preisach plane corresponding to increasing and decreasing field (the grey regions in Fig.2.3).
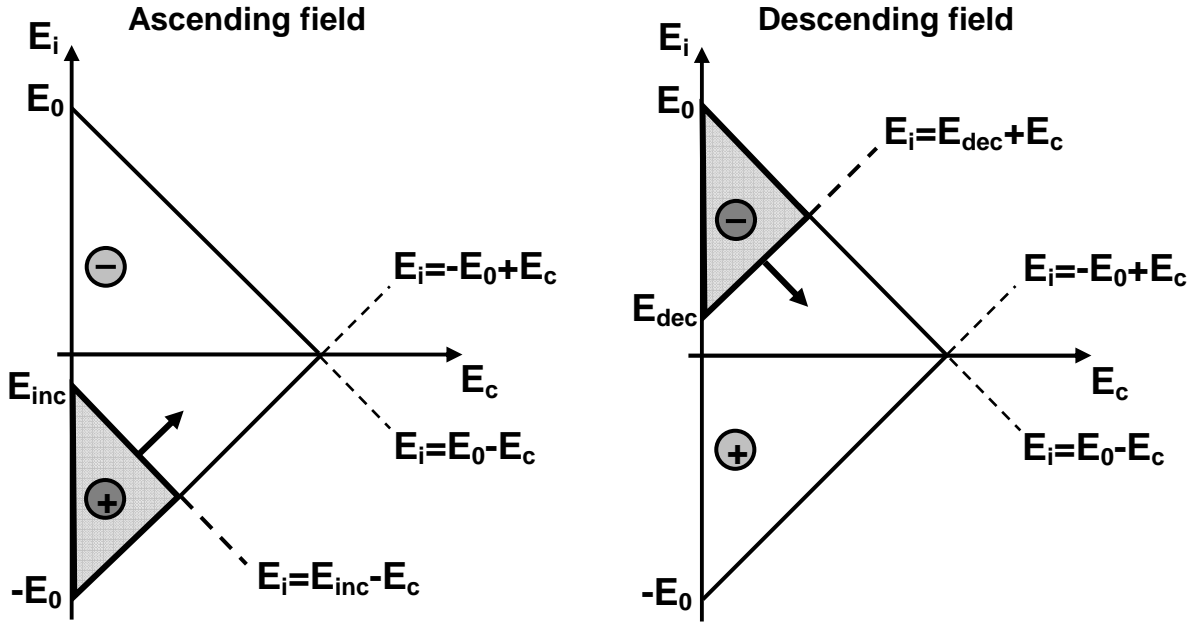
Figure 2.3. *Schematic view of the switched bistable units for an external field alternating between* $-E_0$ *and* $+E_0$. E_{inc} *and* E_{dec} *stand for increasing and decreasing applied field (E) respectively.*

Taking into account that each bistable unit contributes to the total polarization by $\pm P_0$, and hence, each switching units change its contribution by $\pm 2P_0$, the total nonlinear contribution P_m, and branches for descending (P^-) and ascending (P^+) field dependences are expressed as following:

$$P_m = P_0 \int_{0}^{E_0} \int_{-E_0+E_c}^{E_0-E_c} f(E_i, E_c) dE_i dE_c \tag{2.2}$$

$$P^- = P_m - 2P_0 \int_{0}^{\frac{E_0-E}{2}} \int_{E+E_c}^{E_0-E_c} f(E_i, E_c) dE_i dE_c \tag{2.3}$$

$$P^+ = -P_m + 2P_0 \int\limits_{0}^{\frac{E_0+E}{2}} \int\limits_{-E_0+E_c}^{E-E_c} f(E_i, E_c) dE_i dE_c \qquad (2.4)$$

The first application of this approach was represented by its author, F.Preisach [16], to interpret Rayleigh-type magnetization process. Indeed, for constant distribution function $f(E_i, E_c) = \alpha$, the solutions of (2.2) - (2.4) are:

$$\frac{P_m}{P_0} = \alpha E_0^2 \qquad (2.5)$$

$$\frac{P^\pm}{P_0} = \alpha E_0 E \mp \tfrac{1}{2} \alpha (E_0^2 - E^2) \qquad (2.6)$$

The total polarization response, including the linear term of intrinsic dielectric polarization $P = \chi_r E$ and nonlinear part given by formula (2.6) can be expressed as:

$$P = (\chi_{init} + \alpha_\chi E_0) E \mp \frac{\alpha_\chi}{2} (E_0^2 - E^2) \qquad (2.7)$$

and, correspondingly, the dielectric displacement is:

$$D = (\varepsilon_{init} + \alpha_\varepsilon E_0) E \mp \frac{\alpha_\varepsilon}{2} (E_0^2 - E^2) \qquad (2.8)$$

The linear terms of dependence in equations (2.7) and (2.8) describe anhysteretic part of material response, and quadratic terms express hysteresis. The effective susceptibility and permittivity, determining the field dependence of material response, are the linear function of the applied field amplitude:

$$\chi^{eff} = (\chi_{init} + \alpha_\chi E_0) \qquad (2.9)$$

$$\varepsilon^{eff} = (\varepsilon_{init} + \alpha_\varepsilon E_0) \qquad (2.10)$$

The formulas (2.7) – (2.10) describe Rayleigh-type dielectric response to external alternating field **E** with amplitude **E$_0$**. The coefficient $\alpha = \alpha_\chi = \alpha_\varepsilon$ is called Rayleigh coefficient; the sign $\mp$ corresponds to ascending and descending field branches; χ_{init} and ε_{init} designate the zero-field material parameters: the initial relative susceptibility and the initial relative permittivity. Nonlinearity (effective susceptibility dependence on the amplitude of applied field) and hysteresis are interconnected in Rayleigh relations by coefficient α, which implies that higher nonlinearity of material response is accompanied with stronger hysteresis.

In some cases, experimentally observed response of nonlinear materials deviates from Rayleigh relations or demonstrates qualitatively different behaviour. If the requirements of wiping-out and congruency properties are fulfilled, the response of these materials can be described using the Preisach formalism. In practice, even the systems exhibiting Rayleigh-type of behaviour at weaker fields, demonstrate deviations from Rayleigh relations at higher fields [16,19,40]. For magnetization process the transitions from Rayleigh to rectangular form of hysteresis loop was described in terms of Preisach formalism by Akulov and Galenko [40]. They showed that transformation of hysteresis loop from Rayleigh-type to rectangular form can be described using Maclaurin series of distribution function for Preisach model:

$$\mathbf{f(H_c,H_i) = f_0 + c_1 H_i + c_2 H_2 + c_3 H_i H_c + c_4 H_i^2 + c_5 H_c^2 + ...} \qquad (2.11)$$

where H_c, H_i are the coercive and biased magnetic field parameters of Preisach plane for magnetization process. Later, this approach was explored by Turik for ferroelectric hysteresis [19-21]. He considered similar function developed into Maclaurin series but taking into account its symmetry with respect to the sign of internal bias (**E$_i$**) parameter:

$$\mathbf{f(E_c,E_i) = f_0 + g E_c + h E_c^2 + k E_i^2 + l E_c^3 + m E_c E_i^2 + ...} \qquad (2.12)$$

For so-called non-Rayleigh systems such as hard ferroelectrics exhibiting pinched hysteresis loop, the form of distribution function $f(F_i,F_c)$ was outlined in [19] as a double-

ridge function symmetrical with respect to E_c axes. In [24] the forth order polynomial distribution function combined with cut-off at high coercive field level (E^*) was proposed:

$$f(E_i, E_c) = \begin{cases} -cE_i^4 + kE_i^4 & \text{if} \quad E_c < E^* \quad \textbf{and} \quad -cE_i^4 + kE_i^4 > 0 \\ 0 & \text{if} \quad E_c \geq E^* \quad \textbf{and} \quad -cE_i^4 + kE_i^4 \leq 0 \end{cases} \tag{2.13}$$

The Rayleigh-type and pinched propeller-form hysteresis loops are shown in Fig.2.4 with corresponding Preisach distribution functions.
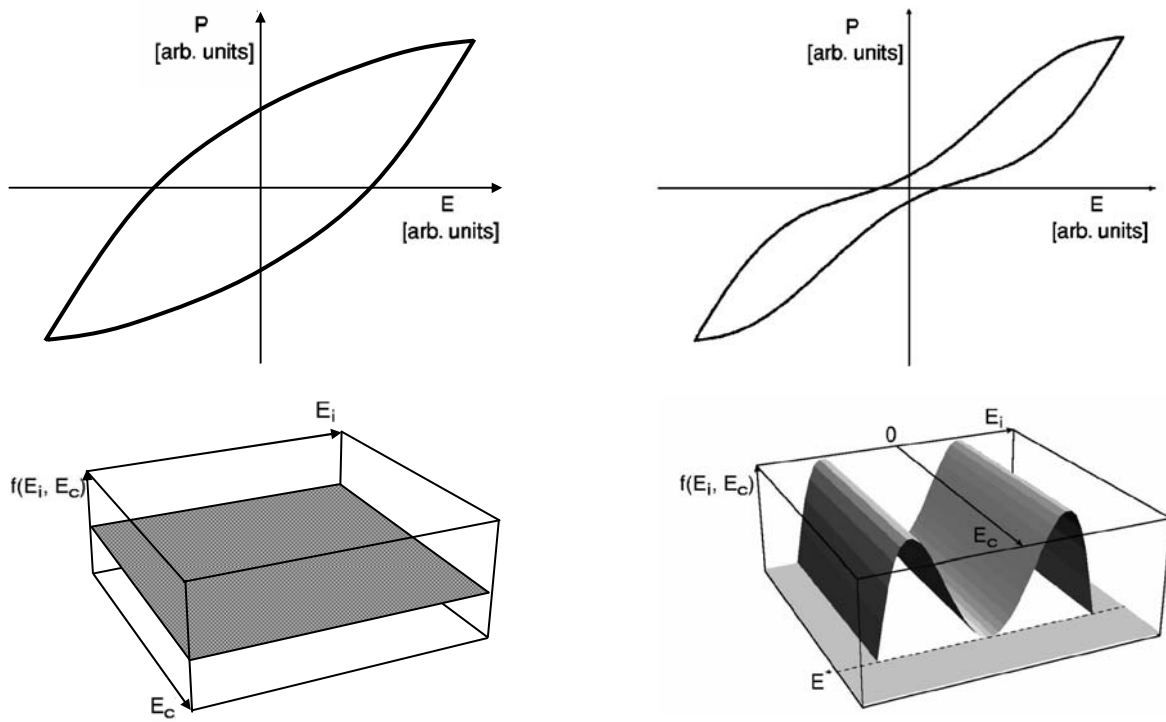
Figure 2.4. *Rayleigh-type (left) and pinched [24] (right) ferroelectric hysteresis loops (top) and corresponding distribution functions for Preisach model (bottom).*

The application of this approach includes modelling nonlinear and hysteretic processes and calculation of the hysteretic losses. However, the presence somewhere in the system of a statistically distributed collection of bistable elements, on which the Preisach formalism is based, has motivated the search of physical mechanism and microscopical

processes leading to the hysteretic and nonlinear behaviour and associating them with the Preisach model. The first theory that attempted to explain the physical origins of the Rayleigh law was proposed by Néel [41] who analyzed Rayleigh law by considering Bloch wall trapped in profiled energy landscape (similar to one shown in Fig. 2.1,b). He assumed that energy, once expressed as a function of the wall position, fluctuates around a constant mean value and represents the random energy profile experienced by the domain wall during the motion. The following approach is proposed by Néel. The complex energy profile is modelled by sequence of equispaced parabolic arcs. The energy gradient (representing the pinning field for a domain wall) is thus represented by a polygonal line made of random slope segments characterized by constant length **2l** (Fig.2.5.). Energy gradient is described by two constants: the distance **2l** between adjacent points of the sequence and the width P_0 of the Gaussian distribution of the slopes. For domain wall displacements lower than **2l,** the domain wall moves reversibly, whereas larger displacement may lead to irreversible jumps if the geometry of neighbouring slopes in a polygon sequence form a barrier separating two local minima. The Rayleigh law was derived by Néel on the assumption of demagnetized state of the domain wall. All the possible stable positions accessible to the domain wall were classified, and the corresponding probabilities to be in each of them were derived. The coefficients of the Rayleigh law found with this method are directly related to the **2l** and P_0 parameterss. The Rayleigh coefficient α was derived and found to be a measure of the irreversible displacement of the domain wall; this irreversible displacement is origin of the nonlinearity of initial magnetization (or polarization in ferroelectrics) curve.
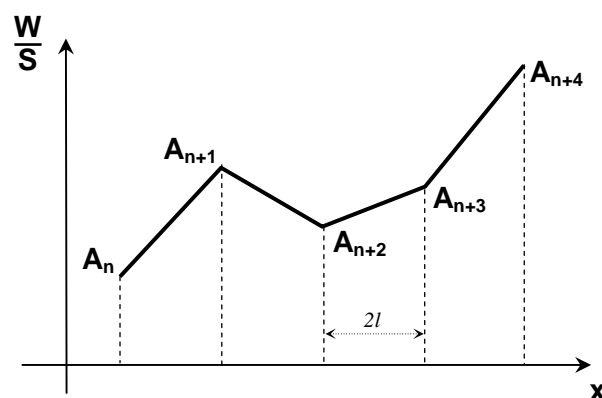
Figure 2.5. Characteristic function used by Néel to describe the profile of domain wall energy. For details see Ref. [41].

Similar statistical approaches to derive nonlinear response of random systems were used in other works [39,42-49]. Kronmüller [42] proposed a statistical theory of Rayleigh's law considering the domain wall motion in the field of force due to lattice defects (in his work – dislocations). The basic of the model is following. The total interaction force between a domain wall and the defects is a sum over all individual forces exerted by the defects on the domain wall. The individual force, **p**, between an isolated defect and a domain wall is a function of the distance **z-z$_j$** between the position of the assumed plane domain wall and position **z$_j$** of the defect. The coordinate axis is chosen parallel to the domain wall normal. The field of force $\upsilon(\mathbf{z})$ is expressed as:

$$\upsilon(\mathbf{z}) = \sum_{\mathbf{j}} \mathbf{p}(\mathbf{z} - \mathbf{z_j}) \tag{2.14}$$

where the sum extends over all dislocations interacting with the domain wall. An example of such a field of force is illustrated in Fig.2.6 and characterized by the following parameters:

(1) The average distance **L$_0$** between neighbouring intersections of the force-distance curve with $\upsilon(\mathbf{z})=\mathbf{0}$;

(2) The average value $\overline{\upsilon}$ of the maxima of the force;

(3) The average value $\overline{\mathbf{1/R}} = \overline{\mathbf{1/(d\upsilon/dz)}}$ of the reciprocal slopes of the force at the positions $\upsilon(\mathbf{z})=\mathbf{0}$.

These parameters were derived in [43,50]. Pfeffer [43] obtained the characteristic parameters by means of correlation functions. He showed that the probability **f** (υ) for the existence of a force between υ and **dυ** is given by the normal distribution

$$\mathbf{f}(\upsilon) = \frac{\mathbf{1}}{\sqrt{\mathbf{2\pi B}}} \mathbf{e}^{-\frac{\upsilon^2}{\mathbf{2B}}} \tag{2.15}$$

with the correlation function **B** defined as

$$B = \frac{F_B N}{L_3} \int\limits_{L_3/2}^{L_3/2} \{p(z)\}^2 \, dz \tag{2.16}$$

where F_B is the domain wall area moving coherently, L_3 is distance between neighbouring domain walls, and N is the density of the defects acting on the domain wall.

Similarly the slopes $\mathbf{R=d\upsilon/dz}$ at the equilibrium positions $\mathbf{\upsilon=0}$ are distributed according to a normal distribution

$$g(R) = \frac{1}{\sqrt{2\pi B_1}} e^{-\frac{R^2}{2B_1}} \tag{2.17}$$

$$B = \frac{F_B N}{L_3} \int\limits_{L_3/2}^{L_3/2} \left\{\frac{dp}{dz}\right\}^2 dz \tag{2.18}$$

The characteristic parameters of the statistical field of force can be expressed in terms of correlation functions **B** and **B₁**.
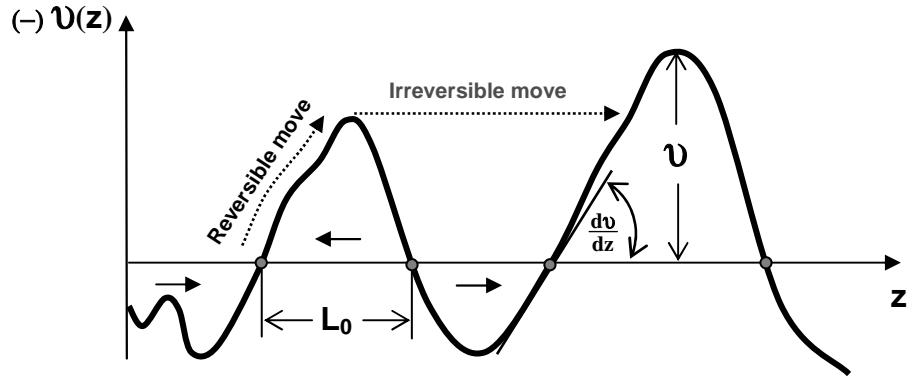
Figure 2.6. Statistical field of force acting on the domain walls proposed by Kronmüller, and its characteristic parameters. After Ref. [42].

The derivation of Rayleigh law proposed by Kronmüller is based on the statistical approach similar to one applied by Néel. The model assumes that domain walls displace

independently from each other, and no restoring forces due to stray fields are generated as a response of the domain wall displacement. Two types of domain wall movements were considered: reversible, characterized by distance $L_{rev}(\upsilon)$, and irreversible, characterized by irreversible displacement $L_{irr}(\upsilon)$. Under the action of external field the domain wall moves reversibly up-hill the force-distance curve towards the force maximum. When the position $d\upsilon/dz = 0$ is reached the domain wall performs irreversible jump into new equilibrium position. The domain wall is stopped when it meets a higher force maximum (Fig.2.6). Considering combination of probabilities for the occurrence of a statistical slope, its occupation by a domain wall, and estimating average irreversible distance, and quantity of domain walls performing irreversible jump in a finite variation of statistical field of force, the Rayleigh law was derived in terms of statistical theory. An important result of the theory is a relationship between the Rayleigh coefficient and microstructural features of the system (provided by (2.16) – (2.18)). Particularly, Kronmüller showed the relations between initial susceptibility (χ_{init}), Rayleigh coefficient (α_χ) and density of defects (N):

$$\chi_{init} \propto \frac{1}{\sqrt{N}} \tag{2.19}$$

$$\alpha_\chi \propto \frac{1}{N} \tag{2.20}$$

Although the results concern magnetization process due to contribution of domain wall motion in ferromagnets with dislocations acting as pinning centres, the equivalent statistical theory of hysteresis in ferroelectric materials based on the analogy between behaviours of magnetic and ferroelectric materials was proposed by Boser [22].

Recent works in ferromagnetics [39,44-49] have shown that if one considers the system with pinning energy profiles E_p described by some defined stochastic process (such as homogeneous Markov process or Wiener-Levy process [39,51]) then the average response of a pinned object exhibits the properties required by the Preisach model. In particular, it was shown in [49] that such stochastic processes give rise to Preisach type hysteresis, and explicit analytical expressions for the Preisach distribution can be derived as a function of the parameters governing the statistics of Markov process. This means that a single element trapped in a random profile of stochastic process contributes, in average, to the total

response in accordance with the Preisach formalism. This result bridges the description proposed in Preisach formalism with physical microscopical features, like Barkhausen jumps of domain wall in a random pinning field [39]. The effect of Barkhausen pulses [52] was observed in barium titanate single crystal [53], and its relations to ferroelectric domain processes are discussed in [54].

Summarizing the brief review on Preisach model of hysteresis loop and related statistic theories, the following important conclusions can be extracted. Hysteresis, in particular ferroelectric hysteresis, has its origin in the multiplicity of metastable states in the system free energy. Preisach model is a powerful tool to describe hysteresis (and nonlinearity) by a collection of a large number of elementary bistable units whose states are determined by two parameters and the final form of the hysteresis loop is related to these parameters distribution. It is applicable to the systems exhibiting congruency and wiping-out properties. The Preisach model clarifies several important aspects of hysteresis phenomena, and its relation to the system free energy is represented in several works in terms of restricted models based on random or stochastic descriptions of the system free energy. The particular case of Preisach hysteresis is the Rayleigh law corresponding to a uniform distribution of Preisach parameters. The important justification of Rayleigh law presence in a disordered system characterized by statistical fluctuation of domain wall potential energy was given in works of Néel and Kronmüller.

2.3. Phenomenological model of domain wall dynamics

The major contribution of the domain walls displacement to polarization response of ferroelectrics was realized as soon as the multidomain structure of ferroelectrics was observed and analyzed [15,55-58]. The domain wall boundary, or domain wall, in a ferroelectric crystal is the region separating domains polarized in different direction. The presence of the domain walls is a result of multidomain structure of many ferroelectric crystals. Multidomain structure of the polar crystal minimizes the electrostatic energy of depolarizing field and the elastic energy associated with mechanical constrains to which the ferroelectric materials is subjected as it is cooled through paraelectric-ferroelectric phase transition [59]. The width of the domain walls in ferroelectric materials is on the order of

one to ten nanometres [59-61]. The electrostatic conditions defining the domain pattern change when an external field is applied and may result in displacement of the domain walls. The surface energy of the wall will be increased when it is set in motion because of the inertia of the ions which change position slightly as their dipoles moments change direction on passage of the wall. The vibration motion of the domain wall as an extrinsic contribution to polarization response of ferroelectric materials was a subject of many theoretical and experimental studies. Kittel proposed the equation of the forced harmonic oscillator to describe the domain wall motion [62]:

$$\rho \frac{\partial^2 \mathbf{x}}{\partial t^2} + \mathbf{r} \frac{\partial \mathbf{x}}{\partial t} + \mathbf{q}\mathbf{x} = 2\mathbf{PE} \qquad (2.21)$$

where **r** represents damping effects, and **q** the restoring force, associated with local trapping of the domain wall. Damping may be occasioned by coupling with lattice vibrations, selective impurity diffusion, local trapping, acoustic radiation, and other causes. This equation was extended by Arlt and Dederichs [63] to include also mechanical driving field:

$$\mathbf{Am}\Delta\ddot{\mathbf{l}} + \mathbf{Ab}\Delta\dot{\mathbf{l}} + \mathbf{kA}\Delta\mathbf{l} = -\left(\frac{\partial \mathbf{W_E}}{\partial \Delta\mathbf{l}} + \frac{\partial \mathbf{W_M}}{\partial \Delta\mathbf{l}} \right) \qquad (2.22)$$

where **A** is the domain wall area, **m** is the effective mass per unit area of the domain wall, **Δl** is the displacement, **b** and **k** are the damping constant and force constant both per area. The driving forces are derived from the electric energy **W_E** and from elastic energy **W_M** of the wall in the applied mechanical stress field. Solutions of equation (2.21) or (2.22) for various systems are based on the assumptions and simplifications for particular domain configurations and geometries. To derive the dependence of complex dielectric, elastic and piezoelectric coefficients on the material properties the model of the damped motions of 90° domain walls was proposed [63]. The essential feature of this model was the geometrical aspect of 90° domain walls contribution in polycrystalline material. The cross section of two domains forming the wall region is shown in Fig.2.7. This model is simplified for two-dimension geometry and considering only 90° domain wall contribution. The wall is treated like a membrane which can be forced to vibrate by electric and/or elastic stresses. The

polarization vectors enclose an angle 90º (for tetragonal distortion) and have the directions of the **x'**, **z'** axes. The primed coordinate system is fixed with the wall, the unprimed one with the net of ceramic polarization, which is parallel to z. The electric dipole moment ($\mathbf{p_i}$) of the wall region in the primed and unprimed system:

$$(\mathbf{p'_i}) = aAP_s \begin{pmatrix} 1 \\ 0 \\ 1 \end{pmatrix}; \quad (\mathbf{p_i}) = aAP_s \begin{pmatrix} \cos\varphi - \sin\varphi \\ 0 \\ \cos\varphi - \sin\varphi \end{pmatrix} \qquad (2.23)$$

where **a** is the thickness, and $\mathbf{P_s}$ is the spontaneous polarization of a domain (Fig.2.7).
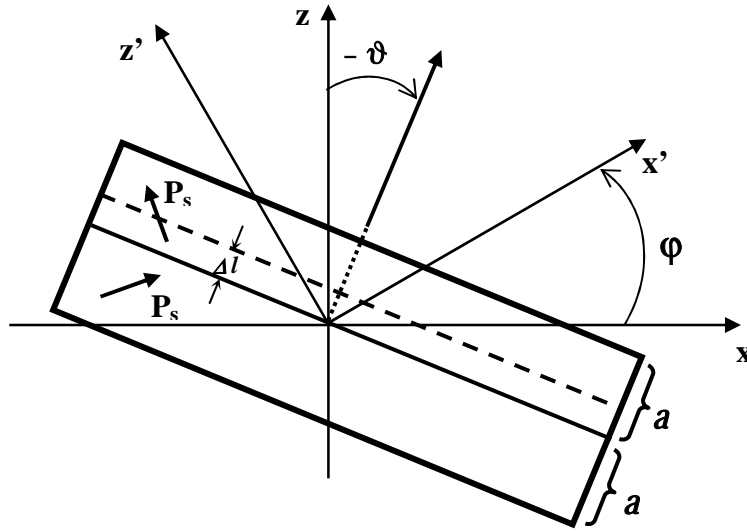
Figure 2.7. *Two 90º domains of a grain of ferroelectric ceramic. From Ref. [63].*

The spontaneous deformation of a domain $\mathbf{S_a}$ and $\mathbf{S_c}$ along the **a** and **c** axis respectively leads to an elastic dipole moment of the wall region represented by a second rank tensor [64.65]:

$$(\varsigma'_{ij}) = a_w A_w \begin{pmatrix} S_c + S_a & 0 & 0 \\ 0 & 2S_a & 0 \\ 0 & 0 & S_c + S_a \end{pmatrix}; \quad (\varsigma_{ij}) = a_{li} a_{mj} \varsigma'_{im} \qquad (2.24)$$

where a_{li} are the direction cosines of the coordinate transformation (Einstein notation of indicies). A displacement $\Delta \mathbf{l}$ of the domain wall (Fig.2.7.) gives rise to changes of the electric and elastic dipole moments of the wall region:

$$(\Delta \mathbf{p_i}) = \mathbf{A_w} \Delta \mathbf{l} \mathbf{P_s} \begin{pmatrix} \cos\varphi - \sin\varphi \\ 0 \\ \cos\varphi - \sin\varphi \end{pmatrix} \tag{2.25}$$

$$(\Delta \varsigma_{\mathbf{ij}}) = \mathbf{A_w} \Delta \mathbf{l} \mathbf{S_0} \begin{pmatrix} \sin^2\varphi - \cos^2\varphi & 0 & -2\sin\varphi\cos\varphi \\ 0 & 0 & 0 \\ -2\sin\varphi\cos\varphi & 0 & \sin^2\varphi - \cos^2\varphi \end{pmatrix} \tag{2.26}$$

with $\mathbf{S_0} = \mathbf{S_c} - \mathbf{S}_a$ standing for a scalar deformation. Then, if $\mathbf{E_i}$ and $\mathbf{T_{ij}}$ are the components of the electric and stress fields at the location of the domain wall, then the energies of the induced electric and elastic dipoles are:

$$W_E = -\frac{1}{2} \Delta p_i E_i ; \quad W_M = -\frac{1}{2} \Delta \varsigma_i T_{ij} \tag{2.27}$$

The resonance frequency ($\omega_0 = \sqrt{\mathbf{q}/\boldsymbol{\rho}}$) of an oscillator represented by (2.21) is evaluated for barium titanate in [62] with assumption of absence any restoring force ($\mathbf{r} = \mathbf{0}$) to be at gigahertz range. For the periodic electric field excitation $\mathbf{E} = \mathbf{E_0} \exp(\mathbf{j}\omega\mathbf{t})$ with frequency ω lower than 10 MHz the inertia term in (2.22) is neglected in [63] and complex displacement amplitude is derived as:

$$\Delta \mathbf{l} = \frac{-\mathbf{P_s}}{\sqrt{2}\mathbf{k}(1+\mathbf{j}\omega\tau)} \left[\mathbf{E_1}\cos\vartheta + \mathbf{E_3}\sin\vartheta \right] +$$

$$+ \frac{\mathbf{S_0}}{\mathbf{k}(1+\mathbf{j}\omega\tau)} \left[(\mathbf{T_{11}} - \mathbf{T_{33}})\sin\vartheta\cos\vartheta - 2\mathbf{T_{13}}(\cos^2\vartheta - \sin^2\vartheta) \right] \tag{2.28}$$

Here the simplifying substitutions $\tau = b/k$ and $\vartheta = \varphi - \pi/4$ (see Fig.2.7) are used. With δn walls per volume and angle having the same orientation between ϑ and $\vartheta+\delta\vartheta$ the change of polarization induced by external field can be expressed as:

$$\delta P_1 = -\delta n A P_S \sqrt{2} \cos\vartheta \Delta l$$

$$\delta P_3 = -\delta n A P_S \sqrt{2} \sin\vartheta \Delta l$$

(2.29)

Equations (2.28) and (2.29) represent the complex matrix equation $\delta P = \delta d_{ij} T_j + \delta \varepsilon_{ik} E_k$ (abbreviated index notation) for polarization caused by those walls with orientation between ϑ and $\vartheta+\delta\vartheta$ in two-dimensional model of domain wall damping [63]. The final response can be derived according to an assumed distribution function $\delta n(\theta)$. Later this model was extended to three-dimensional geometry and included the possible relaxation time distribution $g(\tau)$ [66].

The nonlinear displacements of the domain wall of BaTiO$_3$ single crystal under external periodic field signal were observed through the direct optical measurements with stroboscopic lighting by Fousek and Bezina [67-69], who proposed nonlinear oscillator with non-monotonic restoring force to describe domain wall dynamics. The wall displacement amplitude, however, in most cases increases approximately linearly with increase of the driving field amplitude [67]. Later, Tikhomirov and Red'kin [70] reported on their study of single domain wall oscillations in gadolinium molybdate single crystal under external electric ac-field through the direct optical observation using polarizing microscope technique. They established quasi-linear dependence of the amplitude of domain wall vibration against the strength of driving electric field. However at lower fields, in subcoercive region, the motion of domain wall deviates from linear field dependence. Therefore, the phenomenological model of domain wall dynamics assuming linear displacement describes rather the high field regime [71].

The further extension of domain wall dynamics model including the effect of nonlinear domain wall displacement is proposed by Li, Cao, and Cross [72]. This extension is made by expanding the potential energy U_R of a displaced domain wall due to restoring force into a polynomial function of the domain wall displacement Δl:

$$U_R = U_0 + A\frac{C_1}{2}\Delta l^2 + A\frac{C_2}{2}\Delta l^3 + A\frac{C_3}{2}\Delta l^4 + ... \tag{2.30}$$

where U_0 is the rest energy of a domain boundary, which is assumed to be independent of domain wall motion. Then, the equation (2.22) for nonlinear restoring force may be expressed as follows:

$$Am\ddot{\Delta l} + Ab\dot{\Delta l} + \frac{\partial U_R}{\partial \Delta l} = -\left(\frac{\partial W_E}{\partial \Delta l} + \frac{\partial W_M}{\partial \Delta l}\right) \tag{2.31}$$

The approximate solution of (2.31) for first four terms of (2.30) considering only periodic electric ac-field excitation $E = E_0 \exp(j\omega t)$ with nonresonant frequencies (neglecting the inertia term) is derived in [72] as:

$$\Delta l = \Delta l^0 - \frac{C_2\left(\Delta l^0\right)^2}{C_1(1 + 2j\omega\tau)} - \frac{C_2\left(\Delta l^0\right)^3}{C_1(1 + 3j\omega\tau)}\left(C_3 - \frac{2C_2^2}{C_1(1 + 2j\omega\tau)}\right)$$

$$\Delta l^0 = \frac{e^{j\omega\tau}}{2C_1(1 + 2j\omega\tau)}(P_0\sum_{i=1}^{3}f_i E_{0,i}) \tag{2.32}$$

where $\tau = b/C_1$ is the relaxation time, and f_i designates coordinate transformation cosines of Euler angles Φ, Ψ, and Θ between primed and unprimed coordinates x, y, and z respectively (z' is normal to the domain wall plane). For three-dimension model:

$$\mathbf{f_1} = (\cos\Theta\sin\Phi\sin\Psi - \cos\Psi\sin\Phi$$
$$\mathbf{f_2} = -(\cos\Psi\sin\Phi\sin + \cos\Theta\cos\Phi\sin\Psi \qquad (2.33)$$
$$\mathbf{f_3} = -\sin\Psi\sin\Phi$$

The total induced polarization due to nonlinear displacement of the domain wall:

$$\Delta\mathbf{P_i} = \left[\Delta\boldsymbol{\varepsilon}_{i,j} + \Delta\boldsymbol{\Gamma}_{ijk}\mathbf{E_k}\right]\mathbf{E_j} + \Delta\mathbf{H}_{iklm}\mathbf{E_k}\mathbf{E_l}\mathbf{E_m} \qquad (2.34)$$

$$\Delta\boldsymbol{\varepsilon}_{ij} = \int\limits_0^{2\pi}\int\limits_0^{2\pi}\int\limits_0^{2\pi}\mathbf{P_0^2}\mathbf{K}(\omega)\mathbf{f_i}\mathbf{f_j}\mathbf{Z}(\Theta)\mathbf{d\Phi}\mathbf{d\Psi}\mathbf{d\Theta} \qquad (2.35)$$

$$\Delta\boldsymbol{\Gamma}_{ijk} = \int\limits_0^{2\pi}\int\limits_0^{2\pi}\int\limits_0^{2\pi}\mathbf{P_0^3}\mathbf{K'}(\omega)\mathbf{f_i}\mathbf{f_j}\mathbf{f_z}\mathbf{Z}(\Theta)\mathbf{d\Phi}\mathbf{d\Psi}\mathbf{d\Theta} \qquad (2.36)$$

$$\Delta\mathbf{H}_{iklm} = \int\limits_0^{2\pi}\int\limits_0^{2\pi}\int\limits_0^{2\pi}\mathbf{P_0^4}\mathbf{K''}(\omega)\mathbf{f_i}\mathbf{f_k}\mathbf{f_l}\mathbf{f_m}\mathbf{Z}(\Theta)\mathbf{d\Phi}\mathbf{d\Psi}\mathbf{d\Theta} \qquad (2.37)$$

where $\mathbf{Z}(\Theta)$ is an angular distribution function of domain walls normals, and

$$\mathbf{K}(\omega) = \int\limits_0^\infty\frac{\mathbf{Ag}(\tau)}{2\mathbf{C_1}(1+\mathbf{j}\omega\tau)}\mathbf{d}\tau\,; \quad \mathbf{K'}(\omega) = \int\limits_0^\infty\frac{\mathbf{C_2}\mathbf{Ag}(\tau)}{4\mathbf{C_1^3}(1+\mathbf{j}\omega\tau)^2(1+2\mathbf{j}\omega\tau)}\mathbf{d}\tau\,;$$

$$(2.38)$$

$$\mathbf{K''}(\omega) = \int\limits_0^\infty\frac{\mathbf{Ag}(\tau)}{4\mathbf{C_1^4}(1+\mathbf{j}\omega\tau)^3(1+3\mathbf{j}\omega\tau)}\left(\frac{\mathbf{C_2^2}}{\mathbf{C_1}(1+2\mathbf{j}\omega\tau}-\frac{\mathbf{C_3}}{2}\right)\mathbf{d}\tau$$

2.4. Domain wall contribution through interactions with the charged defects.

The crystal lattice defects act as pinning centres for the domain wall causing its nonuniform motion [73]. A direct observation of pinning and bowing of a single ferroelectric domain wall under weak electric field is described and analyzed by Yang *et al* in a recent paper [74]. Using a simple two-dimensional model shown in Fig.2.8, the domain wall profile **g(x)** was estimated considering two contributions into the change of free energy per unit thickness associated with the domain wall under an external applied field: (1) due to the lowering of the electrostatic free energy by bending of the domain wall, and (2) the increase of free energy due to increased wall length. As the result, the profile **g(x)** is the circle segment of radius $R = \sigma_w/(2P_sE)$, where σ_w is the domain wall energy per unit area, **E** is the strength of the static field applied, and P_s is the spontaneous polarization. Thus the domain wall curvature is unique for a given material at a fixed electric field **E**, and independent of the distance between pinning sites. The movement of the domain wall was revealed to be reversible and unipolar with respect to the applied field.

It is most likely that local Barkhausen jumps observed in ferroelectrics [54,56,75] at switching field conditions are the next step of the domain wall motion under external electric field action after bending between pinning centres.
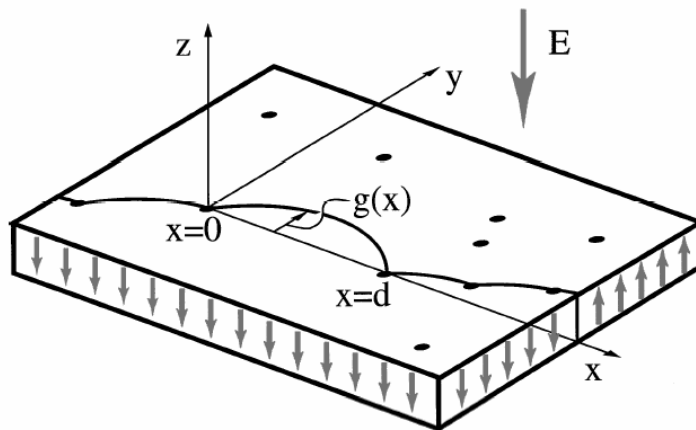
Figure 2.8. *Schematic of bowing of a pinned domain wall under an applied electric field. Dots denote defects. From Ref. [74].*

The switching (or polarization reversal) by an electric field is a defining and the most important characteristic of ferroelectric materials. Application of an electric field reduces the number (in ceramics) or completely removes (in single crystals) domain walls. One consequence of the domain wall switching in ferroelectrics is occurrence of ferroelectric hysteresis loop [59]. An example of ferroelectric hysteresis loop and schematic repartition of two polarization states corresponding to different regions of the loop [76] are shown in Fig.2.9.
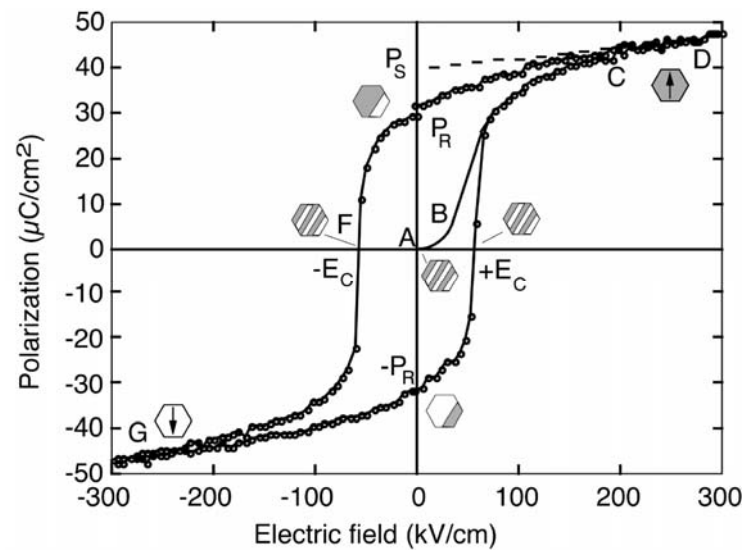
Figure 2.9. *Ferroelectric (P-E) hysteresis loop. Hexagons with grey and white regions represent schematically repartition of two polarization states in the material (e.g. in a grain of a ceramic) at different fields. From Ref. [76].*

In some cases the hysteresis loop is biased or constricted (Fig.2.10). This phenomenon is usually attributed to the effect of the domain pattern stabilization by various mechanisms [77-79], which is well consistent with the direct observation of local biasing, i.e. asymmetry in domain wall motion with the applied field polarity, reported in [74].

a)

b)
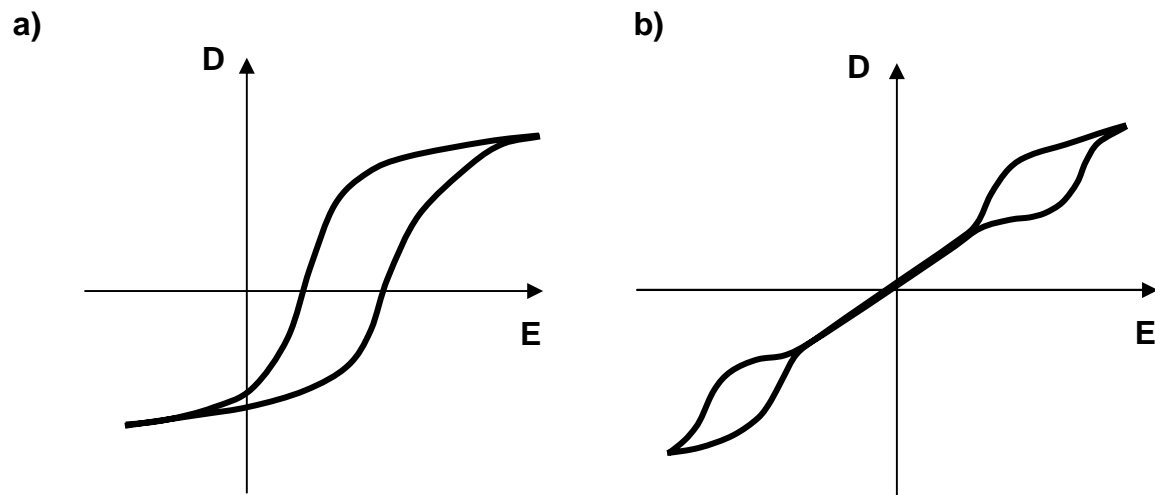
Figure 2.10. *Biased ferroelectric loops which may arise owing to the presence of defects in a ferroelectric crystal: (a) the dipoles have the same sense; (b) the dipole orientations are ordered over large regions, but different regions are antiparallel in the same way as ferroelectric domains. From Ref. [59].*

The effect of the hysteresis loop asymmetry or constriction was observed in many ferroelectrics both non-perovskite [80-84], and perovskite polycrystalline [77,79,85-88] and single crystal [74,89-92] materials; however the mechanisms of the effect and its origin of the domain wall stabilization are investigated in most detail in Rochelle salt [80-82] and triglycine sulfate (TGS) [83,84]. For example, the microscopic mechanism of the spontaneous polarization stabilization in TGS doped with alanine impurities during growth is understood and explained by structural unidirectional orientations of dipoles associated with the alanine molecule partially substituting for the glycine molecule [83]. In perovskite ferroelectrics the stabilization of the domain pattern also may be caused by ordering of charged defects, however, in these cases the main difficulties lay in their unambiguous identification [59]; nevertheless some progress in this direction has been achieved recently [93-95].

Classifications of possible mechanisms that might be responsible for the stabilization of domain wall configuration have been given by several authors [77,79,96,97]. In summary, there are three basic effects that may cause domain pattern stabilization in bulk ferroelectrics [79]:

1) Volume effect. All the solids contain defects in the form of foreign atoms or vacancies. These defects can occupy energetically preferred sites in the lattice and then form anisotropic centres which, locally or within a domain, favour a certain direction for the spontaneous polarization. This favouring of a certain direction of a particular direction of spontaneous polarization reveals itself experimentally as an internal bias or a constriction of the hysteresis loop (Fig.2.10). This scenario is the most used in literature to interpret biased or pinched hysteresis loop in bulk ferroelectrics in general [59], in perovskites [93-95], and, in particular, in TGS [83], Rochelle salt [80], and barium titanate [78,89] single crystals, doped with impurities or subjected to X-ray or gamma radiation.

2) Domain wall effect. This effect is also caused by defects. It is assumed that defects may diffuse in the course of time into the domain walls and fix their position. The driving forces may be elastic (neutralization of internal stresses) or electric (compensation of electric charges, for example, by valency changes of the foreign atoms). This domain wall effect has been suggested as an explanation of hysteresis features in barium titanate [77,89] and lead titanate zirconate [98,99].

3) Grain boundary effect [79]. In many cases the polycrystalline materials contain a small portion of phase which is liquid at the sintering temperature and covers the grain surface as a thin film. Such second phase always occur at high dopant concentrations, when the dopant concentration exceeds the solubility limit. Second phase lead to surface charges at the grain boundaries, which stabilize the domain configurations once these have established: the individual crystallite is biased by an overall preferred direction of polarization, but the individual domain wall remains mobile.

It is clear, that if each mechanism may exist independently, in a real ferroelectric material all of them may play a major or minor role. Simultaneously, the first two mechanisms are related to the domain wall interaction with the crystal defects. They are schematically represented in Fig. 2.11. The first mechanism may be realized through ordering of dipoles formed by charged defect complexes such as $[\mathbf{Fe^-_{Ti,Zr} - V^{2+}_0}]$ in a hard PZT doped with iron. In ferroelectric state, within a domain, these dipoles will have preferable orientation along the direction of the domain spontaneous polarization. Thus, in

course of time, when the system is equilibrated, the domain wall position becomes stabilized by the microdipoles differently oriented on the both sides of the domain wall (Fig.2.11,a). The second mechanism may be realized through two scenarios proposed in [98,99]. One scenario assumes damping vibration of 90° domain boundaries caused by their interaction with mobile point defects. The domain wall displacement from the equilibrium position causes the quasi-elastic interaction force with point defects which remained in the original position. After a certain period of time sufficient for diffusive displacement of point defects to a new position of the wall, the interaction force disappears. Another scenario assumes motionless domain wall interaction with charged point defects. Under an external action, the domain wall does not move but becomes charged which causes the diffusion of the mobile charged defects towards the domain walls to screen the bound charges. These two scenarios are considered as models for calculation of the energy losses due to the first or second mechanism; however it is possible to assume that real process of the domain effect lies somewhere in between two mentioned scenarios. Schematically the domain wall effect is shown in Fig.2.11,b.
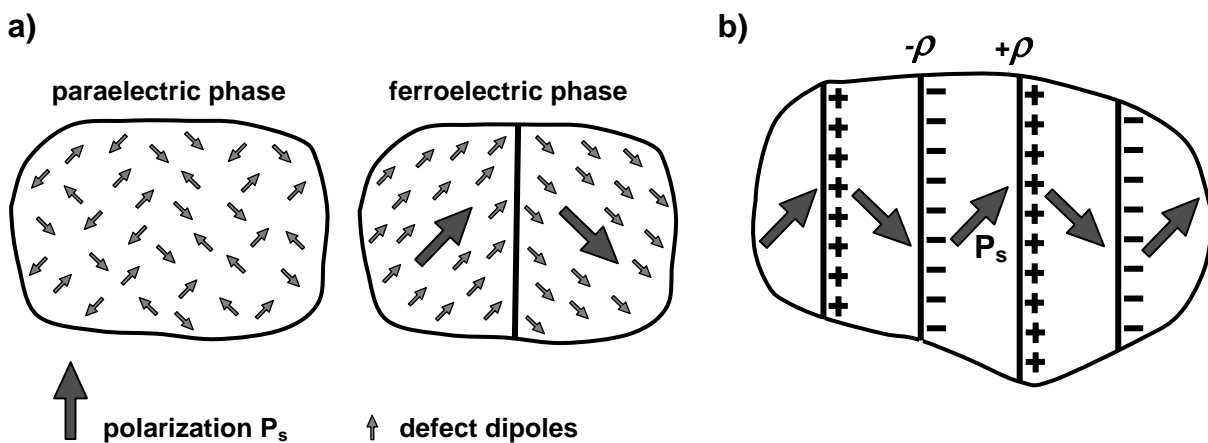
Figure 2.11. *Stabilization of the domain wall position through interaction with charged defects. (a) The bulk effect of charged dipole ordering along spontaneous polarization (P_s); (b) Domain wall effect (after Ref. [98,99]).*

The alignment of defect dipoles in polycrystalline $Pb(Zr,Ti)O_3$ and $BaTiO_3$ ceramics was studied in [94] using electron paramagnetic resonance (EPR) technique. It was shown that defect dipoles can become aligned by oxygen vacancies motion in the octahedron about a negatively charged centre for the oxygen vacancy-related dipole complexes or by defect

displacement and domain realignment in the lattice for isolated defect centres. No alignment was observed in paraelectric phases. This suggests an interplay between distortion in the unit cell and the ability to align defect dipoles. The ceramics investigated in [94] were not deliberately doped with any impurities, however the paramagnetic defect dipoles related to oxygen vacancy was observed. In case of $BaTiO_3$, the Fe^{3+}-$V_{O^{..}}$ and Fe^{1+}-$V_{O^{..}}$ complexes were observed and their alignment was studied. In PZT ceramics the Fe^{3+}-$V_{O^{..}}$ complex and isolated Ti^{3+} (d^1), Pb^{3+} ($6s^1$), and Cu^{2+} (d^9) centres were observed and the alignment of Ti^{3+} isolated centres was studied in detail [93-95].

For hard perovskite ceramics deliberately doped with iron, where oxygen vacancies presence is anticipated due to interaction with holes during thermal treatment ($2h + O^{2-} \rightarrow$ $\frac{1}{2}O_2\uparrow + V_0^{..}$) [8], it is most likely to expect the alignment of the defect dipoles associated with oxygen vacancies similarly to those observed in $BaTiO_3$. The mechanism and kinetics of Fe^{3+}-$V_{O^{..}}$ complexes alignment in tetragonal ceramics of $BaTiO_3$ along applied electric field direction are investigated and analyzed in detail [93-95]. The time-temperature dependencies of aligned complex dipole fractions under dc bias of -4.5 kV/cm are shown in Fig.2.12,a. The alignment kinetics was found to be temperature dependent according to the exponential function: $[Fe^{3+}$-$V_{O^{..}}] = [1-2/3exp(-t/\tau)]$. The equation describes number of dipoles registered by EPR technique and aligned in the tetragonal perovskite lattice along (both spectroscopically equal parallel and antiparallel) the direction of applied bias field [95]. Thus, one third of dipoles are detected to be oriented parallel to the alignment direction before the field is applied. The activation energy of $V_{O^{..}}$ motion to align the defect dipole in tetragonal $BaTiO_3$ ceramics was found to be [95]:

$$E_a^{(V_{\ddot{O}} \text{ in tetragonal } BaTiO_3)} \approx 0.91 \, eV \tag{2.39}$$

The kinetics of the alignment-unalignment-realignment dipole process according to the polarity of applied field bias is shown in Fig.2.12,b. When the polarity of biasing field was switched, the kinetics of realignment process is described by two detected processes: realignment (oxygen vacancy moves from position A to one of four equivalent positions P in Fig.2.12,b); and then realignment (from position P to B). Both processes satisfy the exponential decrease of defect concentrations on positions A and P with the same decay constant that correspond to the general kinetics curve with the minimum at ($1/e \approx 37\%$) of

the aligned fraction, shown in Fig.2.12,b. Thus, these results provide compelling, but nonetheless somewhat intuitive, evidence that $V_{O^{..}}$ motion does indeed occur within the oxygen octahedron in the perovskite lattice. The considered mechanism is well consistent with calculations in [100], which show that the jump distance of defects, whose unidirectional movement was considered as a cause of observed fatigue in thin film, is very close to the lattice parameter.
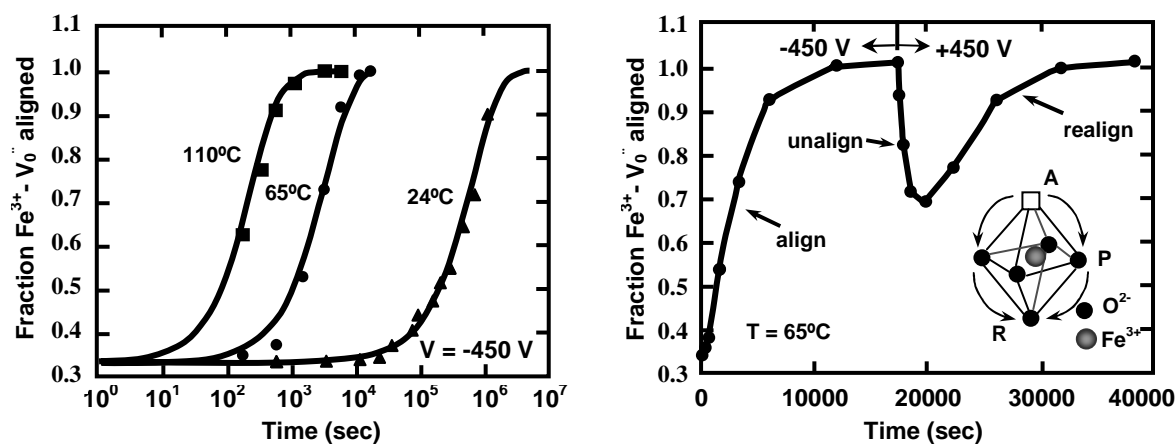
Figure 2.12. *(a) Alignment kinetics of the Fe^{3+}-$V_{O^{..}}$ complex. (b) Field switching experiment showing the alignment, unalignment and realignment of the Fe^{3+}-$V_{O^{..}}$ complex. The inset shows the Fe^{3+}-$V_{O^{..}}$ complex in the oxygen octahedron. The arrows indicate two of the four pathways in which the $V_{O^{..}}$ can move in the lattice. The switching bias of 450 V corresponds to the electric field strength 4.5 kV/cm. (From Ref. [95]).*

Oxygen vacancies and other point defects in the lattice form also the elastic dipoles (Fig.2.13), hence the arrangement of elastic dipoles towards their thermodynamical equilibrium may also contribute to the domain wall clamping [101,102]. In the three dimensional space three orientations are possible for the elastic dipole shown in Fig.2.13 for two dimensional **a-c** plane of tetragonal lattice. Due to low lattice symmetry (in ferroelectric states with non-cubic symmetry) an elastic distortional energy ΔW_m caused by defect position with **c-**axis distortion is different from others causing distortion in **a-** and **b-** axis directions. The splitting mechanical energy ΔW_m is comparable with one associated with an electric dipole (ΔW_e) [101,102]. Random orientation of the elastic dipoles implies **1/3** of their total density **n** to be in each of the three positions. After orientation to the lowest energy there will be an excess Δn of elastic dipoles in the low energy position reducing the

total energy by $\Delta G = \Delta n \; \Delta W_m$. This contribution however is difficult to evaluate, but analysis of the domain wall clamping due to orientation of elastic dipoles can proceed without shifting the electric hysteresis curve [102,103]. In this case a shift of elastic hysteresis curve is expected and was observed [104].
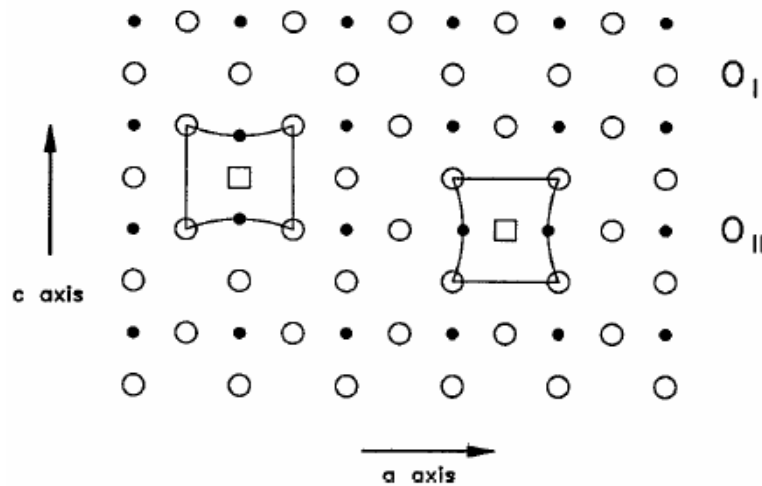
Figure 2.13. *A (100) lattice plane of tetragonal perovskite ABO₃ (solid dots – B-ions, circles – oxygen ions) with an oxygen vacancies (rectangles) on the O_I site (left) and another one on the O_II site (right). The disturbed lattice cells are deformed by 90º to each other and are elastic dipoles which can orient by diffusion of the vacancy. (From Ref. [102]).*

The discussion on which of the domain wall clamping mechanisms dominates in bulk ferroelectrics has been the subject of several publications [77,79,97] and still remains open. Calculations in [105] show that for one-dimensional model of domain wall clamping the clamping pressure exerted by oriented defect dipoles is up to three orders of magnitude weaker than one exerted by the same amount of charges accumulated on grain boundaries. Thus, the authors in [105] conclude that the drift of charged point defects dominates the ageing phenomenon and the domain structure stabilization. In addition, the oxygen vacancy ordering, segregation and gathering at the grain boundary even in some perovskite oxides free of ferroelectric domains have been ascertained through direct experimental evidence in recent study using scanning transition electron microscopy technique [106].

The arguments for the volume effect are based on direct observations of dipole alignments [93-95] and some experimental studies, such as observing the biased hysteresis

loop on Mn-doped BaTiO$_3$ single crystals both before and after the surface layer removal by etching to half of initial thickness within the time much shorter than the relaxation time of the stabilization process [97]. Another recent study [107] describes the direct evidence of domain pattern conservation during switching process by in situ microscopy observation of 90º ferroelectric domains of Mn-doped BaTiO$_3$ during electric field cycling, which can only be explained by volume effect since the restoring of domain pattern was observed in volume.

2.5. Phenomenological description of the domain wall state for the systems with an ordered and disordered state of charged defects.

The considered mechanisms of domain wall stabilization due to interaction with point defects have one similar feature – they assume a kind of electrostatic arrangement of the charged defects based on their mobility resulting in redistribution, pinning or clamping of domain walls. Macroscopically, this is manifested in biased hysteresis loop. The existing quantitative models for domain wall clamping due to volume [102], domain wall [98,99], and grain boundary (charge drift) [105] effects lead to qualitative or quantitative contradictions [97,105] partly due to assumed simplifications such as considering only one mechanism whose contributing scale is difficult to estimate. It makes sense, hence, to find a descriptive phenomenological model which can at least qualitatively characterize dielectric response due to domain wall interaction with charged defects whose electrostatic arrangement irrespectively to exact geometry would be the main regulating parameter. It can be realized by assuming an appropriate energy profile for the domain wall according to the state of electrostatic arrangement of charged defects.

Among the mentioned models such an approach was used by Robels and Arlt [102] who proposed a V-shaped potential to describe the volume effect of domain wall clamping by orientation of defects (Fig.2.14,a). This potential is valid for an infinitely thin domain wall where the force exerted by aligned dipoles on the both sides of the domain wall does not change with the distance from the wall. When a wall changes its position by a distance **Δl**, the dipoles in this region do not reorient immediately, and thus the free energy of a wall increases by:
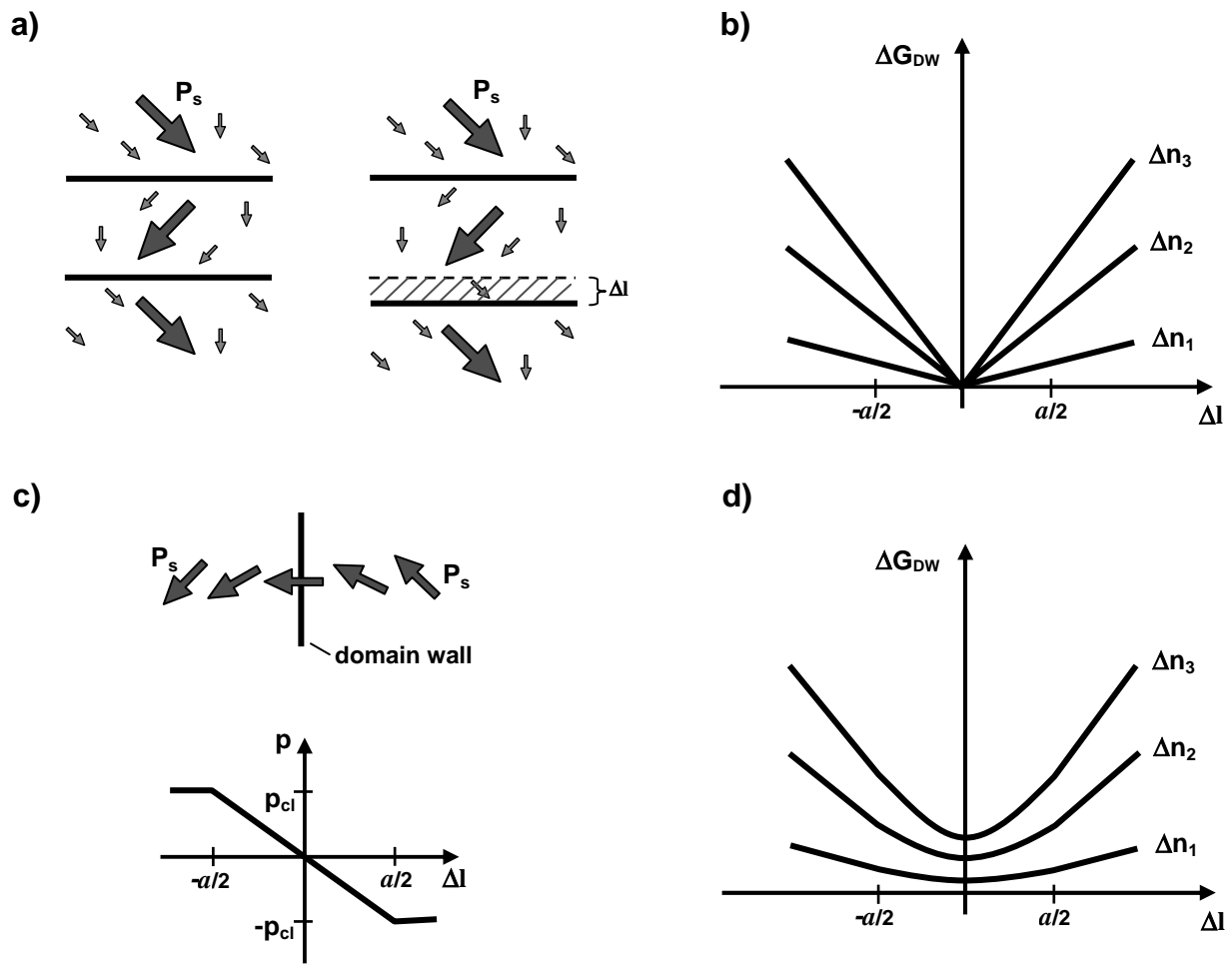
Figure 2.14. *Robles's and Arlt's model of 90° domains in an aged acceptor doped ceramics: (a) Orientation of most of the dipoles parallel to spontaneous polarization P_s within the domains, the dipoles are misaligned in the shaded area if the domain wall displaced by Δl (right); (b) The free energy ΔG of a domain wall as a function of its displacement and number of aligned defects per volume Δn for an infinitesimal domain wall width; (c) Model of a 90° domain wall with the finite width a: gradual change of spontaneous polarization at the domain wall (top) and the resulting clamping pressure as a function of domain wall displacement (bottom); (d) The free energy of a domain wall with the finite width a. (From Ref. [102]).*

$$\Delta G_{DW} = \Delta n(t) A |\Delta l| \Delta W_e \qquad (2.40)$$

where A is the surface of wall, $\Delta n(t)$ is the concentration of dipoles in the shifted region as a function of time t, and ΔW_e is the energy associated with a defect oriented in unfavourable

direction with respect to the spontaneous polarization (it is estimated as **10...30 meV** depending on temperature in range of **40...80 ºC** [101]). Thus the model considers the domain wall trapped in a potential discontinuity (2.40) as shown in Fig.2.14,b. The aligned defect dipoles exert a clamping pressure $\mathbf{p_{cl}(t)}$ to both sides of domain wall in order to keep it in its position:

$$\left|\mathbf{p_{cl}(t)}\right| = \frac{1}{A_w}\left|\frac{\partial\Delta G_{dw}}{\partial\Delta l}\right| = \Delta n(t)\Delta W_e \tag{2.41}$$

To avoid abrupt change of the clamping pressure at $\mathbf{\Delta l = 0}$, the finite domain wall width **a** (Fig.2.14,c) is introduced into the model [102]. Thus the clamping pressure discontinuity can be replaced with the simple assumption of linear change from **-$\mathbf{p_{cl}}$** to **+$\mathbf{p_{cl}}$** within the domain thickness:

$$\mathbf{p_{cl}(t)} = \frac{2\Delta n(t)\Delta W_e}{a}\Delta l, \quad \left|\Delta l\right| \le \frac{a}{2} \tag{2.42}$$

In this case the domain wall is trapped in parabolic potential well (Fig.2.14,d) whose steepness depends on the number of aligned dipoles **Δn** (Fig.2.14,d).

Considering the contribution to the domain wall clamping pressure due to ordering of dipoles, the total effective clamping force per area can be expressed as:

$$\mathbf{k_{eff}(t) = k + k_{cl}(t)} \tag{2.43}$$

where $\mathbf{k_{cl}(t)}$ is exerted from the contribution of the oriented defects and **k** is the restoring force constant in equation of the domain wall dynamics (2.22); the derivation of k is provided in [108]. From (2.42) the contribution of the ordered defects to the force per area is:

$$\mathbf{k_{cl}(t)} = \frac{2\Delta n(t)\Delta W_e}{a} \tag{2.44}$$

Instead of density of oriented defects $\Delta n(t)$ which is difficult to determine directly, Robels and Arlt propose to substitute by microscopic internal bias field that can be determined from hysteresis characterization. Then

$$k_{cl}(t) = \frac{2P_s E_i(t)}{af_E} \tag{2.45}$$

The coefficient f_E depends on the distribution of coercive field and on the strength of the applied ac field, and it is less dependent on the remanent polarization. For tetragonal ceramics it is estimated as $f_E \approx 1.1$ [102] . Then the dielectric permittivity extracted from (2.28) – (2.29) can be expressed as:

$$\Delta\varepsilon_{ij}(t) \propto \frac{P_s^2}{k + k_{cl}(t)} f_{\varepsilon_{ij}} \propto \frac{1}{b + mE_i(t)} \tag{2.46}$$

where b and m are some constants. The experimental verification of (2.46) was performed by deageing experiments on hard barium titanate zirconate and lead titanate zirconate ceramics demonstrated the linear dependence of reverse permittivity $1/\Delta\varepsilon_{33}$ as a function of observed internal bias E_i during ageing and deageing achieved by field cycling [102].

The model proposed by Robels and Arlt can be used as phenomenological model of defect contribution to the domain wall clamping irrespectively of the exact mechanism of defect arrangements[1]. It is based on the domain wall energy and establishes phenomenological links between macroscopically observed bias field E_i appearing in D-E hysteresis loop resulting from electrostatic arrangement of microscopic defects with concentration Δn, and the domain wall energy change ΔW_e. The latter is sensitive to the exact mechanism of electrostatic process (volume, domain or grain boundary) leading to clamping. For example, the clamping pressure caused by drift of charge carriers calculated in [105] is found to be much higher than one exerted by orientation of defects, hence in framework of this model will result in much higher steepness of the potential energy profile shown in Fig.2.14.

---

[1] In the original model of domain wall clamping, proposed by Robels and Arlt, only the effect of orientation of defects was assumed.

2.6. Summary

The literature review identifies the following approaches to build phenomenological models of the domain wall contribution to the polarization response in ferroelectric materials:

The first approach is based on the Preisach formalism that is a universal mathematical model of many hysteretic systems and considers the hysteresis as an assembly of a large number of elementary bistable units whose states are determined by two parameters. The statistical distribution of these parameters usually presented on the Preisach plane defines the final form of the hysteresis loop revealed by the hysteretic system. The physical meaning of Preisach model is analyzed in several works in terms of restricted models based on random or stochastic descriptions of the system free energy. It has been shown that the response described by Rayleigh relations is the particular case of Preisach hysteresis and corresponds to a uniform distribution of Preisach parameters. Rayleigh relations are often used as phenomenological model describing nonlinearity and hysteresis in the magnetic, ferroelectric, and piezoelectric materials. Owing to works of Néel and Kronmüller the Rayleigh relations have been derived for a domain wall contribution due to motion in medium with pinning centers characterized by statistical fluctuation of domain wall potential energy.

The second approach is based on the description of the domain wall dynamics using an appropriate model of harmonic oscillator. The advantage of such approach is the possibility to take into account some domain wall clamping mechanisms directly, e.g. effect of dipoles orientation on domain wall clamping can be included by restoring force in the equation of domain wall dynamics

The domain wall motion under influence of electric field has been a subject of many studies since the multidomain structure of ferroelectrics was discovered. Some of these studies are based on direct observations of domain wall behaviour using optical instruments. Thus the local Barkhausen jumps of domain wall have been observed under switching conditions, while under weaker fields, a bowing of the domain wall pinned on defects has been observed.

The role of structural defects on domain wall motion has been analyzed in recent work of Zhang and Ren by observation of domain pattern transformation under applied field in aged and quenched (thermally disordered) states of ferroelectric crystal. The observed stability of domain configuration to a cycle of applied electric field in aged material and its absence in quenched material strongly suggests, that ordering defect plays a key role in the mechanisms of domain wall clamping in hard ferroelectrics.

One of possible mechanism of defects ordering in perovskite ferroelectrics has been studied using electron paramagnetic resonance (EPR) technique. In these studies the qualitative analysis of EPR spectra indicated the orientation of dipoles formed by charged defect associates (oxygen vacancies with transition metal ions) along the direction of applied field. The mechanism of alignment of local dipoles and its effect on domain wall clamping is also known from early studies of properties of TGS crystals doped with alanine.

The qualitative model of polarization response due to domain wall contribution and accounting for the clamping effect of dipoles alignment along the spontaneous polarization within a domain has been proposed by Robel and Arlt. This model describes the linear polarization response to electric field depending on the number of oriented dipoles. The phenomenological model of domain wall dynamics accounting for the nonlinear effects has been outlined by Li, Cao and Cross.

Chapter 3

The goals and structure of the thesis

The review of literature on dielectric behaviour of hard and soft ferroelectric materials reveals several approaches to describe extrinsic contribution of the domain wall motion to polarization response. In a very general case these approaches can be understood through phenomenological description of domain wall trapping in certain potential profiles. There are two limiting cases that can be considered and attributed to soft and hard ferroelectric system. In the first limiting case, applicable to the soft ferroelectrics, the domain wall moves irreversibly in a random potential energy profile; in the second limiting case, applicable to the hard ferroelectrics, the domain wall is clamped in "V-shaped" potential energy profile and can perform only reversible movements. This phenomenological description of hard and soft system predicts a possibility for ferroelectric system to transform between these two limiting cases under an external influence. This can happen if the shape of domain wall energy potential is controlled by distribution of pinning centers. In cases considered here the randomness or ordering in distribution of pinning centers is usually assumed to be related to the state of arrangement of charged point defects with respect to polarization within domains. An indication that this assumption may be correct is the difference in mobility of defects in hard and soft materials (Fig.3.1). In hard ferroelectric materials with perovskite structure doped with acceptors, such as Fe^{3+} replacing (Zr^{4+},Ti^{4+}) in PZT, the local charge misbalance favours the formation of oxygen vacancies that tend to form dipole associates with the acceptor dopant ions (Fig.3.1,a). In the soft materials the dipole formations of the cation vacancies with the donor dopant ions are anticipated (Fig.3.1,b). However the mobilities, and thus tendency to order, are not equal for all defects.

If the diffusive motion of oxygen vacancies in the crystals with perovskite structure have been a subject of more or less direct observations and extensively discussed in literature [93-95,100,107,109-111], there is relatively little information about the mobility of cation-site defects. Nevertheless, taking into account the geometry of the perovskite structure and the coordination of atoms in it, it is reasonable to assume that oxygen-site defects have advantageous prerequisites for diffusion. Hence the anticipated ordering and disordering structure of defects in, correspondingly, hard and soft ferroelectric materials may serve as basic assumption in the understanding of hardening and softening mechanisms.

The experimental study of hardening-softening transitions under various conditions in modified PZT ceramics is one of the main thesis objectives
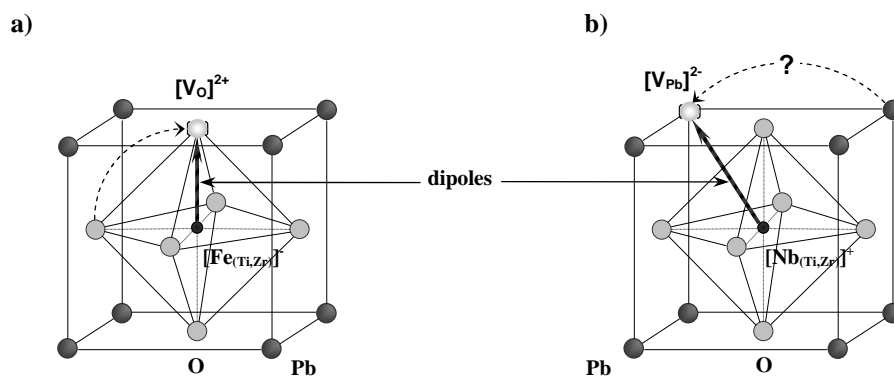
Figure 3.1. *Possible associated defect dipoles in PZT doped with acceptor dopant (a) and donor dopant (b). Due to higher mobility of anion vacancies the ordering of dipoles in acceptor-doped hard ceramics is expected. Dipoles associated with immobile cation vacancies are disordered most likely.*

Another thesis objective is a contribution to a more general task of building a unified model of polarization nonlinearity and hysteresis in ferroelectrics with various state of order of domain wall pinning centres[2]. The unified model is based on the following principles.

The V-shaped potential profile proposed by Robels and Arlt is considered as ultra-hard limiting case corresponding to anhysteretic reversible motion of domain wall clamped by electrostatically arranged charged defects. Nonlinear effects of domain wall motion can be included into this model similarly to the way proposed in [72]. The original V-shaped potential that describes the movement of a domain wall beyond the position of its minimum can be smeared at the origin to account for the linear reversible movement of the domain wall very near its initial position[3]. As in the original model of Robels and Arlt [102], an additional restoring force described by a parabolic potential may be added to describe movement of the wall when concentration of electrostatically arranged dipoles approaches zero. And, finally, the free energy of the wall is modified by the external field E. Then the final expression for the domain wall free energy change per unit area in the simplified one-dimensional case is given by:

$$\Delta G = \frac{1}{2}k(\Delta l)^2 + k_{cl}\left(\sqrt{(\Delta l)^2 + (\Delta l_0)^2} - \Delta l_0\right) - 2P_s E \Delta l \qquad (3.1)$$

Here, k describes the steepness of the additional harmonic potential resulting from other factors causing restoring force; k_{cl} describes the steepness of the modified V-shaped potential caused by arrangement of charged defects; Δl_0 defines the smearing region width around initial wall position $\Delta l = 0$. In general case, k_{cl} is described by (2.44), and both clamping constants can be determined from ageing experiment accordingly to (2.46). The domain wall displacement $\Delta l(E)$ and proportional polarization response suggested by (2.29) can be obtained by solution of the equation describing the equilibrium position:

$$\frac{\partial \Delta G}{\partial \Delta l} = 0 \qquad (3.2)$$

This equation can be solved analytically[4] and one of its solutions is shown in Fig.3.2

---

[3] Smearing of the V-potential has been proposed by A.K. Tagantsev
[4] First analytical solution for the modified V-potential was given by J.Dorn (semester project, LC, 2001)

Obviously, the anhysteretic, nonlinear dielectric behaviour described by (3.1), (3.2) and shown in Fig.3.2 is only an approximation for very hard ceramics. Comparing the potential energy profiles shown for the Rayleigh-type system shown in Fig.2.5 and Fig.2.6 with one for a system with clamping force exerted by ordered defects shown in Fig.2.14 and Fig.3.2, the complete phenomenological model describing mechanisms of the domain wall contribution to polarization nonlinearity and hysteresis can be proposed as schematically shown in Fig.3.3. This model considers the steepness and randomness of the domain wall free energy as a function of degree of order in the electrostatic arrangement of charged defects. Thus, according to this model, the softening or hardening of ferroelectric system is described in terms of the roughness, steepness and randomness of the potential describing the free energy of the domain wall (Fig.3.3).
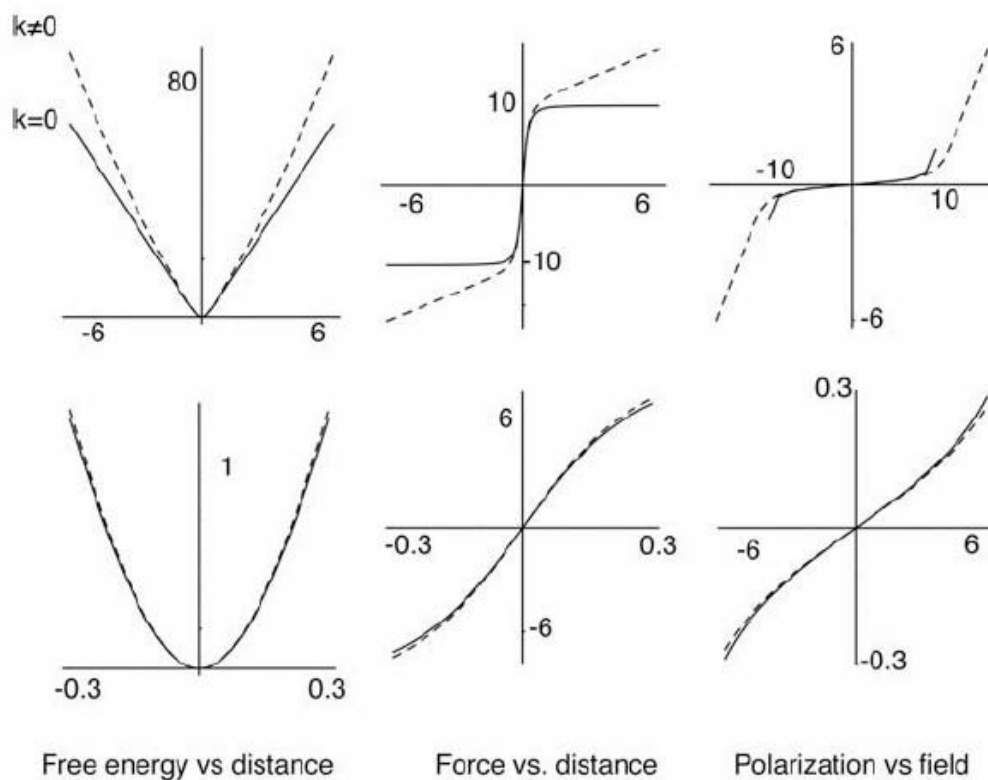
Figure 3.2. *Modified V-potential for a domain wall, force acting on the wall, and polarization caused by the domain wall displacement in a hard material. Top: at large distance from the wall position at rest. Bottom: In the smeared region. The numbers (whose values have no physical meaning) on the axis are included to indicate order of magnitude and enable comparison of effects at large distances and in the smeared region. Dashed lines indicate case k 0 in (3.1)-(3.2)*
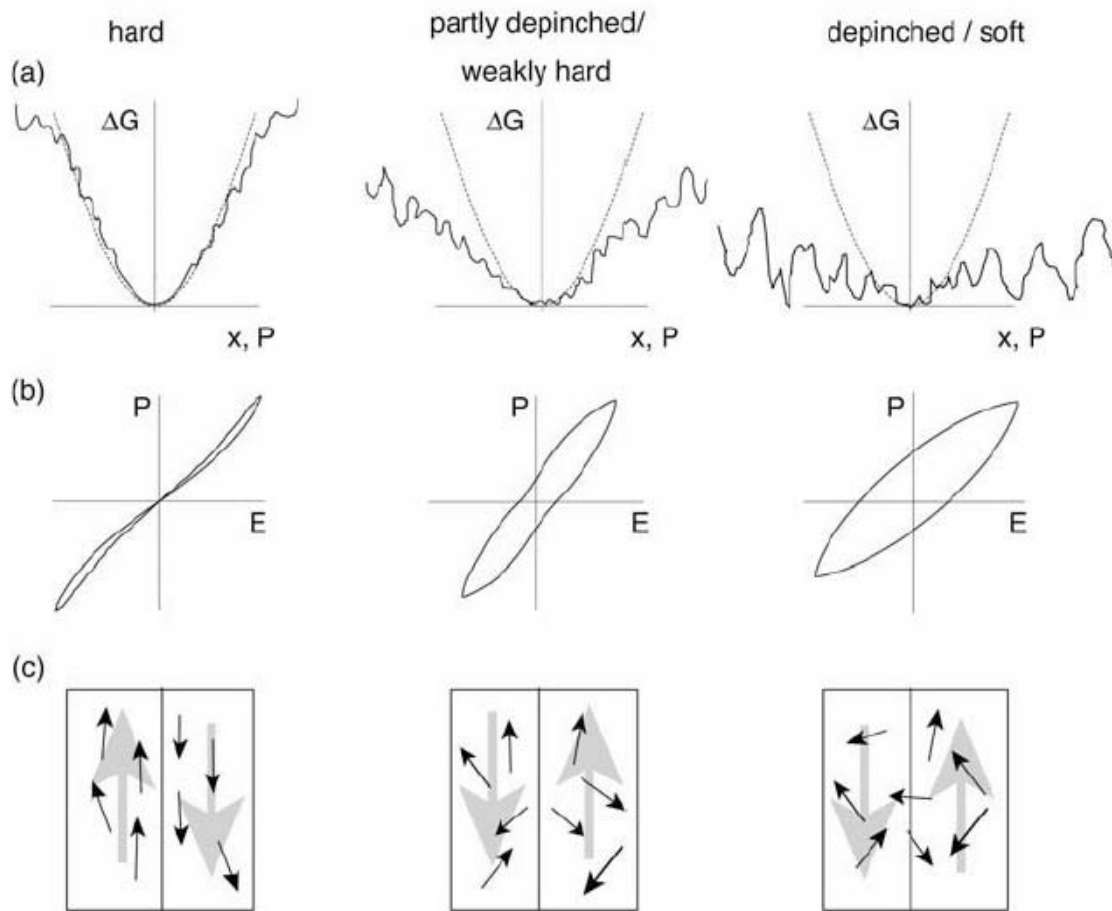
Figure 3.3. *V-potential, with introduced roughness, in the smeared region for a very hard, a partially depinched or a weakly hard material, and for a field relaxed or soft sample. (a) Energy profile of a domain wall; (b) polarization-field hysteresis; (c) schematic of ordering of defect centres within domains which gives rise to the bias field.*

Further model development towards detailed qualitative and quantitative description, as well as its verification, requires collection and deep analysis of experimental data on polarization response in a real ferroelectric system experiencing transitions between hard and soft states under the influence of various physical effects, such as applied electric field of different strength and frequency, temperature, and type and concentration of dopants.

In this work PZT ceramics doped with Fe and Nb impurities are used for analysis of polarization nonlinearity and hysteresis in the context described above. Thus, the aim of study is the systematic analysis of the hard and soft ferroelectric ceramics behaviour under switching and subswitching field conditions. The experimental study includes analysis of various external effects

causing order-disorder transitions and their relations to the models considered in this and previous chapters.

The particular interest of the following study is to find out which nonlinear parameters of polarization response are the most critical to hardening-softening of ferroelectric system and which may thus serve as the model parameters.

The following structure of the thesis is based on specific goals:

- **Chapter 4: Processing and characterization of Pb(Zr,Ti)O$_3$ ceramics**

This chapter describes the details of processing of modified PZT ceramics and the characterization of their basic properties. It will help to find the optimal composition range at which the main goals of thesis can be realized. Namely, ferroelectric ceramics should clearly and reproducibly reveal the inherent properties of hard and soft materials. These properties should also reveal explicit and regular dependence of dopants type and concentration and should not be much affected by other effects such as microstructural parameters, fluctuation of density or composition. However not all of characterized properties will be presented in this chapter, some of them will appear later, in the chapters describing the detailed studies of material properties.

The quality of prepared ceramics is evaluated by classical set of characterization methods including density, grain size control, X-ray diffraction and scanning electron microscopy. The positron annihilation study as a special characterization method will be described in a separate section. The aim of this particular study is both to characterize PZT ceramics and to adopt the method of positron annihilation lifetime analysis as a tool of defect structure analysis in ferroelectric ceramics.

- **Chapter 5: Electrical characterization**

In this chapter the details of dielectric spectroscopy study and important features of polarization response to periodic field signal are discussed. Particularly, the links between nonlinear parameters of polarization response (which may easily be obtained using the dielectric spectroscopy technique) and features of ferroelectric hysteresis are demonstrated. These links are then related to models of the ferroelectric hysteresis and nonlinearity.

- **Chapter 6: Dielectric properties of hard and soft ceramics at subswitching conditions**

The features of hardening and softening of ferroelectric system revealing themselves under subswitching range of electric field are studied and analyzed. The special emphasis is devoted to analysis of material properties (expressed directly or by nonlinear parameters) in terms of conceptual models considered in the present and previous chapters. The detailed study using dielectric spectroscopy methods in broad frequency and temperature ranges will be provided in order to accomplish two main tasks: 1) to characterize the specifics of the domain wall dynamics in hard and soft ferroelectrics and to verify in a wide frequency range the applicability of the models that are developed previously without accounting for frequency effects; 2) to study the processes of ac-conductivity provided by hopping charge carriers whose role in hardening mechanism has been discussed above.

- **Chapter 7: Study at switching conditions**

Several effects of softening and hardening in ferroelectric PZT ceramics under switching conditions will be considered in this chapter: effects of composition (mainly, dopants type and concentration), amplitude of the driving field, thermal treatment, and time. Each analyzed effect is considered separately, but the possible coupling of the various effects is analyzed throughout the chapter.

- **Summary and conclusions**

The brief revision of main thesis results followed by the conclusions will be provided in the thesis summary.

Chapter 4

Processing and characterization of Pb(Zr,Ti)O$_3$ ceramics

4.1. Composition range

The thesis aim assumes synthesis of lead zirconate titanate compositions modified with hardening and softening impurities in order to obtain two sorts of dominating defects – presumed immobile cation vacancies in soft ceramics, and oxygen vacancies in hard ceramics [8]. The oxygen vacancies are considered by many authors as the most mobile intrinsic ionic defects in perovskite-type materials [109-111]. The appropriate concentration of Fe and Nb dopants can be added in the range of their solubility (up to 1% for iron dopant) [112]. To cover a reasonable range of compositions, PZT ceramics are prepared with the dopant concentration fixed as 1 at.% Fe, 0.5 at.% Fe, 0.1 at.% Fe, undoped, 0.2 at.% Nb, 0.5 at.% Nb, 1.0 at.% Nb.

The phasee diagram PbTiO$_3$ – PbZrO$_3$ (Fig.2.1) contains several regions with different structure and related property features [8,113-116]. Roughly, four compositional regions of PbZr$_{1-x}$Ti$_x$O$_3$ solid solution can be classified accordingly to their properties and applications [115]:
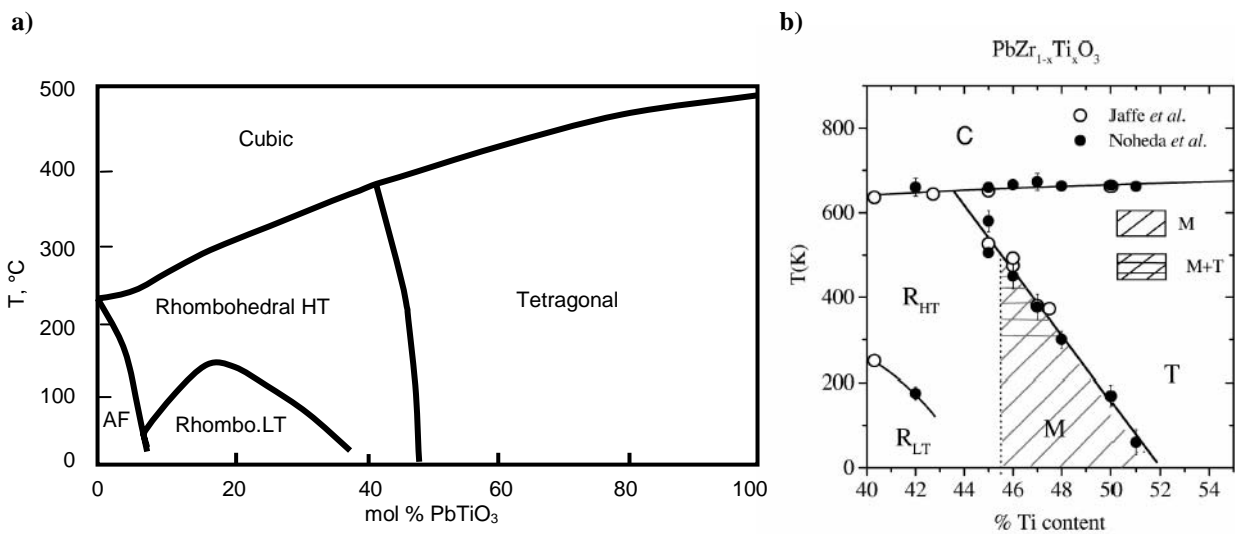
Figure 4.1. *Phase diagram for lead zirconate titanate below the solidus line. a) General view, from ref. [8]; b) detailed refinement of MPB region, from ref. [113].*

1) **0 < x < 0.1:** Antiferroelectric and rhombic phase exists at the normal conditions, however, in some application the antiferroelectric to ferroelectric phase transitions induced by external electric field are used in applications. Ceramics based on these compositions are promising for shape memory applications due to relatively high coefficients of electroelasticity. The deformation of these ceramics can be controlled by various domain configurations and structures [117]. Another interesting application of these ceramics is fabrication of elements with high electron emission obtained during ferroelectric – antiferroelectric phase transition controlled by external electric field and mechanic stress [118]

2) **0.1 < x < 0.4:** There are two rhombohedral phases. The ferroelectric phase transition from the low-temperature to the high temperature phase is accompanied with the loss of oxygen octahedron tilt angle and corresponding superstructure [119]. The phase transition feature calls forth the high pyroelectric properties used in pyroelectric detectors. These ceramics are characterized by relatively low spontaneous deformations and low range of dielectric constants and are used in electromechanical transducers and surface acoustic wave devices. Another feature of this compositional range with added dopants is the experimentally observed states of metastable polarization which is typical for relaxors [120,121].

3) **0.4 < x < 0.6:** This area of solid solutions includes the morphotropic phase boundary (MPB) (around **x = 0.48**) separating rhombohedral and tetragonal regions, where crystal structure and properties are very sensitive to the fluctuation of composition. Recent structural studies of ferroelectric PZT with Zr/Ti = 52/48, have revealed a monoclinic phase in the vicinity of the MPB [113,114] (Fig.2.1,b). In this region most of the properties are very pronounced and reach the extremum values. The close relationship between the monoclinic phase and the striking piezoelectric properties of PZT has been shown in [116]; in particular, it has been revealed that the monoclinic distortion is the origin of the unusually high piezoelectric response of PZT. This feature of MPB region is widely used in applications of these materials [1,8,121].

4) **0.6 < x < 1.0:** Compounds in wide range of the solid solutions with tetragonal crystal structure possess relatively high anisotropy of piezoelectric coefficients d_{33} and d_{31} and corresponding electromechanical coupling factors k_t and k_p [122,123]. Other features of these compositions are relatively high coercive fields and high spontaneous deformations. Some applications of these materials include filters and frequency stabilizers.

For the experimental study of various aspects of polarization response in hard and soft PZT ceramics, the third (MPB) region is most appropriate due to the most pronounced properties and high values of dielectric constant. Three basic compositions for modified $Pb(Zr_xTi_{1-x})O_3$ ceramics are chosen near the morphotropic phase boundary, corresponding to **x = 42**(tetragonal)**, 50**(MPB)**, and 58**(rhombohedral) in order to characterise their properties and conduct the study on the compositions with the most reliable and reproducible dielectric response. For simplicity, in the following, these compositions will be also mentioned as PZT(42/58), PZT(50/50), and PZT(58/42) correspondingly.

4.2. Bulk ceramic processing[5]

The PZT ceramics have longer than 50 years history and the technology of their ceramic processing is rather well developed and has been described in many books [8,116,124], review papers [1,125], and separate articles dedicated to some aspects of PZT processing[126-135]. A chart describing the main steps of the mixed oxide route of PZT processing is shown in Fig.4.2.

.

PbO, ZrO$_2$, TiO$_2$, (Fe$_2$O$_3$ or Nb$_2$O$_5$) powders

1 → **Mixing & milling**

2 → **Drying & sieving**

3 → **Calcining 5°C/min, 780°C, 90 min**

4 → **Ball milling**

5 → **Drying & sieving**

6 →

6 → **Powder characterization**

7 → **Cold pressing**

8 → **Sintering 2°C/min, 1180°C, 90 min**

9 → **Bulk ceramic characterization**

10 → **Slicing, polishing, electroding**

→ **Bulk ceramic samples for electric characterization**
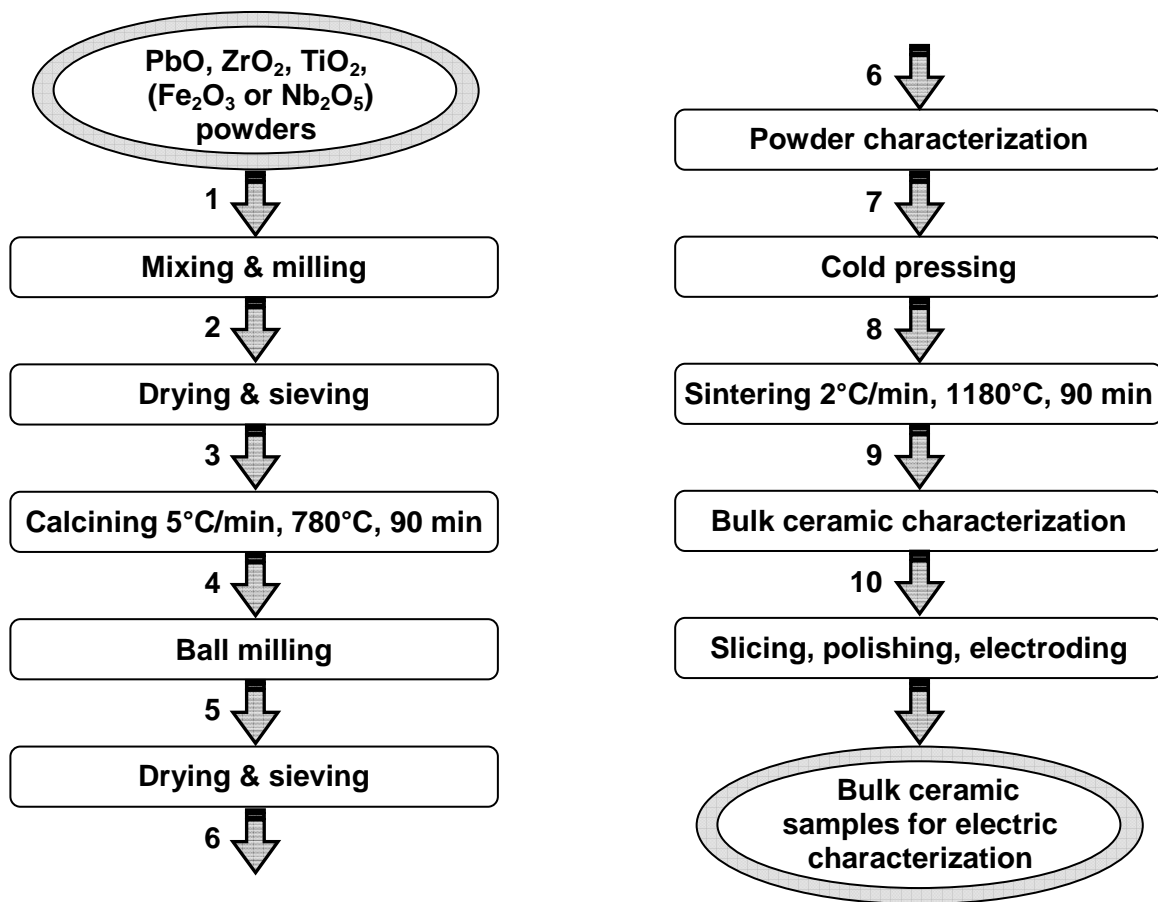
Figure 4.2. Processing for PZT bulk ceramics preparation

The mixed oxide route is the most common technique of PZT preparation. The following procedure has been used in this work. The first step was mixing of oxides powders taken in stoichiometrical proportions followed by ball milling during about 18 hours with yttrium-stabilized zirconia balls in slurry obtained with isopropanol. After milling the powder mixture was dried out and sieved with 100 micron filter in order to avoid too large particle agglomerates. At the next stage, powder was calcined in lead oxide saturated alumina crucibles covered by alumina plates. The second stage of milling and sieving was performed with the calcined powder. The sintering was performed on pellets uniaxially pressed at 40 MPa and packed into covered alumina crucibles whose volume was a little larger than the volume of pellets. The inner space of the crucibles was filled up with the powder of the same composition as the pressed pellet in order to prevent intensive lead oxide evaporation during the thermal treatment. The sintered samples were cut in slices then ground, polished, and electroded with gold or platinum evaporated in a vacuum chamber. The weight loss was monitored at all processing stages. The powder processing weight loss during steps 1 and 2 was **0.2÷0.7 wt.%**, the weight loss during calcinations was **0.34 ± 0.03 wt.%**, or **0.19 ± 0.03 wt.%** excluding the water contained in ZrO_2 powder. Weight loss during sintering was **0.65 ± 0.08 wt.%**. The density of bulk ceramics $Pb(Zr_{0.5}Ti_{0.5})O_3$ doped with Fe (up to 2 at.%) and Nb (up to 3 at.%) was within the interval **7.79...7.98 (± 0.08) g/cm^3**.

The processing parameters are variable with respect to the initial state of precursors and final density and porosity of the bulk ceramic. The preliminary study of pressed oxides mixture (so-called "green-body") behaviour during heating was performed in order to determine the temperatures of calcination and sintering (Fig.4.3). The sample extension during synthesis due to chemical interactions between the components has two steps most likely corresponding to two temperatures of chemical reaction activation: first, between PbO and TiO_2 up to 700 ºC, than, activation of the reaction with ZrO_2. The dilatation process was completed at 800 ºC, and was followed by the densification process occurring up to 1180 ºC (Fig.4.3,b). Similar results are reported in [126].

a)

b)
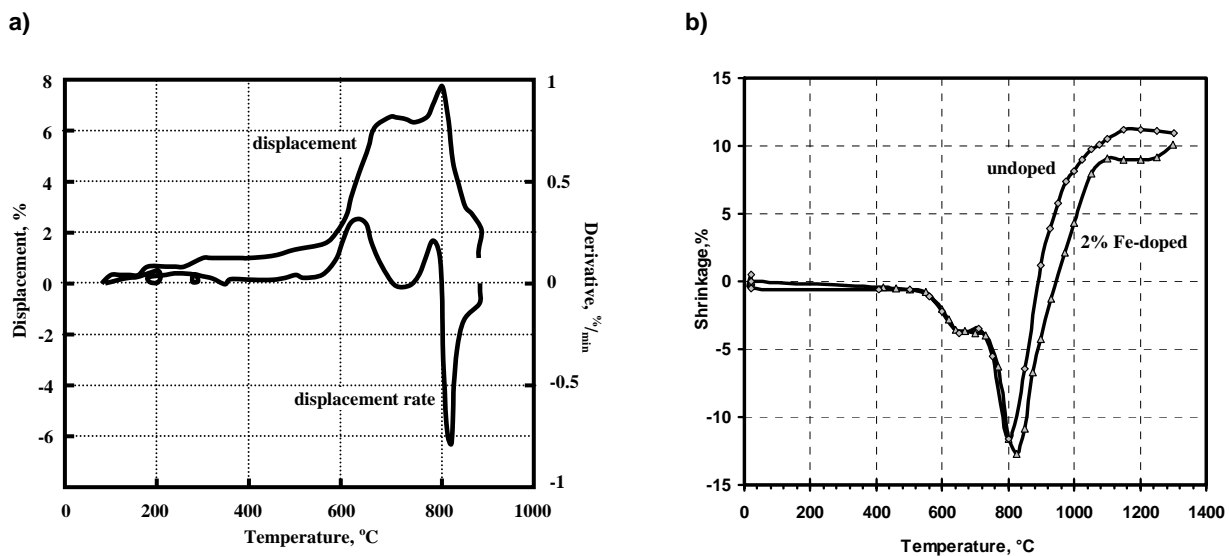
Figure 4.3. *Extension/shrinkage of green body sample during heating measured with different techniques and on different powders: (a) dilatometry of $Pb(Zr_{0.5}Ti_{0.5})O_3$ synthesis; (b) extension during heating of $Pb(Zr_{0.5}Ti_{0.5})O_3$ and $Pb(Zr_{0.5}Ti_{0.5})_{0.98}Fe_{0.02}O_3$ samples observed using optical microscope.*

4.3.**Material characterization and processing control**

The control of processing parameters and quality of material is important at each stage of processing. Initial powders of the main components were subjected to termogravimetry analysis (Fig.4.4) in order to determine igniting losses predominantly due to evaporation of water present in the form of intercrystalline or surface absorbed molecules or hydroxogroups. The weight of lead oxide increased during heating as a result of its oxidation at higher temperature. The experiment in nitrogen atmosphere did not demonstrate any significant weight loss during the heating. Titanium oxide demonstrated almost negligible weight loss during heating. Only zirconium oxide (fine-grade powder "TZ-0", TOSOH) demonstrated noticeable weight loss during heating (about 0.75 wt.%, at 900 ºC, manufacturer data is 1.2 wt. % at 1000 ºC). The igniting loss of zirconium dioxide is taken into account for the stoichiometry and weight control.

Particle size distribution after ball milling was characterized using granulometer or by visual control using scanning electron microscope (SEM). Some examples are shown in Fig.4.5.
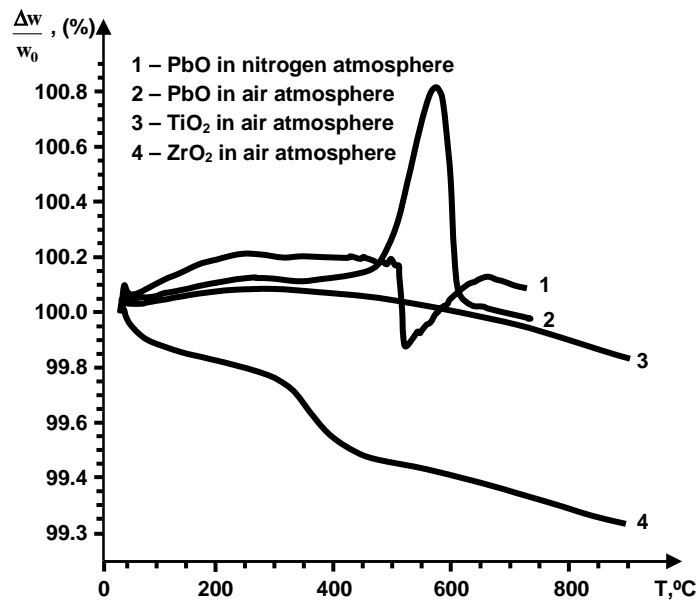
Figure 4.4. *Termogravimetry of initial precursors. Igniting weight loss versus temperature*

a)

b)
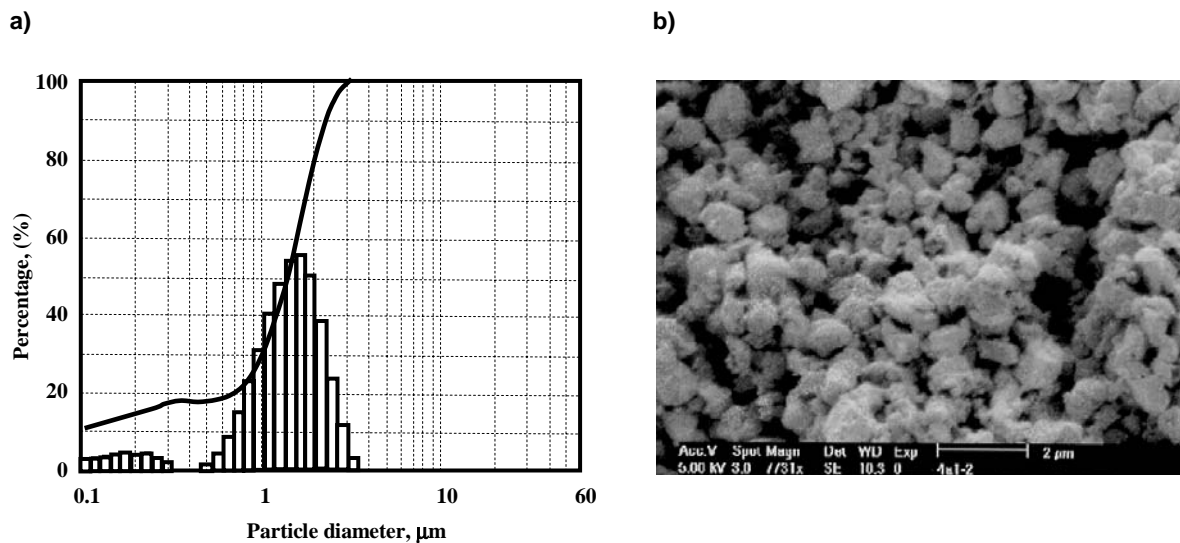
Fig.4.5. *Two methods of particle size distribution control: (a) using granulometer (calcined and milled $Pb(Ti_{0.5}Zr_{0.5})_{0.998}Fe_{0.002}O_3$); and (b) by scanning electron microscopy (calcined and milled $Pb(Ti_{0.5}Zr_{0.5})O_3$)*

The solid state reaction does not complete entirely during calcination. As seen from X-Ray diffraction patterns shown in Fig.4.6, the peaks of both rhombohedral and tetragonal compositions are presented on X-Ray diffraction patterns of calcined powders but not of sintered ceramics. An additional homogenization of calcined powder and thermal treatment

during sintering has stabilized the fluctuation of composition in ceramics. X-ray diffraction patterns of sintered bulk ceramics are shown in Fig.4.7.

The homogeneity of the ceramic compositions has not been specially investigated. The substitution of Fe and Nb into the lead zirconate titanate solid solution in the 6-coordinated site in the perovskite structure is presumed based on the fairly small difference between the ionic radii of the substituent ions (Fe^{3+} and Nb^{5+}) and those of Ti^{4+} and Zr^{4+}. The qualitative reproducibility of ceramics' properties and their regularities, with respect to the type and concentration of dopants, were used as the main criteria of ceramics quality. The exact mechanism of ceramic hardening/softening may depend on the type of dopants incorporation within the ceramic (bulk, surface or interface) [79]. For this reason, the qualitative studies of the hardening-softening transitions were performed in this thesis only when a regular and unambigous trend was observed in the polarization response of ceramics as a function of the type and concentration of dopants.
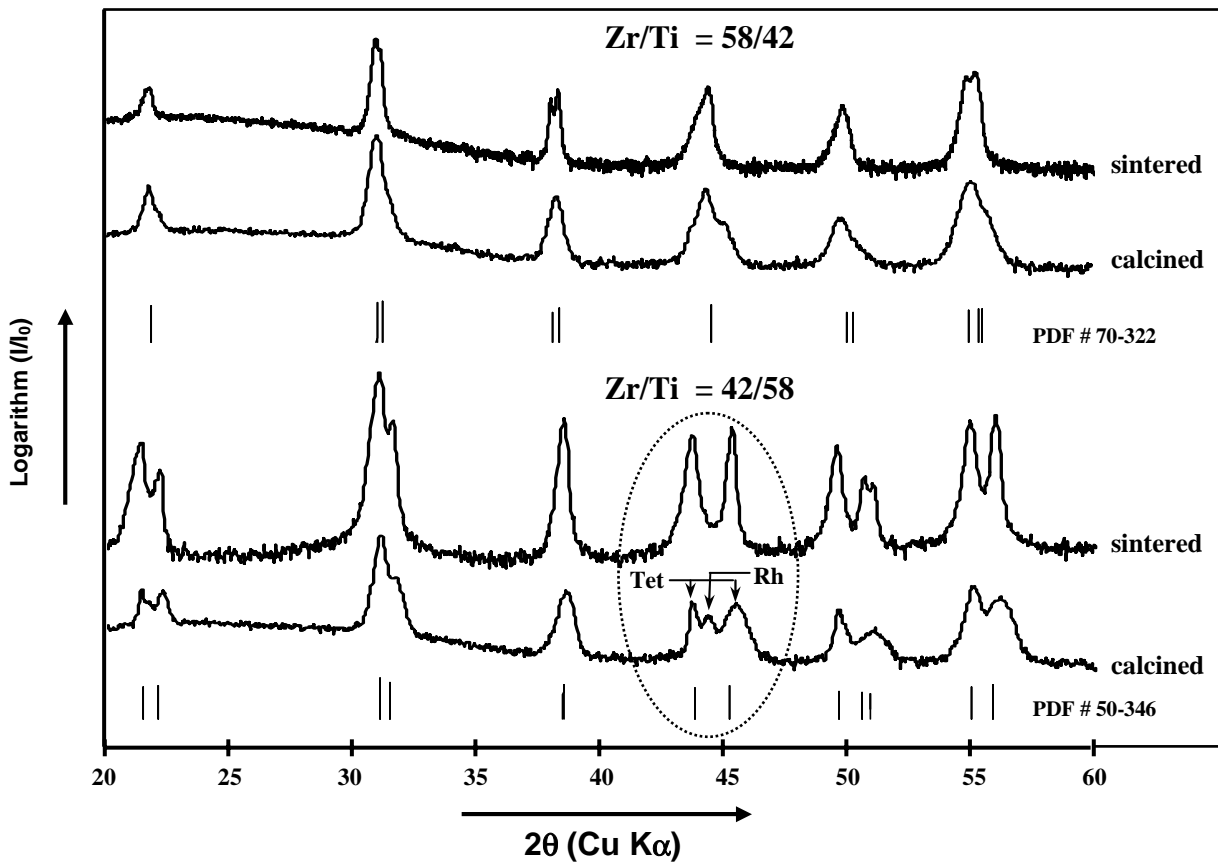
Figure 4.6. *X-Ray diffraction analysis of calcined powders and sintered ceramics of PZT in tetragonal and rhombohedral regions of phase diagram. Bar lines correspond to database diagrams of $Pb(Zr_{0.44}Ti_{0.56})O_3$ (PDF # 50-346) and $Pb(Zr_{0.58}Ti_{0.42})O_3$ (PDF # 73-2022).*
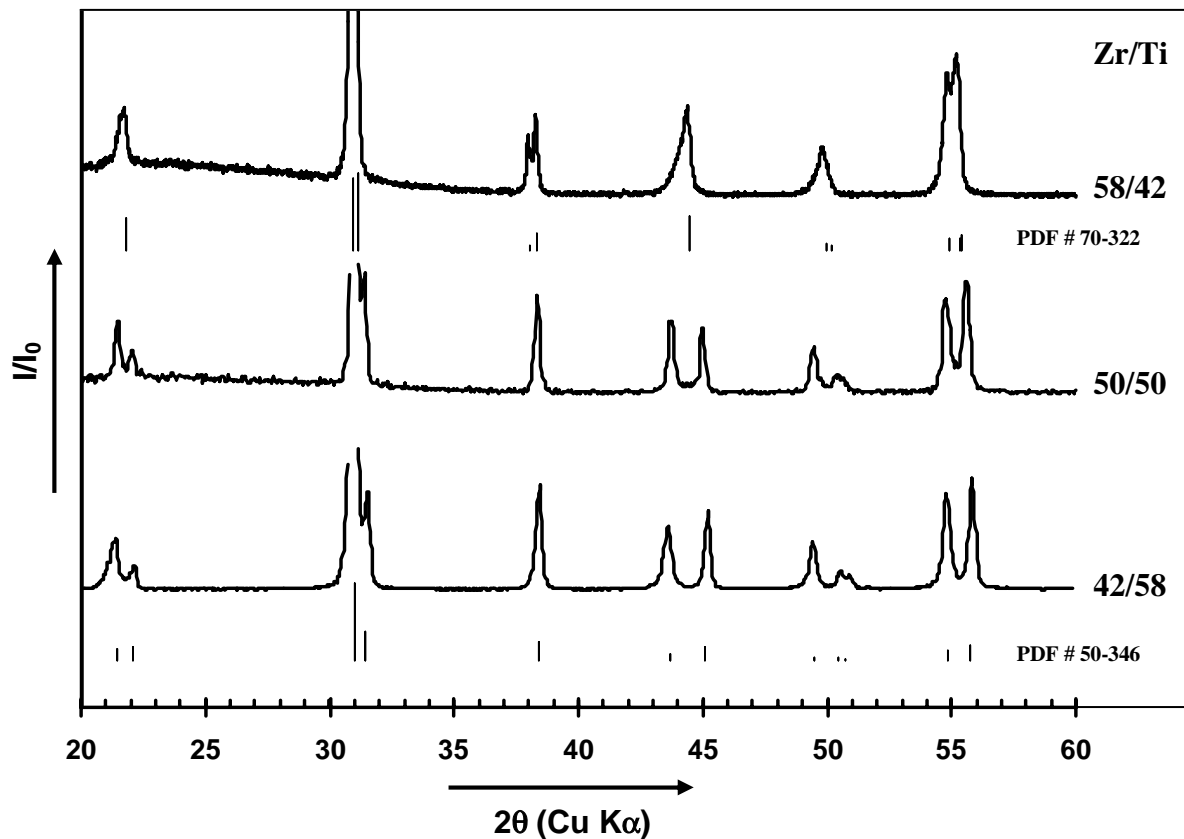
Figure 4.7. *X-Ray diffraction analysis of sintered ceramics PbZr$_x$Ti$_{1-z}$O$_3$ in tetragonal, MPB, and rhombohedral regions of phase diagram. Bar lines correspond to database diagrams of Pb(Zr$_{0.44}$Ti$_{0.56}$)O$_3$ (PDF # 50-346) and Pb(Zr$_{0.58}$Ti$_{0.42}$)O$_3$ (PDF # 73-2022).*

4.4. Characterization of basic properties of bulk PZT ceramics

4.4.1. Ceramic microstructure

The microstructure of sintered ceramics was characterized by SEM (Fig.4.8.). There is no second phase observable on microphotographs of ceramic surfaces and porosity is small. Typical for ferroelectric ceramics, "watermarks" are observable due to the presence of 180° domains; on some microphotographs the 90° domain walls are also observable. Dopants have a profound effect on the grain size of the ceramics. The average grain size decreases by an order of magnitude when the material is doped with 2 at.% of either niobium or iron. Grains are also observable through the optical microscope. A complementary analysis of the ceramic surfaces with the optical microscope has shown, that adding of

0.1 at.% of Fe dopant decreases the grain size of $Pb(Zr_{0.58}Ti_{0.42})O_3$ ceramics 2-3 times greater than the addition of 0.2 at.% of Nb dopant does. This indicates that low concentration of iron has a stronger effect on the grain size than niobium.
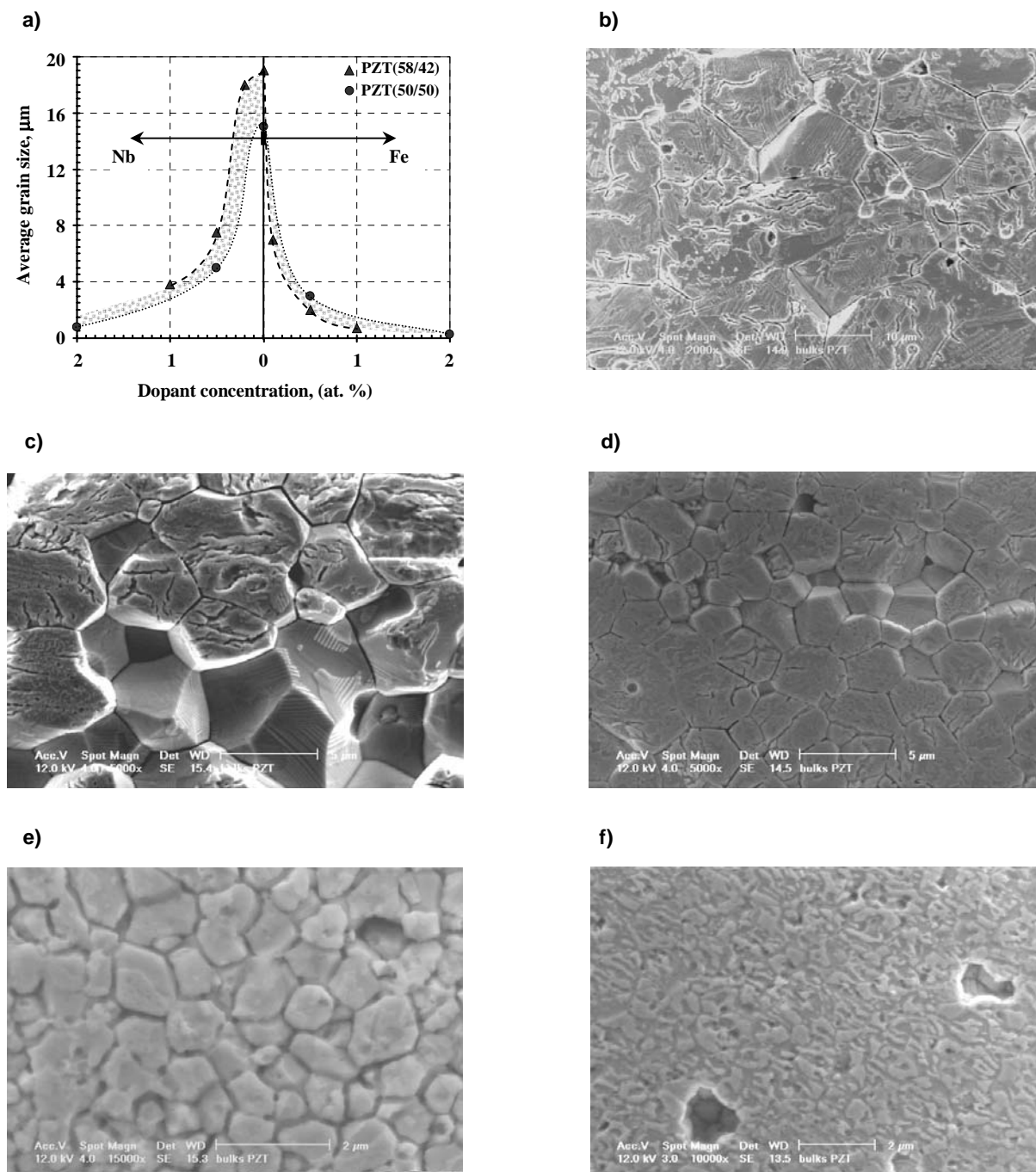
Figure 4.8. *Scanning electron microscopy of bulk ceramics. (a) average grain size dependence on the type and concentration of dopants; (b-f) microphotographs of etched ceramic surface: (b) $Pb(Zr_{0.5}Ti_{0.5})O_3$; (c) $Pb(Zr_{0.5}Ti_{0.5})_{0.995}Nb_{0.005}O_3$; (d) $Pb(Zr_{0.5}Ti_{0.5})_{0.995}Fe_{0.005}O_3$; (e) $Pb(Zr_{0.5}Ti_{0.5})_{0.98}Nb_{0.02}O_3$; (f) $Pb(Zr_{0.5}Ti_{0.5})_{0.98}Fe_{0.02}O_3$.*

4.4.2. Positron lifetime study[6]

Detection of positron annihilation lifetime and intensity in a solid is a tool to study the properties of open-volume and substitutional defect centres that trap positrons and effect its lifetime until annihilation with an electron from the bulk. In the past, the method of positron lifetime study has been extensively used to investigate defects in metals, semiconductors, and polymers. Recently, the application of this method has been adopted also for bulk forms of metal oxides with the perovskite structure, as well as for thin films of these materials. The study of bulk PZT ceramics by positron lifetime study here is an attempt to adopt this recent and developing method to the analysis of defects in modified PZT ceramics and thus to use it as additional means for materials characterization.

The positron wavefunction is more intense in the interstitial regions, away from the positive atomic cores. Positron annihilation from perfect solids is characterized by a single decay constant and hence the mean lifetime is a material parameter which is called the bulk lifetime. The missing atom core associated with vacancy defects results in a potential well for the positron. In insulators, the local charge of defects must also be considered, if the vacancy is positively charged the positron may be repelled by the Coulomb interaction before it can be trapped; neutral or negative vacancy defects are positron traps. The electron density is lower at the vacancy site so the trapped positron lives longer than the normal bulk lifetime for the material. Theoretical values for some perovskites are calculated in [136] and given in Table 4.1.

Table 4.1. *Theoretical positron lifetimes (ps) for some perovskites ABO_3. From Ref. [136]*

Material	Bulk	V_A	V_B	V_O	V_AV_O	$2V_O$	$3V_O$	V_BV_O	$V_BV_OV_O$
$PbTiO_3$	147	280	175	152	284				252
$BaTiO_3$	152	293	204	162					
$LaCoO_3$	129	275	173	145	280	160	170	202	

---

[6] The positron annihilation analysis has been provided by S.Singh and D.J.Keeble, University of Dundee, Scotland, UK.

These calculations do not take into account valence electrons correctly and do not predict trapping rates. The simplest form of the trapping model describes the spectrum predicted when a single positron trap is introduced into an otherwise perfect material [137]. Two lifetime components result. The first, τ_1, quantifies annihilations from perfect sites; if there are no defects it is equal to the bulk lifetime, τ_b. With defect appearance the trapping is increased, and lifetime τ_1 shortens, $\tau_1 < \tau_b$. The second lifetime, τ_2, is predicted to be fixed and to characterize the defect type, $\tau_1 = \tau_d$. In the limit that each positron implanted becomes trapped the corresponding intensity I_2 reaches **100%** and this is termed saturation trapping. The trapping rate, **K**, characterizing the trapping model, is a product of the specific trapping rate for particular defect type, μ, and the defect concentration, **[c]**. An algebraic interpretation of the trapping model can be expressed as:

$$\mathbf{K} = \mu[\mathbf{c}] = \mathbf{I}_2 \left(\frac{1}{\tau_1} - \frac{1}{\tau_2} \right) = \frac{\mathbf{I}_2}{\mathbf{I}_1} \left(\frac{1}{\tau_b} - \frac{1}{\tau_d} \right) \tag{4.1}$$

$$\frac{1}{\tau_b} = \frac{1 - \mathbf{I}_2}{\tau_1} + \frac{\mathbf{I}_2}{\tau_2} \tag{4.2}$$

The experimental spectrum is complicated by the presence of a finite width instrument resolution function. This can normally be described by superposition of several Gaussian functions, typically one of these functions dominates with >80% intensity. The resolution function can be experimentally determined and deconvolved from lifetime spectra. The positron source material, ^{22}NaCl, is deposited onto a thin support foil, protecting the sample under study and allowing the source to be re-used. A small fraction of positrons annihilate with the salt crystals and also within the source support foil, these source annihilation must be correctly subtracted to allow accurate analysis. The inverse problem is solved either by fitting a model to the spectrum using non-linear least-squares or by a maximum entropy method. The finite experimental resolution function width, the counting statistics, and the inverse problem algorithm limit the ability to resolve lifetime components, commonly $\tau_{n+1} > 1.5\tau_n$.

Four PbZr$_{0.42}$Ti$_{0.58}$O$_3$ ceramics were studied, an undoped pair and pairs doped with 0.1, 0.5 and 1.0 at. % Fe. The undoped samples were subsequently subjected to a vacuum

anneal. The vacuum was better than 1.3x10-6 mbar; the samples were at or above 500° C for 3 hours, out of which the samples were at ~750° C for 1 hour.

The positron lifetime spectra after source correction were found to give a broader distribution of acceptable fits than is normally found. In consequence a large number of spectra were recorded using several types of positron source and the statistical distribution of fits analysed. To aid the process, directly deposited positron sources were made on the undoped and the 1.0% Fe doped PZT samples, these spectra have only a single source correction term that is straightforwardly obtained. The majority of the lowest "χ^2" fits were two-component fits, the low variance three component fits had two main components in agreement with the two-component fits and a third 0.1% long lifetime component supporting the validity of the two term fits. The results are shown in Figure 4.9. The second lifetime component was found to be in the 280-290 ps range which is much closer to theoretical calculations for the A-site vacancy or its associate with an oxygen vacancy shown in Table 4.1.
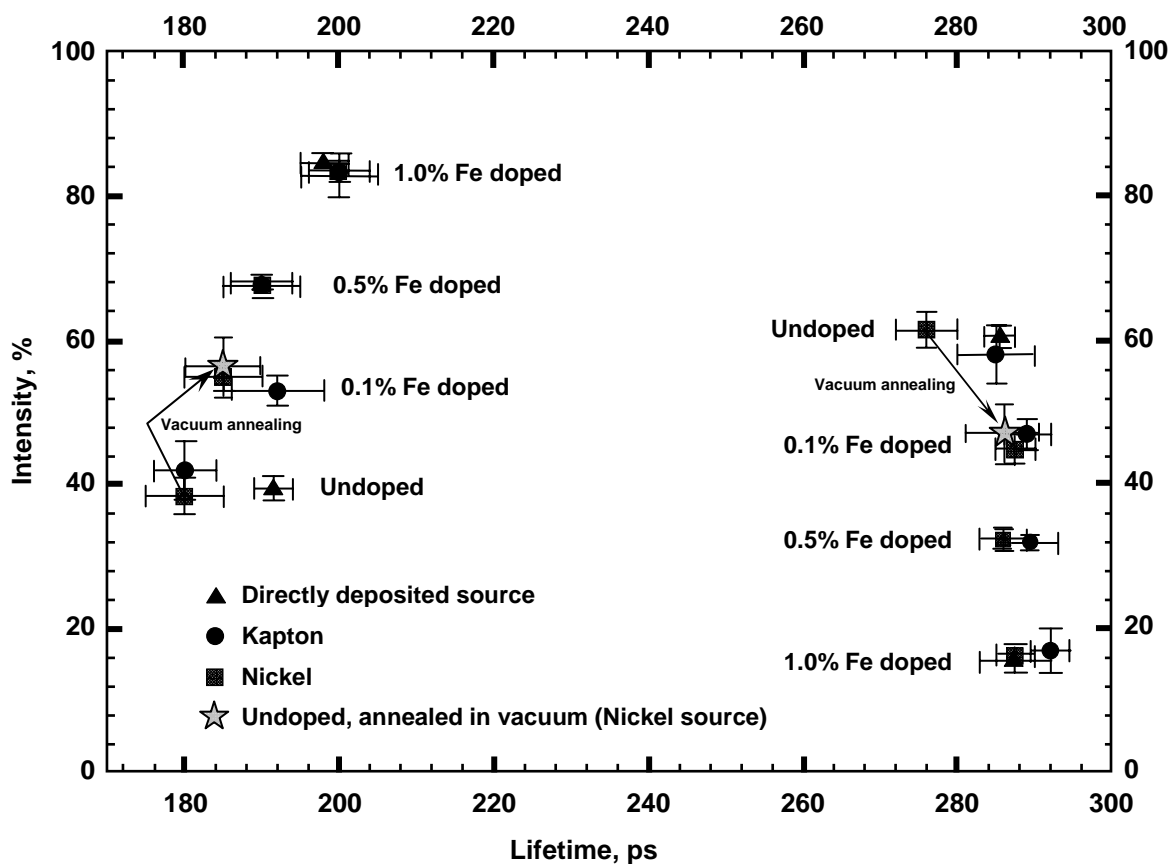

Figure 4.9. *Positron lifetime results for undoped and iron doped Pb(Zr$_{0.42}$Ti$_{0.58}$)O$_3$ ceramics*

The first lifetime component was found to be in the range 180-200 ps, this lifetime is too long to include positron annihilations from perfect lattice. The use of the trapping model gives a calculated bulk lifetime some 100 ps longer than the theoretical value for perovskite oxides. This first lifetime component is either a single defect lifetime or an average resulting from two or more defect states. The 180-200 ps value is in the range calculated for the B-site vacancy. All the samples studied showed saturation trapping, all implanted positrons annihilate from vacancy defect sites.

For saturation trapping the lifetimes observed are either defect lifetimes or average values obtained from two or more unresolved defect states. The intensity of the component is determined by competition between the $\mu \cdot [c]$ products for the defects detected. Considering the results shown in Fig.4.9, the simplest interpretation considers the two lifetime values as characteristic defect lifetimes. A clear trend is observed; with increasing [Fe], there is a decrease in the intensity of the second lifetime at the expense of the first component. Two limiting cases can be readily identified: (1) the concentration and/or defect specific trapping rate for the 280 ps defect reduces with increasing [Fe], or (2) the concentration and/or defect specific trapping rate increases for the 180 ps component with increasing [Fe].

The assignment of the well separated 280–290 ps component to A-site vacancies and/or $V_A V_O$ complex defects is fully consistent with theory and previous single crystal $PbTiO_3$ results. From Table 4.1 it can be seen that in the region ~150–200 ps in addition to the isolated V_B and V_O defects, there are a series of possible vacancy complex defects involving V_O. These states can not be resolved with the current instrument resolution width. Reviewing again the cases outlined above, case (1) would require that increasing [Fe] decreases [V_{Pb}], case (2) would require increasing [Fe] increases the concentration of the defects with lifetime components in ~150–200 ps region. Case (1) is in a reasonable agreement with defect chemistry principles. Indeed, it is expected that an increase of [Fe^{3+}] substituting for B^{4+} ions should increase [V_O], and decrease [V_{Pb}]. The lifetime τ_1 shift towards τ_2 can be interpreted as a result of increase of the total amount of defects which are interfering and contributing into longer life for the trapped positrons in bulk thus affecting τ_1. Another effect is the formation of defect complexes, whose positron lifetimes are expected to be longer than those at individual defects as discussed in [137]. These

complexes may be charge-neutral combinations of anion-cation vacancies, or clusters of oxygen vacancies.

The undoped samples were subjected to a vacuum anneal at temperatures up to ~750 °C. The preliminary positron lifetime results seem to be similar to those obtained from the 0.1% Fe doped samples (Fig.4.9). The intensity of the first lifetime component increases, which is consistent with the increase in trapping to vacancy defects with lifetimes in the ~150–200 ps range. Since annealing in vacuum can only increase but not decrease the concentration of any vacancies, it becomes apparent that the similarity in positron annihilation response in annealed undoped and acceptor-doped (with 0.1%Fe) samples strongly indicates that lifetime τ_1 is intimately related to the oxygen vacancy concentration. In a positron lifetime study on donor-doped PZT ceramics [138], the detected lifetime τ_1 of about 150 ps is attributed to single oxygen vacancies. The existence of a positron bound state at positively charged vacancies is predicted in [139]. The trapping rate of such states is strongly reduced due to the potential barrier surrounding the positive vacancy. Even though the trapping rate for positively charged vacancies is much lower than in the case of neutral or negatively charged defects, trapping could be possible if the defect concentration is extremely high [140].

In conclusion, the positron annihilation study was tested on $Pb(Zr_{0.42}Ti_{0.58})_{1-x}Fe_xO_3$ (x = 0, 0.1, 0.5, 1.0) ceramics. The spectra of all studied samples are best fitted with two lifetime components, one in the region 180–200 ps, the second in the region 280–290 ps. Saturation trapping was observed for all samples, all positrons annihilate from vacancy defect states. Increasing the concentration of Fe doping was found to increase the intensity of the first lifetime component. A vacuum annealing experiment on the undoped sample also caused an increase in the intensity of positron trapping to the first lifetime component. These results are consistent with a competition between positron trapping to A-site vacancies on the one hand, and several possible defect states related to oxygen or B-site vacancies and defect associates, on the other hand. The predominant formation of oxygen vacancies with iron doping and vacuum annealing is anticipated while formation of B-site vacancies is rather improbable.

4.4.3. Dielectric permittivity and losses

Characterization of the dielectric permittivity dependence upon temperature is the most common tool to observe phase transition in ferroelectric system. The measurements performed at various frequencies and characterization of the dielectric losses gives some additional information on the dielectric properties of the material.

The dielectric measurements were performed using the LCR meter (HP 4284A) connected to the electroded sample with platinum probes. Samples were heated in a mini-furnace with heating rate 4 ºC/min; the temperature was controlled by a thermocouple contacting the sapphire sample holder near where the sample was situated.

Figure 4.10. *Temperature dependences of dielectric permittivity (top) and losses in log-linear scales (bottom) for PZT ceramics doped with 0.5 at.% Fe in rhombohedral, MPB, and tetragonal regions (from left to right). Curves from up to down correspond to increase of frequency.*

Three composition of hard PZT (doped with 0.5 at.% Fe) in rhombohedral, MPB, and tetragonal regions have been characterized with the described dielectric measurements. The results are shown in Fig.4.10. The losses at higher temperatures are extremely high and are evidence of high conductivity and related dielectric dispersion that has well pronounced frequency dependence. However, the dielectric response is strong enough to observe the ferroelectric phase transition. Curie-Weiss behaviour is observable at higher frequencies. The conductivity dominates the relatively high dielectric response at lower frequencies, so the measurements performed at lower frequency are not precise enough to determine the dielectric part of the response, which results in very high apparent values of the dielectric permittivity. This effect becomes more pronounced if composition changes from rhombohedral to tetragonal via MPB. If this effect is attributed to oxygen vacancy diffusion, it is probable that the related diffusion coefficient is higher for tetragonal compositions.

Comparison of the dielectric permittivity and loss thermal behaviours for hard and soft samples (Fig.4.11) reveals the absence of the frequency dispersion in dielectric response in soft PZT. It gives further support to the assumption that oxygen vacancies contribute to the conductivity, as their concentration is reduced in donor-doped ceramics.
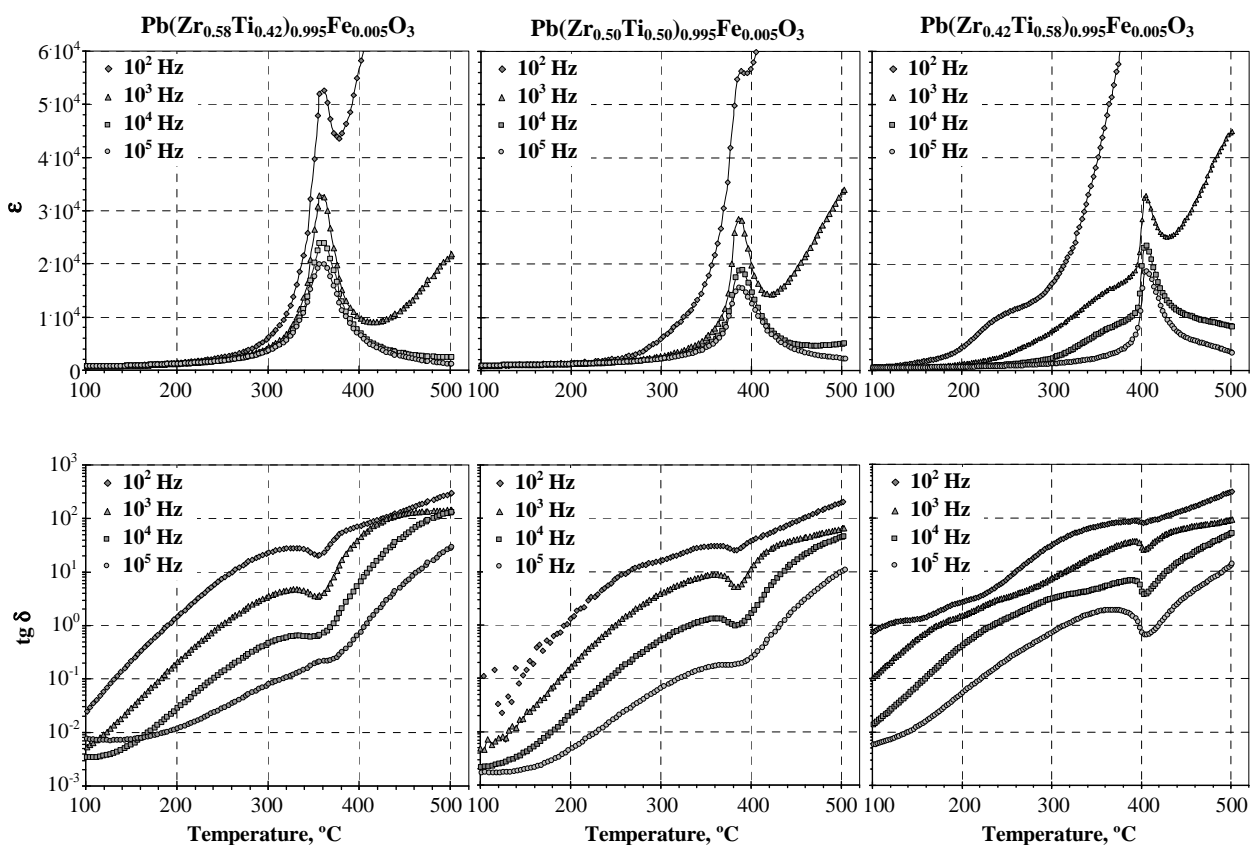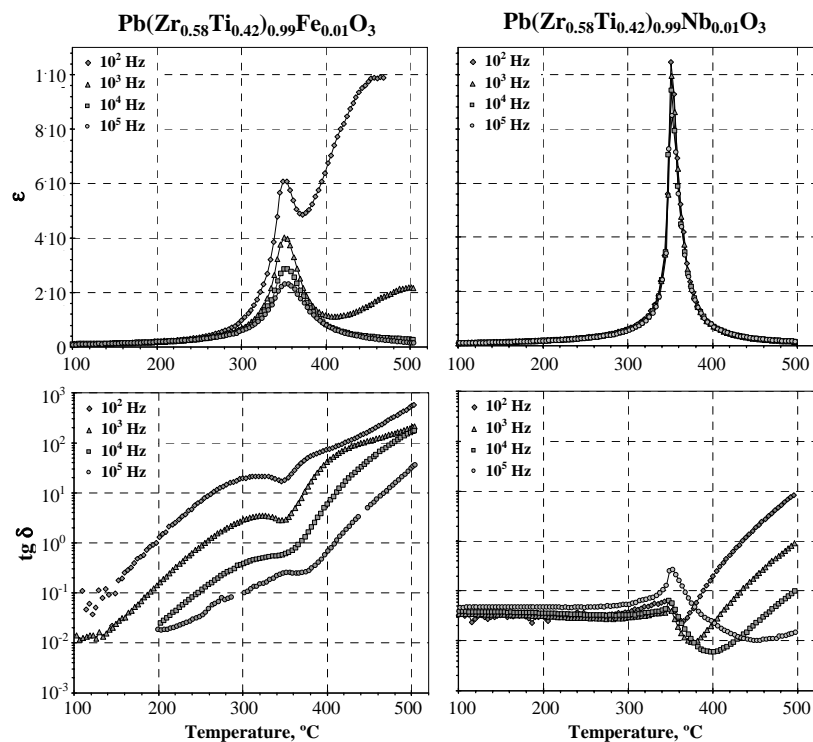

Figure 4.11. *Temperature dependences of dielectric permittivity (top) and losses in log-linear scales (bottom) for rhombohedral PZT ceramics doped with 1.0 at.% Fe (left) and 1.0 at.% Nb (right). Curves from up to down correspond to increase of frequency.*

4.5.Summary

The highest electromechanical properties of PZT ceramics occur near the morphotropic phase boundary (MPB). However, for better reproducibility of material properties, it is desirable to obtain ceramics with composition slightly distant from the MPB region so that the properties are less dependent on fluctuation of the Zr/Ti ratio, and therefore, would vary less from sample to sample. For the property characterization and reproducibility tests, three basic compositions covering the rhombohedral (58/42), MPB (50/50), and tetragonal (42/58) regions of phase diagram have been chosen. The analysis of a large amount of experimental data (not all are presented) has revealed that among the three mentioned compositions, the best reproducibility is observed in PZT (58/42). The majority of the results presented in the following are obtained on samples of PZT (58/42) ceramics doped with iron or niobium up to 1 at.%.

In the literature, there are many sources dealing directly or indirectly with processing of PZT ceramics and offering ifferent ways of sample preparation by the mixed oxide processing route. It indicates that there is no established procedure with known parameters of synthesis, which could be easily used for sample preparation. The tailored processing route is adapted to the laboratory facilities and states of initial oxide precursors.

The solid state chemical reaction between components passes in two steps; the major part of the reaction between oxide components occurs at the calcination step, but complete homogeneity is achieved only at the sintering stage.

Analysis of the ceramic microstructure revealed that doping, especially with iron, affects the grain size. Both iron and niobium additives lead to dramatic decrease in grain size of bulk ceramics. This aspect should be taken into account for characterization of the properties of the ceramics. The anticorrelations between grain sizes and properties of the hard and soft ceramics would indicate that the grain size effect is a minor factor and can be neglected.

The study of positron annihilation has been performed on $Pb(Zr_{0.42}Ti_{0.58})_{1-x}Fe_xO_3$ (x = 0, 0.1, 0.5, 1.0) ceramics. The analysis of the obtained spectra revealed two lifetime components, one in the region 180–200 ps, the second in the region 280–290 ps. Saturation trapping was observed for all samples, which suggests that all positrons annihilate from vacancy defect states. Increasing the concentration of Fe doping was found to increase the

intensity of the first lifetime component. A vacuum annealing experiment on the undoped sample also caused an increase in the intensity of positron trapping of the first lifetime component. These results are consistent with a competition between positron trapping to A-site vacancies and trapping to defects associated with oxygen vacancies.

Analysis of the temperature dependencies of the dielectric permittivity and losses revealed by hard and soft samples with various compositions and at various frequencies shows that the frequency dispersion of these dielectric parameters becomes stronger when the composition changes from soft to hard, and, for hard ceramics, when the composition changes phase from rhombohedral to tetragonal.

Chapter 5

Characterization of nonlinearity and hysteresis

The main purpose of electrical characterization in this work is to investigate the nonlinear and hysteretic response of the materials. The usage of dielectric spectroscopy methods has an advantage in obtaining details of the nonlinear response. The characterization technique employed for the study is described in this chapter, and the advantages of using dielectric spectroscopy as a characterization tool are demonstrated and discussed. These results will be used in the subsequent chapters to gain understanding of processes in the materials

5.1. Dielectric spectroscopy

In order to study in detail the polarization response to low field signals, the lock-in technique was used as shown in Fig.5.1. The output voltage, gauged by lock-in amplifier (SR 830), was synchronized with the input sinusoidal signal. The input signal was created by the same lock-in amplifier and, if necessary, amplified by wideband power amplifier (Krohn-Hite 7602M). The test sample is represented in the circuit by capacitor C_S. The charge amplifier transforms the measured charge into an output voltage (Fig.5.1,a). This device has a wide range of operating frequencies and amplitudes of input signal. However, its applicability is limited for high operating voltages. For measurements at fixed frequency, the circuit can be simplified in order to avoid use of the charge amplifier (Fig.5.1,b).

a)

C$_S$

**Kistler 5011
charge amplifier**

Q

U$_{in}$

U$_{out}$

**SR 830 lock-in
amplifier**

**Tektronix TDS 430A
oscilloscope**

b)

C$_S$

U$_{in}$

R

U$_{out}$

**SR 830 lock-in
amplifier**
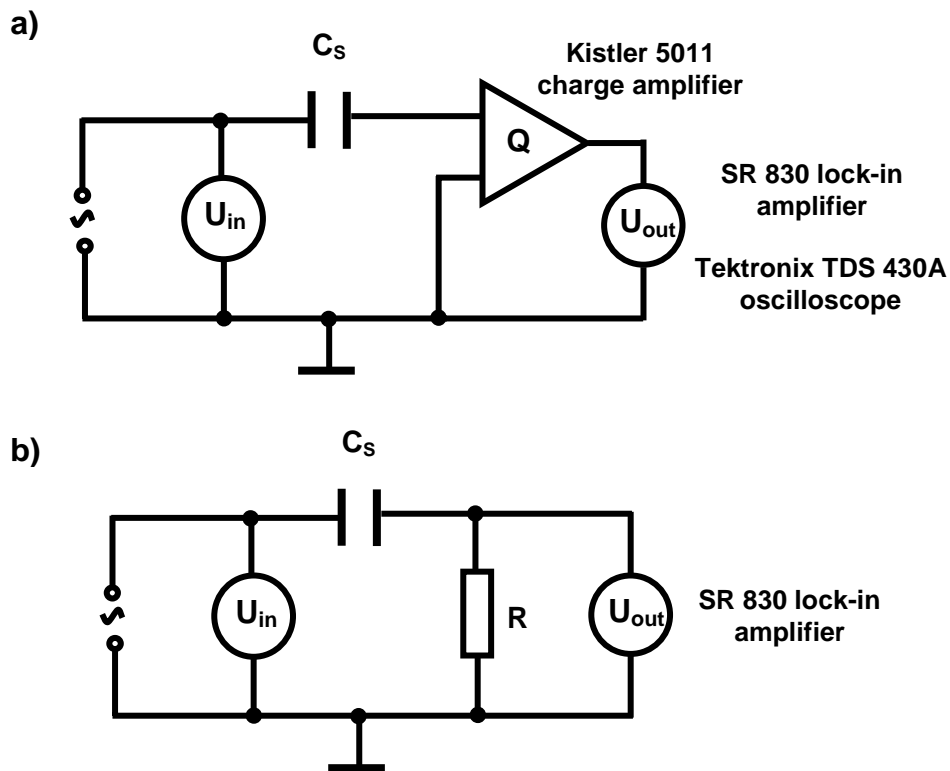
Figure 5.1. *Electrical circuits for measurements of complex amplitudes of polarization.*

The voltage across the resistor is proportional to the current **I(t) = dQ(t)/dt**. The requirement applied to the resistor is to be only a tool to measure the current determined by the voltage dropped across the capacitor. This condition is satisfied if **R << 1/ωC**, where ω is the cyclic frequency of the voltage generator. For accuracy purposes, this requirement should take into account the instrument sensitivity. In this case the resistor should be chosen according to

$$\mathbf{R\omega C} \approx \frac{\mathbf{U_{out}}}{\mathbf{U_{in}}} \leq \mathbf{0.01} \tag{5.1}$$

where the amplitude of **U$_{out}$** should be within the best range of voltage detector sensitivity, and **U$_{in}$** is the amplitude of the driving voltage. Another variable parameter is the sample capacitance, which can be easily regulated by the sample's geometry. Considering the input signal

$$U_{in}(t) = U_0 \sin(\omega t) \tag{5.2}$$

the driving field $E(t)$ is applied to the sample with thickness d:

$$E(t) = E_0 \sin(\omega t) \approx \frac{U_0}{d} \sin(\omega t) \tag{5.3}$$

The measured voltage $U_{out}(t)$ dropped on the resistor is proportional to the current $I(t)$ in the circuit:

$$U_{out}(t) = I(t)R \tag{5.4}$$

The current $I(t)$ is the result of sample polarization. If the polarization response $P(E)$ is described by nonlinear function and is unknown, its Fourier components can be derived from amplitudes and phase angles of the measured current. The Fourier series of polarization response in the general case can be written as:

$$P(t) = P_0 + \sum_{n=1,2,3...} \left(P_n' \sin(n\omega t) + P_n'' \cos(n\omega t) \right) \tag{5.5}$$

Hence, the current can be expressed as:

$$I(t) = \frac{\partial Q(t)}{\partial t} \approx A \frac{\partial P}{\partial t} = \sum_{n=1,2,3...} \left(An\omega P_n' \cos(n\omega t) - An\omega P_n'' \sin(n\omega t) \right) \tag{5.6}$$

The voltage $U_{out}(t)$ is detected by the lock-in amplifier as amplitudes (U_{n_0}) and phase angles (φ_n) of several first harmonics with respect to the phase and frequency of source voltage $U_{in}(t)$, so the detected voltage signal U_{out} is composed as:

$$U_{out}(t) = \sum_{n=1,2,3...}\left(U_{n_0}\sin(n\omega t)\cos\varphi_n + U_{n_0}\cos(n\omega t)\sin\varphi_n\right) \tag{5.7}$$

The current through the circuit is in-phase with the measured voltage across the resistor $U_{out}(t)$, and scaled as $I(t) \approx U_{out}(t)/R$ if requirement (5.1) is satisfied. Accordingly (5.6), the experimentally measured current resulting from sample polarization can be expressed as:

$$I(t) = \sum_{n=1,2,3...}\left(I'_n\sin(n\omega t) + I''_n\cos(n\omega t)\right)$$

$$\tag{5.8}$$

$$I'_n = \frac{U_{n_0}}{R}\cos\varphi_n, \quad I''_n = \frac{U_{n_0}}{R}\sin\varphi_n$$

Comparing (5.6) and (5.8) the Fourier components of polarization response (the complex amplitudes) can be expressed through experimentally measured voltage amplitudes (U_{n_0}) and phase angles (φ_n):

$$P'_n = \frac{I''_n}{An\omega} = \frac{U_{n_0}}{An\omega R}\sin\varphi_n$$

$$\tag{5.9}$$

$$P''_n = \frac{-I'_n}{An\omega} = \frac{-U_{n_0}}{An\omega R}\cos\varphi_n$$

The primed components are used to designate the in-phase amplitudes with respect to the phase of the source signal, and double-primed components designate the out-phase amplitudes with 90º phase advance. These parameters are used to characterize the ac-signal on complex plane, where the real part of the complex amplitude is in-phase with respect to the reference driving signal, and the imaginary part is out-phase. Alternatively, one may use the absolute amplitude of the signal and its phase angle whose cosine and sine determine correspondingly the in-phase and out-phase amplitudes of ac-signal. Thus, any response to the periodic signal can be represented as a combination of in-phase and out-phase response. It is seen from (5.9) that amplitudes of polarization and current are differed in phase for a quarter of period.

5.2. Some features of polarization response to periodic electric field signal

The representation of an ac-signal through harmonic amplitudes and phase angles is convenient for the monitoring of nonlinear systems.

Firstly, the harmonic analysis using the discrete Fourier transform permits the separate study of various contributions to nonlinearity. If the apparent nonlinearity of material response is the result of several contributions differently depending on time (e.g. additional nonlinearity possibly imposed by aging), the harmonic analysis may be very helpful in studying such phenomena manifesting themselves in the frequency domain [141-143]. According to the principles of Fourier transformation, any existing waveform can be decomposed into an equivalent series of sine waves (with possible phase shift) and a dc component; the representations of this waveform in time domain and in frequency domain will contain the exact same information but in different form [142,143].

Secondly, there is an advantagein directly obtaining the information on hysteretic behaviour of a system by monitoring separately the in-phase and out-phase components of the nonlinear polarization response. The anhysteretic part of the symmetrical response of the material to the sine signal would result in in-phase response of polarization with respect to the driving field. However, due to dielectric losses, the conductivity of the sample, and inductive wires in the circuit, a phase lag is usually observed. The phase lag caused by various processes manifests itself in the out-phase component of material response.

It is convenient for the following analysis to define a periodic signal by a trigonometric function, for example, sine:

$$\mathbf{E=E_0\sin(\omega t)} \tag{5.10}$$

Thus, the perfectly symmetrical response of s material, when $\mathbf{P(E) = -P(-E)}$, implies so-called half-wave symmetry:

$$\mathbf{P(\omega t) = -P(\omega t+\pi)} \tag{5.11}$$

Half-wave symmetry of polarization response is provided in unpoled and non-textured ceramics by the random orientation of grains. In this case, the amplitudes of all even harmonics are equal to zero [144]. The polarization response, hence, can be expressed as:

$$
\begin{aligned}
P(t) = &P_1' \sin(\omega t) + P_1'' \cos(\omega t) + P_3' \sin(3\omega t) + P_3'' \cos(3\omega t) + \\
&+ P_5' \sin(5\omega t) + P_5'' \cos(5\omega t) + P_7' \sin(7\omega t) + P_7'' \cos(7\omega t) + ...
\end{aligned}
$$

(5.12)

The running value of electric field $\mathbf{E}$ reaches the extrema $\pm\mathbf{E_0}$ when $\boldsymbol{\omega t} = \pm\boldsymbol{\pi/2}$, and crosses zero when $\boldsymbol{\omega t} = \pm\boldsymbol{\pi}$. Hence, the running value of polarization response each quarter period is determined by either only in-phase or only out-phase components:

$$
\begin{aligned}
\omega t &= \frac{\pi}{2} + 2\pi n: \quad P = +P_1' - P_3' + P_5' - P_7' + ... \\
\omega t &= \pi + 2\pi n: \quad P = -P_1'' - P_3'' - P_5'' - P_7'' + ... \\
\omega t &= \frac{3\pi}{2} + 2\pi n: \quad P = -P_1' + P_3' - P_5' + P_7' + ... \\
\omega t &= 2\pi n: \qquad\quad P = +P_1'' + P_3'' + P_5'' + P_7'' + ...
\end{aligned}
$$

(5.13)

Thus, the in-phase and out-phase amplitudes contain information on the hysteresis loop geometry as shown in Fig.5.2.

Two limiting cases of polarization response can be considered as references: (1) response due to domain wall motion in a random potential energy profile described by Rayleigh relations (2.7) – (2.10); and (2) response due to domain wall motion in regular V-shaped potential described by (2.46).

The development of the Rayleigh formula (2.7) into Fourier series for periodic field signal (5.10) yields

$$
P = (\chi_{init} + \alpha_\chi E_0)E_0 \sin(\omega t) + \sum_{1,3,5,..} \frac{4\alpha_\chi E_0^2 \sin(\frac{\pi n}{2})}{\pi n(n^2 - 4)} \cos(n\omega t)
$$

(5.14)

$$P = +P_1' - P_3' + P_5' - P_7' + \dots \qquad P = -P_1'' - P_3'' - P_5'' - P_7'' - \dots \qquad P = -P_1' + P_3' - P_5' + P_7' + \dots \qquad P = +P_1'' + P_3'' + P_5'' + P_7'' + \dots$$
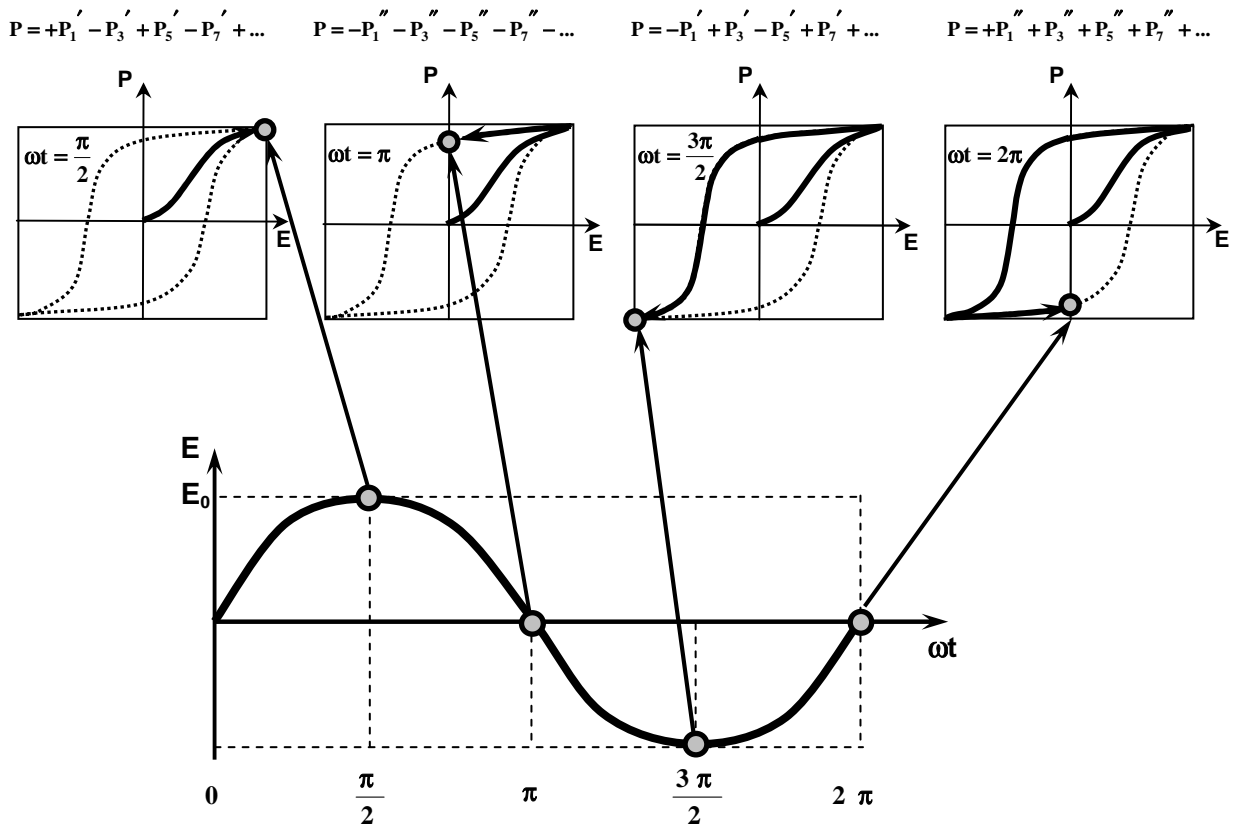
*Figure 5.2. The relations between hysteresis geometry and complex amplitudes of **P(E)** dependence.*

There are several interesting features of equation (5.14) that can be useful for further analysis:

(1) The half-wave symmetry (5.11) holds and only odd-number harmonics have nonzero amplitudes

(2) All higher harmonics are quadratic functions of the field amplitude

(3) All higher harmonics are out-phase with the driving field signal

(4) The ratios of out-phase components are constant ratios of integer numbers.

The third feature implies that the phase angle δ_n of all higher harmonics is ±90°. The phase angle of the polarization response is defined using the following representation of Eq. (5.5):

$$P = \sum_n P_n \sin(n\omega t + \delta_n) \qquad (5.15)$$

where $P_n = \sqrt{(P_n' + P_n'')}$ is the amplitude and $\delta_n = \arctan\left(\dfrac{P_n''}{P_n'}\right)$ is the phase angle of the nth harmonic of the polarization response.

The experimental verification of these features of ideal Rayleigh response to periodic signal allows one to study in detail the applicability of the model based on Rayleigh relations to real ferroelectric ceramics. The reason of such detailed verification approach is that the Eq. (2.7) – (2.10), representing ideal Rayleigh response, may fit experimental data in certain range of driving field amplitudes beyond which the discrepancy between model and experimental hysteresis becomes apparent even with the rough evaluation through direct fitting of Rayleigh relations to the experimental data [14]. The analysis of complex amplitudes of nonlinear response gives higher precision of the real response deviation from ideal Rayleigh model. For example, the Rayleigh-looking hysteresis of piezoelectric response with slight asymmetry described in [32] does not satisfy the requirement of half-wave symmetry (5.11), so the presence of even-number harmonics should be well pronounced [72] and detected with lock-in technique. This discrepancy can, in turn, give additional information on processes occurring in real materials.

Another limiting case of polarization response caused by reversible movement of hardly clamped domain wall yields the linear anhysteretic polarization response to the applied electric field. Spectral analysis of such ideal case would contain only first harmonic with nonzero amplitude and in-phase with the driving field.

Beside these two limiting cases of non-linear hysteretic and linear anhysteretic responses there is the third type of possible idealized response which is nonlinear and anhysteretic. This case corresponds to the nonlinear, reversible, and rate-independent domain wall motion (e.g. in the potential well such as the modified V-potential (Fig.3.2)). In this case the spectral analysis of polarization response has a limited applicability unless the analytical expression of the potential profile is known. Fourier development of polarization-field dependence obtained by solution of Eq. (3.1) and (3.2) gives complex hypergeometric functions for the harmonic amplitudes that can be verified experimentally. Another way is to substitute the unknown form of the potential energy by the equivalent Maclaurin series similar to (2.30) and consider appropriate polynomial expansion of the polarization response

as a function of applied electric field. Such approach was used in [141] to study the polarization response in ageing $Pb(Mg_{1/3}Nb_{2/3})O_3$-based ceramics. However, the relations between polynomial terms and generated harmonics allow only a decrease of the odd harmonic's amplitude with increasing harmonic number, which was not in agreement with the experimental results. The observation made in [141] suggests that if the amplitude of any $(2n+1)^{th}$ harmonic exceeds by magnitude the amplitude of $(2n-1)^{th}$ harmonic, the polynomial expansion of polarization as a function of applied field does not represent a real process adequately.

If the polarization response is symmetrical (5.11) and expanded into series of in-phase and out-phase components (5.12), it is evident from Fig.5.2, that hysteresis is provided by out-phase components $\mathbf{P_n''}$. The same response can be represented as (5.15), in terms of amplitudes $\mathbf{P_n}$ and phase angles $\mathbf{\delta_n}$, If $\mathbf{\delta_n} \quad 0 \pm 180^o$ than the response is hysteretic and remnant polarization is determined as the sum of out-phase components of all harmonics (Eq.(5.13) and Fig.5.2). Contrary, if all odd polarization harmonics are in-phase with driving field the hysteresis does not occur. According to the causality principle, the response always lags behind the signal, so the phase lag $\mathbf{\delta_n}$ is always nonzero, but its magnitude noticeably depends on the polarization process. As a rule, the lag in response due to an extrinsic contribution to polarization is higher than one of intrinsic process. So, usually, the phase lag due to intrinsic processes can be disregarded, at least at not very low fields. In case of extrinsic contribution due to domain wall motions, the phase lag is different for reversible and irreversible process of domain wall movement. The harmonic series of ideal Rayleigh response (5.14) can be analyzed from this point. If one considers a random potential profile with "V-shaped" minima and domain wall motions due to reversible movement within the minima and irreversible jumps between them, then the hysteresis and nonlinearity are both the consequence of irreversible process. The linear term of Rayleigh equation (2.7) is entirely included in the first harmonic of the Fourier expansion form (5.14), hence the nonlinear part is entirely represented by the series of only out-phase components. Any deviation from ideal Rayleigh process which accounts only for extrinsic contribution may imply either nonlinearity of reversible process or lack of randomness that is statistically in the background of Rayleigh relations.

To underline the meaning of in-phase and out-phase components, the polynomial expansions of the polarization response with half-wave symmetry and the corresponding

Fourier development into in-phase and out-phase harmonics will be considered (for sine field signal (5.10)). In the most general case, the ascending and descending branches of a symmetric polarization response can be expressed as follows:

$$P^{\uparrow\downarrow} = \pm a_0 + a_1 E \pm a_2 E^2 + a_3 E^3 \pm a_4 E^4 + ... + a_{2n-1} E^{2n-1} \pm a_{2n} E^{2n}$$

(5.16)

In a particular case of anhysteretic response in a centrosymmetric material, the polarization-field dependence can be expressed by only odd power polynomial:

$$P_{anhyst} = a_1 E + a_3 E^3 + ... + a_{2n-1} E^{2n-1}$$ (5.17)

It is possible to show, that Fourier expansion of anhysteretic response (5.17) contains **(2n-1)** harmonics, where only in-phase components in **n** (odd) harmonics are nonzero. The Fourier expansion of hysteretic response (5.16) contains **n** (odd) in-phase components and infinite number of odd out-of-phase components. The structure of the harmonic series is organized in the way that the in-phase components include only polynomial terms that are not related to hysteresis. This "anhysteretic" terms account for nonlinear reversible process. The out-phase components include only polynomial terms that are related to the difference in ascending and descending branches of the polarization response and hence can be called "hysteretic terms". The irreversible processes are entirely described by them.

The presence of even harmonics in a spectrum may denote asymmetry of response if internal polarization within ceramics is not compensated on average. In the unpoled state, this compensation is provided by spontaneous, random, orientation of polarized items (such as domains and grains), but since the electric field is applied, the compensational equilibrium may be destroyed, so the response will be not symmetrical with respect to the field polarity. For dynamic mode of characterization when driving field changes polarity relatively fast, this effect is usually negligible. If the magnitude of even harmonic is significantly smaller than the magnitude of any higher numbered odd harmonic, they are for simplicity not considered.

5.3.Summary

The use of dielectric spectroscopy in analysis of nonlinear and hysteretic response of materials has the advantages in gaining in depth details of the polarization response. Firstly, as shown in [141-143], if the nonlinearity is a result of several contributions differently depending on time (e.g. additional nonlinearity possibly imposed by aging), than these contributions may reveal themselves noticeably in the frequency domain and can be studied using harmonic analysis of the response. Secondly, the analysis of the reversible and irreversible harmonic components of the polarization response permits distinguishing between nonlinearity and hysteresis. This is because the in-phase and out-phase components of dielectric spectra represent independently the information of reversible and irreversible rate independent processes. As a consequence of this matter, the features of some idealistic models can be established for the harmonics of the response spectrum. Thus, the idealistic Rayleigh model of response assumes nonlinearity and hysteresis of the same origins (rate-independent irreversible movement of the domain walls in a medium of random energy fluctuation); the Fourier analysis of Rayleigh formula demonstrates the number of well defined features of the spectral form of polarization response to the sinusoidal electric field signal. These features can be adequately expressed by the number of nonlinear parameters such as ratios of out-phase amplitudes, phase angles of harmonics, etc. Some of these nonlinear parameters are very sensitive even to small deviations of the behaviour of real materials from the ideal models. However, these deviations may be not noticeable without the use of harmonic analysis.

Chapter 6

Dielectric properties of hard and soft PZT ceramics at subswitching conditions.

The term "switching" designates the reorientation of the remanent polarization by applying external force. Switching conditions are usually achieved by applying higher than coercive field strength to provide the full switching of polarization. The external field with the strength amplitude less than the macroscopic coercive field is considered here as subswitching field. In terms of the polarization mechanism, the subswitching field affects the polarization mostly via the process of domain rearrangements and does not involve large scale reconstruction of domain structure. Some very hard ferroelectric ceramics have negligible remanent polarization due to the constriction of the hysteresis loop and thus, can not be completely switched. However it is possible to distinguish the field range where domain rearrangements predominantly contribute to the polarization response. As the study is focused on the domain wall contribution, this distinction is essential. The term "subswitching conditions" is used in this study to designate the polarization response under fields lower than macroscopic coercive fields of ferroelectric materials. The threshold field range separating subswitching and switching range is approximately 10 kV/cm for soft ceramics and higher for hard ceramics. In the next chapter this transition field range will be more defined. The experimental studies in this chapter are performed under the subswitching field range and aim to investigate the relations between polarization response of hard and soft ceramics and nonlinear parameters of dielectric spectroscopy in order to estimate the applicability limits of idealized models considered in previous chapters and to characterize with nonlinear parameters the intermediate states between these limits.

6.1. **Electric field induced nonlinearity**

As nonlinear dielectric materials, the hard and soft PZT ceramics demonstrate field dependent properties (Fig.6.1). The nonlinearity, which is defined as the nonlinear dependence of material response on the amplitude of the applied force, manifests itself in the driving field amplitude dependence of dielectric permittivity (Fig.6.1,a) and piezoelectric coefficient (Fig.6.1,b). Obviously the nonlinearity increases as the material composition changes from "hard" (acceptor doped) to "soft" (donor doped). These dependences may be interpolated by linear functions relatively well and, thus, satisfy the second part of the Rayleigh relations (2.9)-(2.10). Nevertheless, the applicability of the Rayleigh relations to the material response requires some deeper verification. While Fig.6.1,a shows the permittivity of the response measured at the first harmonic, it is interesting to look at information that can be obtained by analyzing other nonlinear parameters.

The experimentally measured phase angles of the first and third harmonics of polarization response as functions of increasing and decreasing electric field amplitude are shown in Fig.6.1,b,c. The physical meaning of the phase angle, in general, is a delay in response to applied signal, which also results in hysteresis. If the response is nonlinear, the phase lag occurs not only at the first harmonic but at the higher harmonics as well. The polarization response becomes more hysteretic with increasing field amplitude and with the change of the ceramic composition from hard to soft (Fig.6.1,c). The behaviour of materials characterized by measuring the response at the first harmonic (Fig. 6.1,a-c) is regular in the sense that it is well-ordered with respect to the type and concentration of dopants. Meanwhile the behaviour of the phase angle of the third harmonic (δ_3) of polarization is more complex and distributed less adequately with respect to the composition of ceramics (Fig.6.1,d).

To understand this inconsistency in the field amplitude dependence of δ_3 with the ceramics composition, the experimentally obtained characteristics can be evaluated according to the model based on the ideal Rayleigh-type response (2.7) – (2.10) that for the sine signal can be expressed as the Fourier series by Eq. (5.14). As mentioned in section 5.2, all higher harmonics in (5.14) have phase angle **±90°,** and particularly, δ_3 = **-90°**. Since none of the characterized ceramics clearly demonstrated this feature, it can be attributed to the
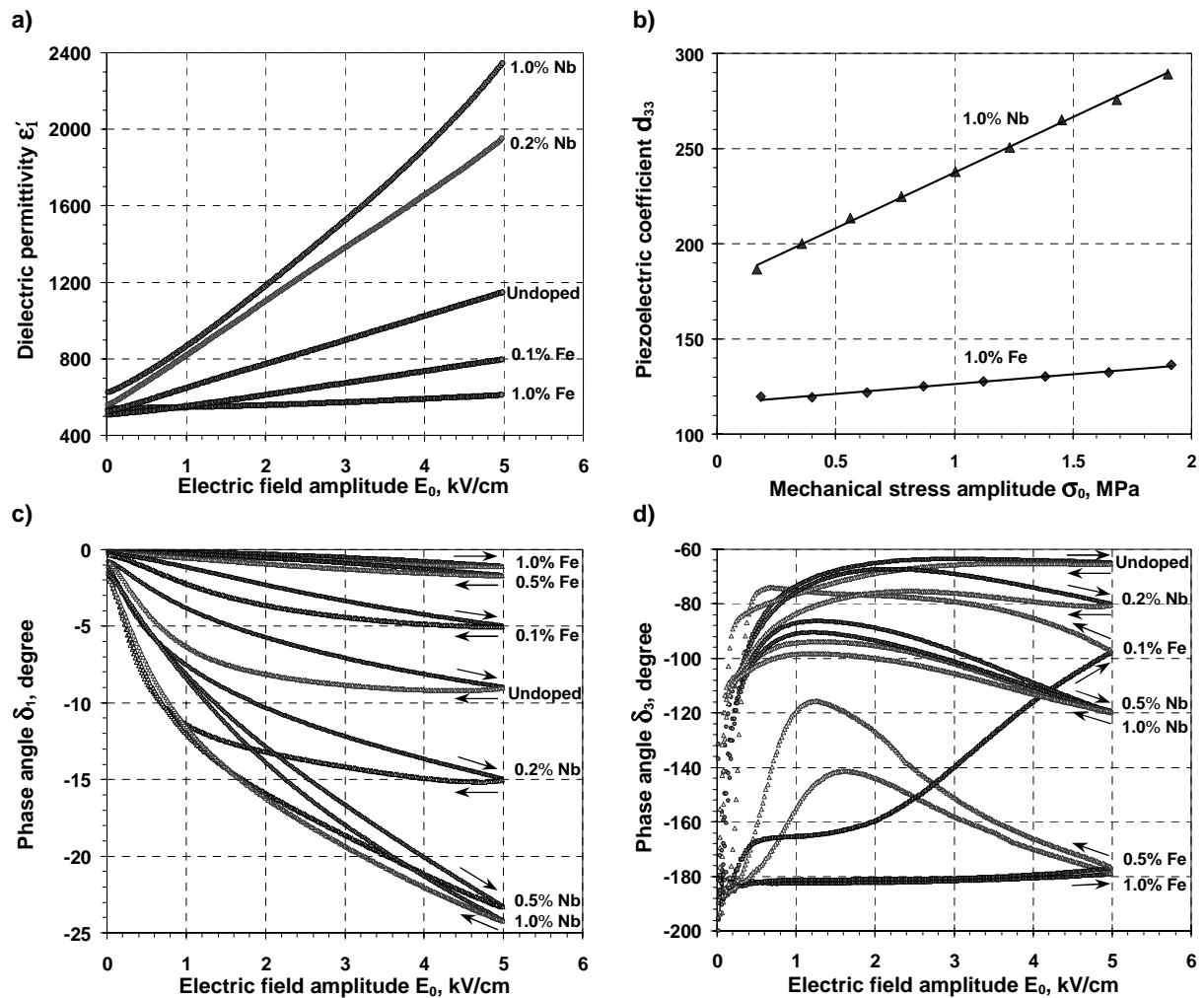
Figure 6.1. *Characterization of soft and hard Pb(Zr₀.₅₈Ti₀.₄₂)O₃ ceramics at subswitching fields. Driving field amplitude dependences of: (a) dielectric permittivity derived from the first harmonic amplitude* $\varepsilon_1' = P_1' / E_0$; *(b) piezoelectric coefficient* d_{33}; *(c) phase angle of the first harmonic of polarization response; (d) phase angle of the third harmonic of polarization response. Dopant concentration is indicated in at.%; arrows indicate the branches corresponding to increasing and decreasing of driving field amplitude.*

deviation from ideal Rayleigh behaviour that is valid only for extrinsic contribution of domain wall movements in a perfectly random energy profile (randomly distributed pinning centres media) and does not account for any intrinsic nonlinear contribution, the presence of conductivity, and many other effects. These deviations also can be found in the response measured at first harmonics. For example, the dependences $\varepsilon_1'(E_0)$ are not perfectly linear

for soft ceramics (Fig.6.1,a). As a result, the Rayleigh coefficients α_ε and α_χ in (2.7) – (2.10) are not constants in the real case. The coefficients used in Rayleigh relations and derived from the experimental data are shown in Fig. 6.2. These plots demonstrate that the material response deviates from ideal Rayleigh model as the softening increases and for higher amplitudes of the applied field.
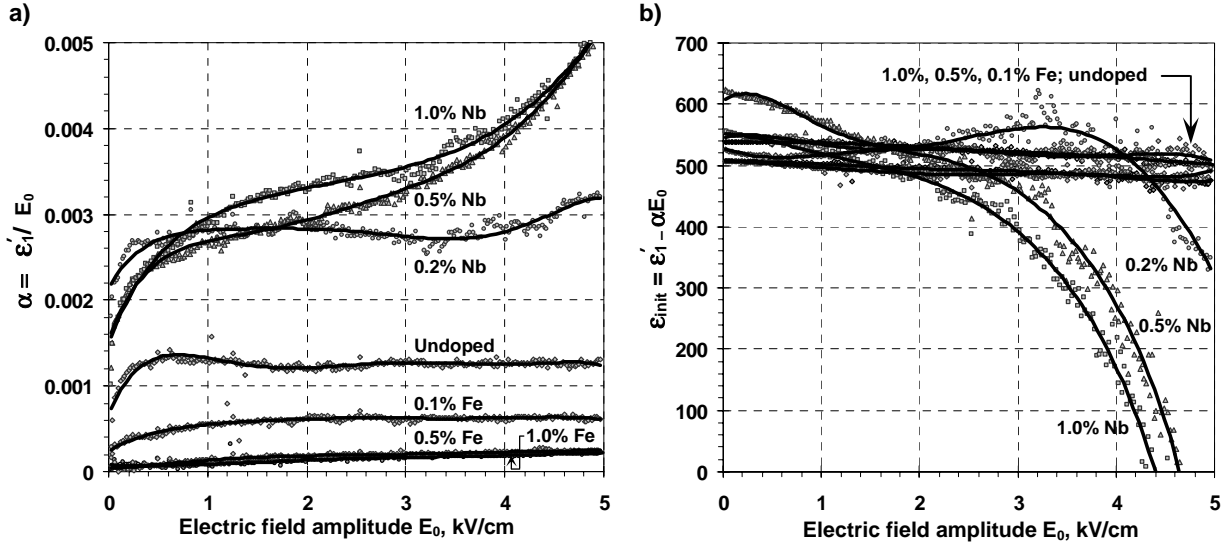
Figure 6.2. *Rayleigh parameters ε_{innt} and α derived from experimental data of $P_1(E_0)$ dependence for hard and soft $Pb(Zr_{0.58}Ti_{0.42})O_3$ ceramics. Dopant concentration is indicated in at.%.*

Nevertheless, the behaviour of the soft ceramics can be described by quasi-Rayleigh model in which the linear relationships (2.9) – (2.10) are replaced by additional terms:

$$\chi(E_0) = \chi_{init} + \alpha_\chi E_0 + \beta_\chi E_0^2 + \gamma_\chi E_0^3 + ... = \chi_{init} + \alpha_\chi^*(E_0)E_0 \qquad (6.1)$$

$$\varepsilon(E_0) = \varepsilon_{init} + \alpha_\varepsilon E_0 + \beta_\varepsilon E_0^2 + \gamma_\varepsilon E_0^3 + ... = \varepsilon_{init} + \alpha_\varepsilon^*(E_0)E_0 \qquad (6.2)$$

The physical justification of these additional terms in the frameworks of Preisach formalism is shown in [32].
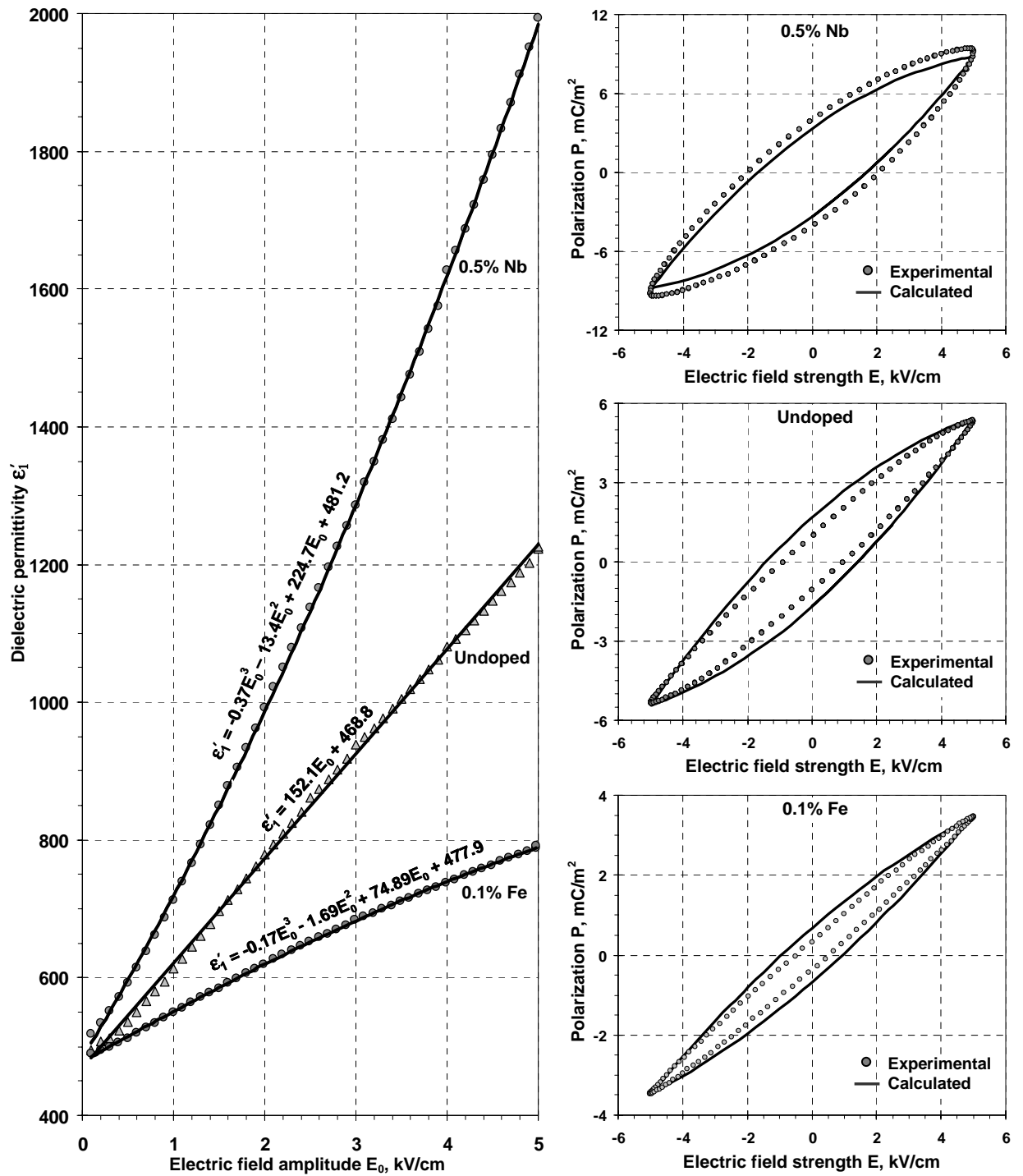
Figure 6.3. *Real part of dielectric permittivity as a function of electric field amplitude (left) and corresponding **P-E** hysteresis loops (right). Dots correspond to experimental data; solid lines are calculated curves accordingly to interpolations (6.2) and hysteresis (2.7) with α replaced by α^{*}. Dopant concentration for hard and soft $Pb(Zr_{0.58}Ti_{0.42})O_3$ ceramics is indicated in at.%. The measurements are performed at 1 kHz.*

Thus, the real behaviour of some ferroelectric ceramics can still be described by Eq. (2.7) – (2.8) if parameter α is replaced by $\alpha^*(E_0)$ defined by Eq. (6.1) – (6.2). The link between hysteresis and nonlinearity is one of the most important implications of the Rayleigh relations. The experimental examination of this link is shown in Fig.6.3. The experimentally measured nonlinearities $\varepsilon_1'(E_0)$ are extrapolated by cubic polynomial (6.2) and the hystereses are calculated using the Rayleigh relations with parameter α replaced by $\alpha^*(E_0)$. The comparison between experimental hystereses with calculated ones demonstrates that only for soft composition the experimentally measured polarization response is higher than the calculated one, which can be attributed to other additional contributions that are not accounted by considered model. The undoped and hard ceramics demonstrate comparatively poor hystereses, with polarization response smaller than the one calculated from quasi-Rayleigh model, thus showing that the applicability of the model is probably not valid for their cases (i.e. the nonlinearity is not linked with hysteresis in a straightforward way).

The replacement of the Rayleigh coefficient α by α^* is only an approximation that apparently works well at the certain field range (Fig.6.4). The measured polarization response remaining slightly higher than the calculated one using the Rayleigh relations is generally in good agreement with the Rayleigh relations for the soft ceramic sample in the electric field amplitude range 1.0 - 2.0 kV/cm. Indeed, in this field amplitude range, the phase angle of the third harmonic is close to -90° implied by Rayleigh relations (Fig 6.1,d). Beyond this region, the deviation from the Rayleigh relation become more apparent and the response of the material can be modelled using the Preisach approach as a more general tool [32,33]. In this work, only the ideal Rayleigh model is considered as a reference of the idealized material response due to the contribution of domain wall movement in perfectly random potential energy profile.

In the case of polarization response insignificantly deviated from the Rayleigh relations, the presence of in-phase nonlinear components originated in other contributing mechanisms results in the deviation of the phase angles of higher harmonics from ±90°. But in many other cases, including hard ferroelectric ceramics, the material response is clearly non-Rayleigh-like. It is most likely that pinning centres in hard ceramics are not randomly distributed but are arranged in such a way to lock the domain wall motion in the potential well with only one minimum. In the idealized case this potential well can be described by a V-shape (Fig.2.14), so the displacement of domain walls at subswitching weak fields would

be linear and anhysteretic. In real very hard ceramics (doped with 0.5 - 1.0% Fe), the third harmonic is presented in the polarization response and is predominantly in-phase; the phase angles of the first and the third harmonics are close to $0\pm180°$, so the displacement of the domain wall is rather nonlinear but essentially anhysteretic, which is in agreement with the V-potential characteristics (see chapters 3 and 5).
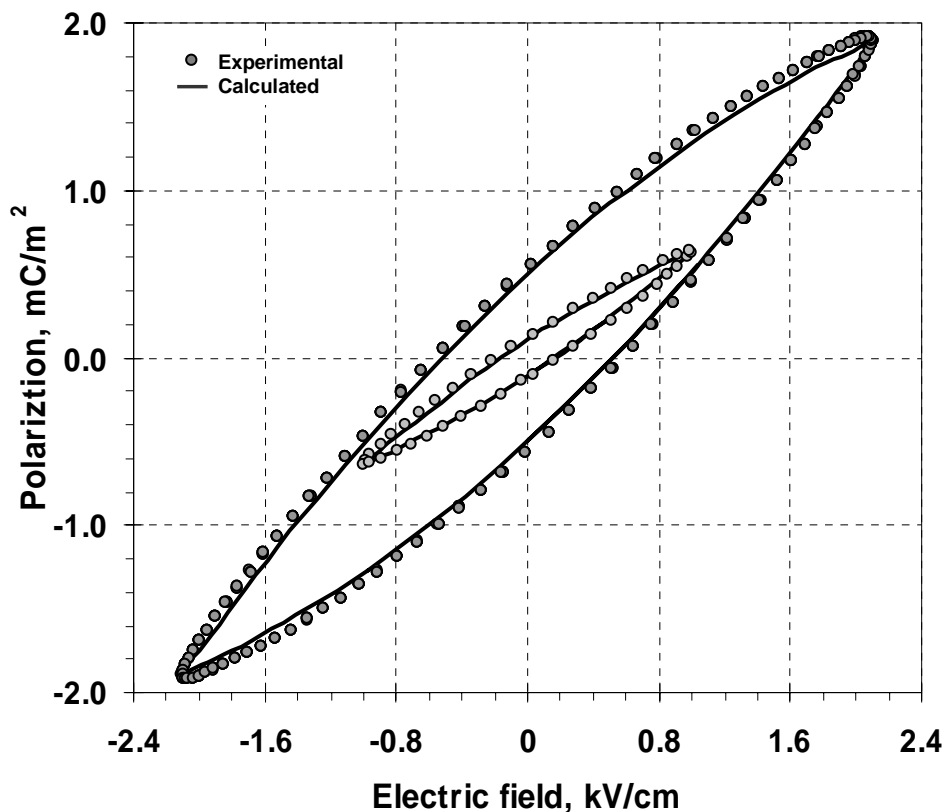
Figure 6.4. P-E hysteresis loops of PZT (58/42) ceramics doped with 0.5%Nb: experimentally measured (dots) and calculated from the nonlinearity shown in Fig.6.3. (solid lines).

These two limiting idealized references based on assumptions of the perfectly ordered and perfectly random states of pinning centres are helpful in interpretation of the ambiguous behaviour of the third harmonic phase angle as a function of the field amplitude and the dopants type and concentration.

Interestingly, one slightly hard sample, doped only with 0.1% Fe, demonstrates the transition from predominantly in-phase to predominantly out-phase third harmonic response

as the field increases. Moreover, while the undoped and soft ceramics demonstrate relatively similar dependence of δ_3 on increasing and decreasing field amplitude, for hard materials, as a rule, the field amplitude dependence of δ_3 is quite different for increasing and decreasing fields.

The following experiment shows in detail the role of δ_3 as a parameter characterising the aging state of a ferroelectric ceramic. The field amplitude cycling has been performed several times with two different hard samples; the results are shown in Fig.6.5. The measurements of $\delta_3(E_0)$ for ascending and descending electric field amplitude E_0 were run in series several times. For the slightly hard ceramic sample (Fig.6.5,a) the phase angle δ_3 reaches the vicinity of -90° with increasing driving field amplitude at the first run and remains in this region with decreasing field amplitude and at all subsequent experiments. (The very low field behaviour below evident threshold field of 0.5 – 1.0 kV/cm is not considered for simplicity). For the harder sample (Fig.6.5,b), the phase angle δ_3 does not reach the region of -90° neither with increasing field (where δ_3 almost does not depend on the field amplitude) nor with decreasing field (where δ_3 noticeably changes towards the region of -90°), but at each subsequent run, the sample demonstrates a sort of "memory" with respect to δ_3 achieved during the previous cycling of the field.

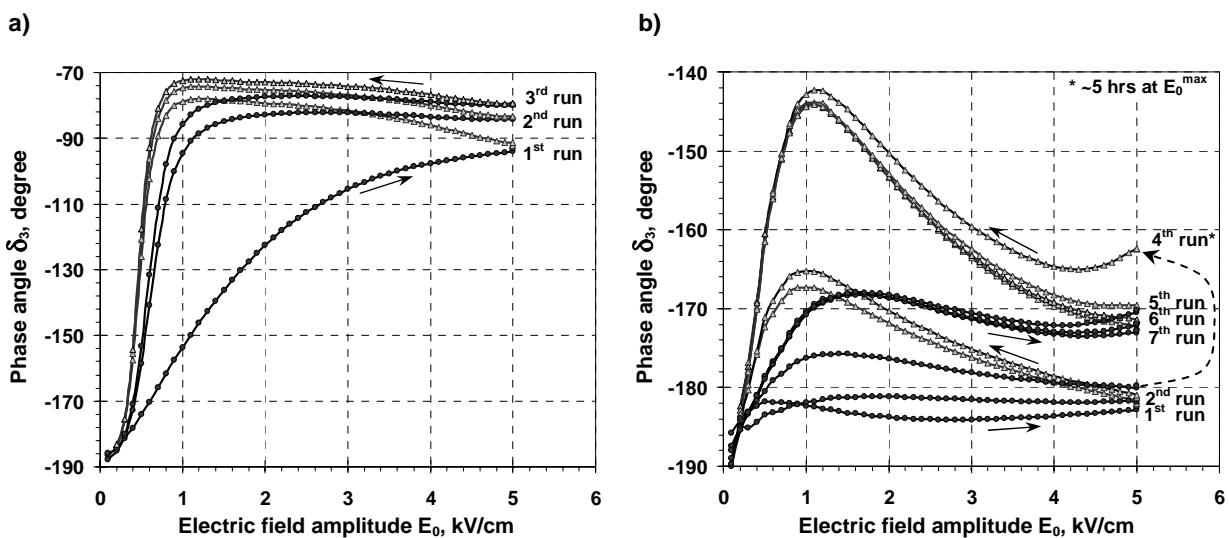**Figure 6.5.** *Phase angle of the third harmonic of polarization response as a function of electric field amplitude (1 kHz) for hard $Pb(Zr_{0.58}Ti_{0.42})O_3$ ceramics doped with (a) 0.1% Fe and (b) 0.5% Fe. Arrows indicate the branches corresponding to increasing and decreasing of driving field amplitude.*

To confirm this "memory effect" the sample was kept during the 4th run at the maximum field amplitude **$E_0 = 5$ kV/cm** for as long as 5 hours. During this time under the ac-field exposure the phase angle **δ_3** had increased and continued to increase when the field amplitude was decreasing. At the next, 5th and other subsequent runs, the value of **δ_3** was noticeably higher than during first three experimental runs. So these experiments demonstrate that electric ac-field, as well as time during which the field is applied, changes the properties of the hard ferroelectric ceramics. This effect may be understood as a consequence of the well-known ageing-deageing effects in hard ferroelectric ceramics [77-79]. In [79] the deageing effect of sample cycling under electric fields at the switching range was shown experimentally for many hard ceramics. Here, the same effect can be attributed for the third harmonic phase angle transition but under subswitching conditions.

The considered effect can be interpreted within the framework of one of the possible scenarios of hardening-softening transition shown schematically in Fig.3.3. This scenario assumes that in aged hard ferroelectrics, all the charged defects are electrostatically arranged and occupy the most preferable positions with respect to the orientation of domain polarization. With increasing amplitude of the ac electric field, the initially ordered pinning centres may be perturbed by the field's action, and become partly disordered. At the same time, with increasing field amplitude, the domain walls, each time, move further and further away from their equilibrium positions, and, thus, become affected by bigger number of pinning centres situated thereabout. With decreasing field amplitude, the amplitude of the domain wall motion decreases and the number of the ordered pinning centres around it also decreases; meanwhile the number of disordered pinning centres remains the same (if the restoring process is not very strong and fast). In practice, the behaviour of the third harmonic phase angle with increasing and decreasing field may be abstractedly compared with carving the way and using it afterwards for the return. Disordering the pinning centres, by displacing them from their potentially preferable states within the domain, results in the appearance of trapping in the domain wall potential profile by additional local minima. Ideally, this process of the potential energy trapping may go on till complete disorder is accomplished and such process would designate the transition from one idealized model of ordered system (V-potential) to another idealized model of the perfectly random system (model based on the Rayleigh law).

The experimental verification of applicability of the model based on Rayleigh relations to the response of soft ferroelectric ceramics can be extended also on higher harmonics response. Accordingly to Eq. (5.14), the ideal Rayleigh response is characterized by the nonlinear parameters that are compared with experiment in Fig.6.6, Fig.6.7, and Table 6.1.

Table 6.1. *Some nonlinear parameters of the polarization response to the sine electric ac-field signal: the experimental data for the soft PZT ceramics[*] and the Rayleigh formula evaluations*

Nonlinear parameter	$\delta_1, °$	$\delta_3, °$	$\delta_5, °$	$\delta_7, °$	$\delta_9, °$	$\dfrac{P_1''}{P_3''}$	$\dfrac{P_3''}{P_5''}$	$\dfrac{P_5''}{P_7''}$
Rayleigh formula evaluations	$\lim\limits_{E_0\to\infty} \mathrm{ctg}\delta_1 = -\dfrac{3\pi}{4} \approx -2.36$	-90	90	-90	90	5	-3	-7
Experimental value in the field amplitude range 2...5 kV/cm	$\delta_1 \approx 0..-25°$ $\mathrm{ctg}\,\delta_1 \approx -4.0 .. -2.34$	-90..-120	57..70	-30 ..-140↑[**] -137..-143↓	-5..15	7..10	-5..-10	-30..-7↑ -7..-9↓
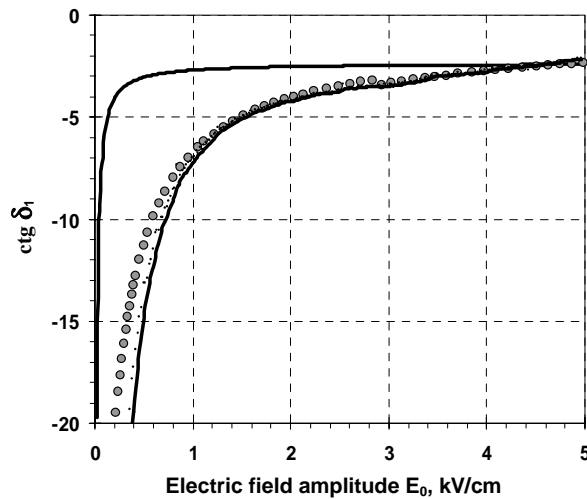
Figure 6.6. *Characterization of the soft $Pb(Zr_{0.58}Ti_{0.42})O_3$ ceramics doped with 1.0% Nb at the first harmonic:* $\dfrac{P_1''}{P_1'} = \dfrac{1}{\mathrm{tg}\delta_1} = \mathrm{ctg}\delta_1$. *Dotted curve corresponds to the experimental data; solid curves correspond to the calculated dependences using Rayleigh formula (top line – using the constant mean values $\varepsilon_{init} \approx 500$, and $\alpha \approx 0.034$; bottom line – using the current values of ε_{init} and α shown in Fig.6.2).*

---

[*] See also Fig. 6.6, Fig. 6.7 and the comments in the figures captions
[**] ↑-increasing field amplitude; ↓-decreasing field amplitude
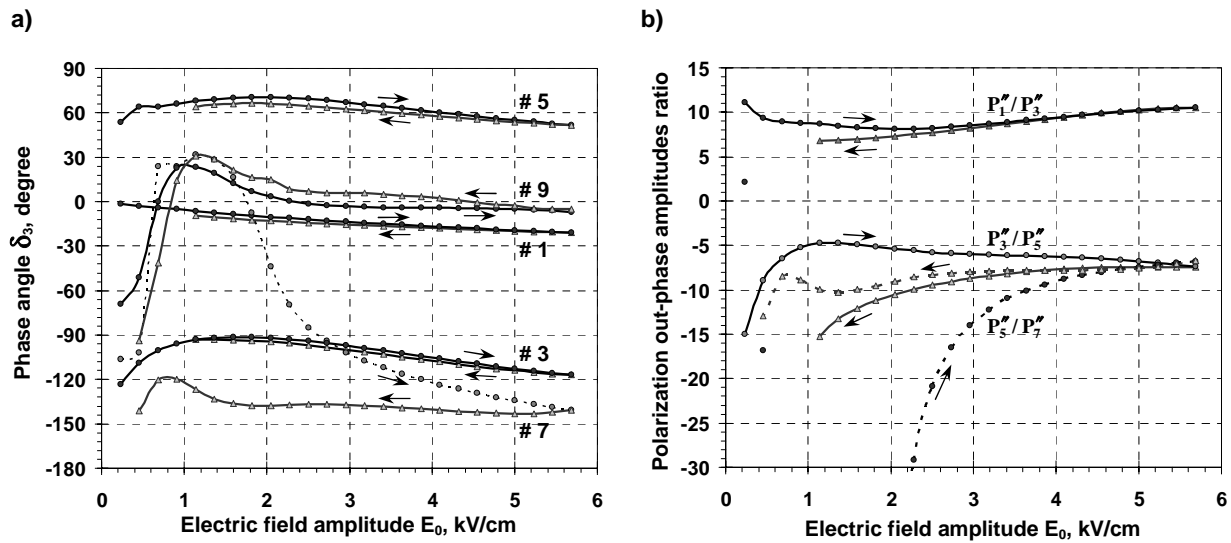
Figure 6.7. *Nonlinear characteristics of the soft Pb(Zr$_{0.58}$Ti$_{0.42}$)O$_3$ ceramics doped with 1.0% Nb: (a) phase angles of first five odd harmonics of polarization response and (b) ratios of out-phase components of polarization response as a function of electric field amplitude (1 kHz). Arrows indicate the branches corresponding to increasing and decreasing of driving field amplitude.*

It is evident that the deviation from the ideal Rayleigh model becomes more apparent at higher harmonics, e.g. at the 9th harmonic Rayleigh formula does not hold for the real response, but for the first three odd harmonics the model works relatively well for the examined sample. In Fig.6.8 the out-phase amplitude ratio of the first to third harmonics of polarization response is compared among the soft compositions (Fig.6.8,a) and between soft and hard samples (Fig.6.8, a and b). For soft ceramics this ratio can be considered as a constant when amplitude of the driving field is higher than 1 kV/cm. This ratio, however, is slightly growing with an increase of the field amplitude. In practice, it may imply an additional contribution (e.g. conductivity or any other linear effect) contributing to the out-phase component of the first harmonic but not to the third harmonic. The extrapolation of these out-phase ratios to the zero-field region gives the value quite close to 5 predicted by the Rayleigh model. For the aged hard ceramics estimation of this out-phase component ratio has no practical sense. As it is shown in Fig.6.8,b, this parameter is not stable and, as expected, differs by several orders of magnitude from one predicted by the Rayleigh model. Quite the contrary is the polarization response of the thermally quenched hard ceramics. The behaviour of out-phase polarization components ratio of quenched hard ceramic sample

reminds one of the soft samples but with some field amplitude scaling effect. It reaches the value of 5 at the field amplitude range of 4..5 kV/cm, and stabilizes at this level.
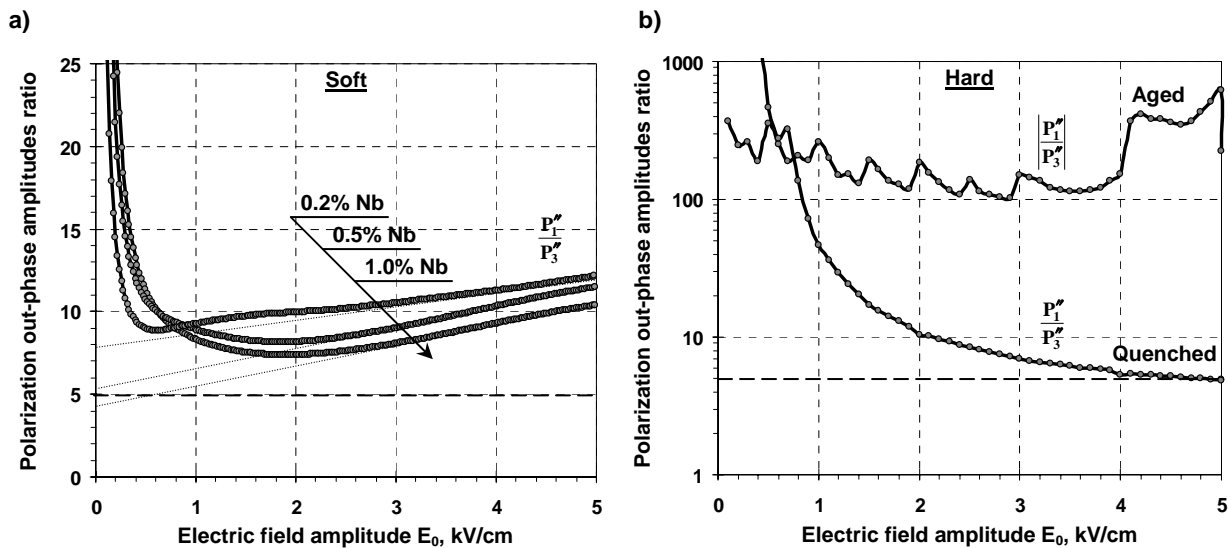
Figure 6.8. Ratios of the out-phase amplitudes of polarization response for (a) soft and (b) aged and quenched hard (doped with 1.0 at.% Fe) $Pb(Zr_{0.58}Ti_{0.42})O_3$ ceramics. Dopant concentration is indicated in at.%; measurements performed at 1 kHz.

The thermal quenching was performed by heating the sample above the Curie temperature (approximately up to 450 – 500 °C), and immediate cooling down to room temperature in water. If the sample passes the phase transition region relatively fast, then the defect states will be mostly frozen and will remain as in the paraelectric phase. If the time of the electrostatic rearrangement of defects (ageing time) in a polarized regions (ferroelectric domains) at room temperature is much longer than the measurement time required to make the experiment, then the experimental results demonstrate the behaviour of thermally deaged material.

The response of thermally quenched hard ceramics is found to be well-consistent with the Rayleigh model (Fig.6.9). The polarization response of quenched sample in comparison with the aged one is higher, and with higher nonlinearity (Fig.6.9,a); out-phase component dominate in the third harmonic response (δ_3 is much closer to **-90°**) (Fig.6.9,b); the out-phase amplitude ratio P_1''/P_3'' reaches the value of **5** (Fig.6.8); the hysteresis loop is more

developed and is in a good agreement with the curve calculated using the Rayleigh relations between hysteresis and nonlinearity (Fig.6.9,c and d).
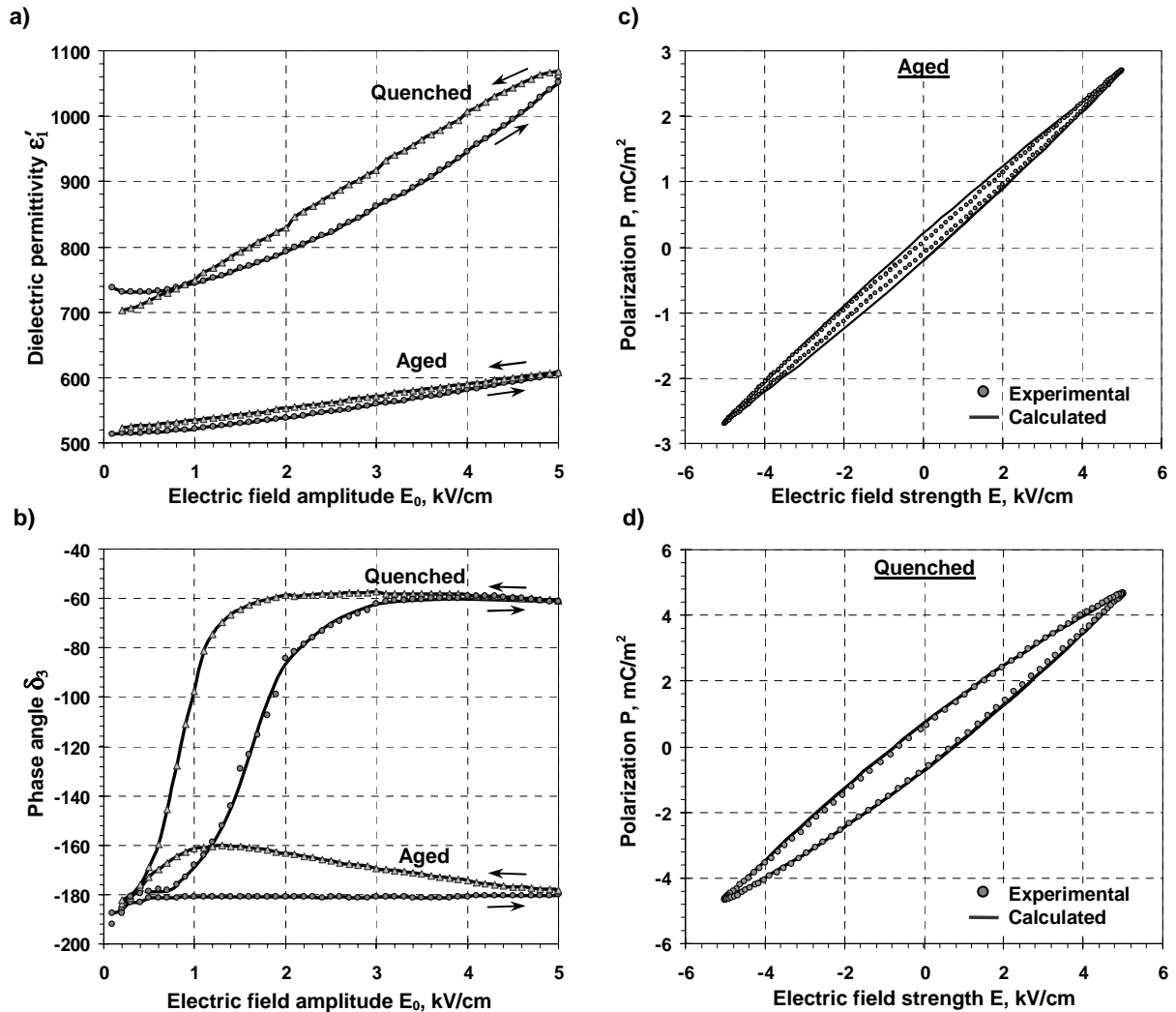
Figure 6.9. *Characterization of aged and quenched hard ceramics soft $Pb(Zr_{0.58}Ti_{0.42})O_3$ doped with 1.0 at.% Fe: Real part of dielectric permittivity (a) and phase angle of the third harmonic of polarization response (b) as a function of electric field amplitude and corresponding **P-E** hysteresis loops for aged (c) and quenched (d) samples. Points correspond to experimental data; solid lines are calculated curves accordingly to (2.7) and (6.2); arrows indicate the branches of increasing and decreasing field amplitude. The measurements are performed at 1 kHz.*

This relative consistency of the experimental data obtained from the quenched sample with Rayleigh relations strongly suggests that the change in the polarization response towards the idealized Rayleigh model predictions after the thermal quenching occurred

mainly due to the loss of the electrostatic arrangement in the defect states. The thermal quenching results in resetting the domain pattern in thermally disordered pinning centres medium so that the extrinsic contribution of the domain wall movement into polarization response acts in accordance with the model based on Rayleigh relations.

In summary, the polarization response of soft and hard ceramics can be approximated by idealized models based on the Rayleigh relations or the V-potential, respectively. However the real response of real materials deviates from these models, the deviation becomes especially apparent when the response is characterized using the harmonic analysis and the behaviour of nonlinear parameters is considered. These observed deviations suggest that the response of real ferroelectric ceramics corresponds to an intermediate situation with respect to the idealized models and thus may be better approximated by some mixture of these idealized models. At least, the gradual enhancing of the hysteresis loop and increasing of nonlinearity with change of dopant type and concentration in PZT ceramics from hard compositions (iron doped) to soft compositions (niobium doped) are in a good agreement with a qualitative model of order-disorder transitions. This model links the state of electrostatic arrangements of charged defects in the bulk with roughness, steepness and randomness of the domain wall potential profile as shown in Fig.3.3. A similar transition has been observed in the quenching experiment. In addition, the idealized models account for macroscopic domain wall dynamics in terms of an energy profile across which the domain wall moves reversibly or irreversibly under the influence of electric field, but neither any intrinsic contribution to the polarization response nor viscosity effects of domain wall dynamics resulting from the roughness of the domain wall energy landscape are considered. The influence of viscosity of domain wall motion will be discussed in section 6.2.2.

6.2. Frequency effects

6.2.1. Introduction

In general, the dielectric and other properties of ferroelectric materials are frequency dependent. The frequency dependence of material parameters, also known as dispersion, is an essential property of all dielectric materials. In most of the cases, the frequency

dispersion of dielectric permittivity or piezoelectric coefficient is described by a Debye or Debye-like model [14,145], broad power law [146], or logarithmic function [147].

In some materials, including PZT, the frequency dispersion is accompanied with nonlinearity with respect to the driving field amplitude. Moreover, these two effects are coupled: nonlinear parameters are frequency dependent and parameters, which describe frequency dispersion, depend on driving field amplitude [14,147,148]. In several works the frequency dispersion is attributed to the same origins as an extrinsic contribution of nonlinearity phenomenon, namely to displacement of domain walls and their interaction with pinning centres, to the state of order of pinning centres [149-152], to the nature of the domain wall motion: reversible or irreversible [153]. In this way, the relative frequency behaviour of hard and soft PZT ceramics is of a particular interest.

Dielectric spectroscopy, on the other hand, is a well known experimental tool covering at various frequencies ranges, many physical phenomena [146, 154-156], and can be, in particular, used to study the relaxation processes intimately related to the dynamics of defects. As many relaxation processes are temperature-activated, the temperature dependences of the materials properties and derived activation energies for the relaxation processes are of interest as well.

The systematic and comprehensive review of the dielectric relaxation in solids has been given by Jonscher in his monograph [146]. In this review, a complete classification of all experimentally observed types of dielectric response in the frequency range below the microwave region and extending to the lowest attainable frequencies of 10^{-4} – 10^{-6} Hz is first presented. The summary of that classification is shown in Fig. 6.10. It takes into consideration not only the generally accepted dipolar response, but also the equally important charge carrier responses of both hopping electronic and ionic nature. The reason of inclusion of charge carriers among the polarising species is based on the experimental evidence that the hopping charge carriers give rise to genuinely dielectric responses, and, in addition, they follow the same law of frequency dependence as the classical dipolar species above the loss peak frequency:

$$\chi'(\omega) \propto \chi''(\omega) \propto \omega^{n-1} \qquad (6.3)$$

with the exponent in the range

$$0 < n < 1 \tag{6.4}$$

The relations (6.3) and (6.4) as shown in [146] represent the universal law, which is obeyed by interactive many-body systems, and whose range of validity extends from frequencies at which the quantum and phonon effects become dominant down to either the loss peak frequency in dipolar systems or to the onset of the strong low-frequency dispersion in the systems where hopping charge carriers have dominating contribution to dielectric response.
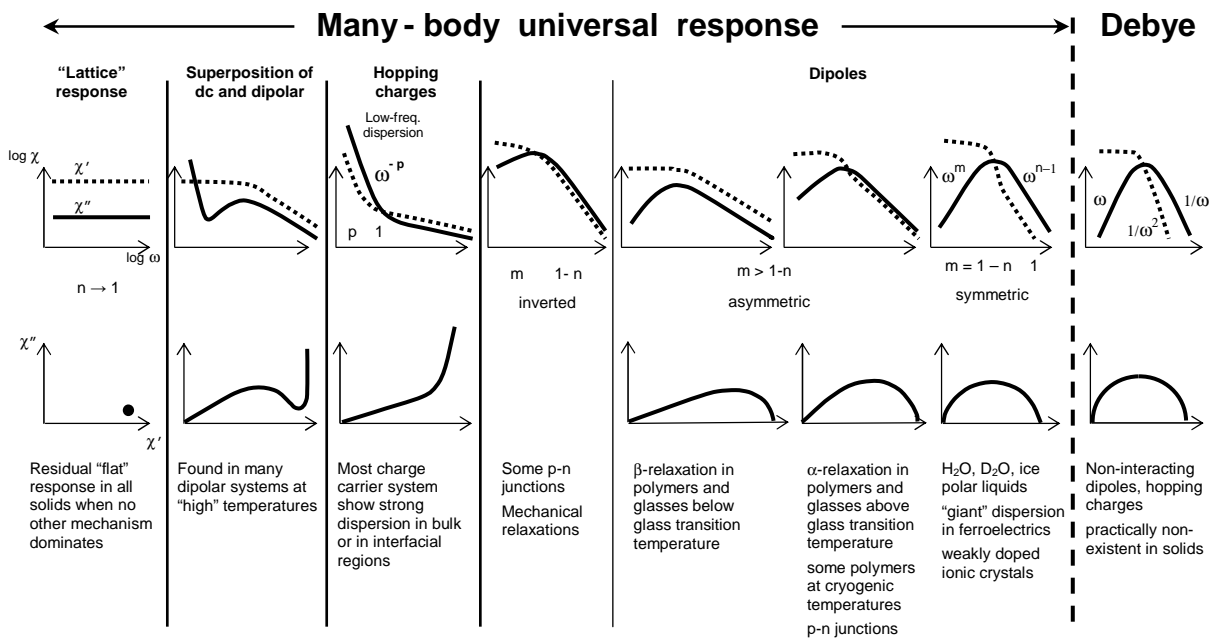
Figure 6.10. *The general classification of all types of dielectric responses found in solids. The upper row gives the diagrammatic representation of the* $\log\chi'(\omega)$ *(dotted line) and* $\log\chi''(\omega)$ *(solid line) against* $\log\omega$, *the lower row gives the corresponding complex susceptibility plots. Typical materials giving the various types of response are indicated. The extreme right gives the practically non-existent case of the Debye response, moving to the left the loss peaks appear increasingly broader for dipolar systems, further to the left the charge carrier responses corresponding to the strong low-frequency dispersion and to dc conductivity. On the extreme left is the limiting case of "flat" frequency- and temperature independent loss. From Ref. [146].*

6.2.2. **Frequency dispersion in hard and soft ceramics at various field amplitudes.**

The polarization response of some soft and thermally quenched hard PZT ceramics to the low-field periodic signal, as described in section 6.1, is consistent with the Rayleigh formalism expressed in Eq. (5.14). While the Rayleigh equations are frequency independent, the real response has apparent frequency dispersion (Fig.6.11 and Fig.6.12).

As discussed above, the Rayleigh relations represent an ideal model of a definite type of domain wall motion. As such, they do not account for many other possible contributions to polarization response. Hence, the question of common origin of the nonlinearity and frequency dispersion of dielectric permittivity is naturally posed. An experimental examination of the frequency dependence of some nonlinear parameters attributed to the Rayleigh model demonstrates ample evidence that the Rayleigh model holds for a very broad frequency range (Fig.6.13). The frequency independent ratio of out-phase polarization components implies that both first and third harmonic components of the polarization response vary with frequency by the same law. An insignificant deflection of characterized parameters at higher frequencies (Fig.6.13) is a result of the instrumental error which was verified by comparing the results obtained with lock-in and charge amplifiers at lower frequencies and with LCR-meter at higher frequencies: the data points are located within one trend except at the transition frequencies of the devices' operating limit. An example of such experimental data conjunction is shown in Fig.6.12.

The validity of the Rayleigh-based model in a wide frequency band suggests that the frequency dependency and nonlinearity probably both originate in the same phenomenon, otherwise the deviation from the ideal Rayleigh model with varying frequency would be more apparent as in the case of varying field amplitude.

The domain wall nature of dielectric permittivity frequency dispersion is discussed in [152] in terms of domain wall motion in a disordered medium energy landscape, and in [153], in terms of an irreversible creep-like viscous domain wall motion and reversible wall relaxation.
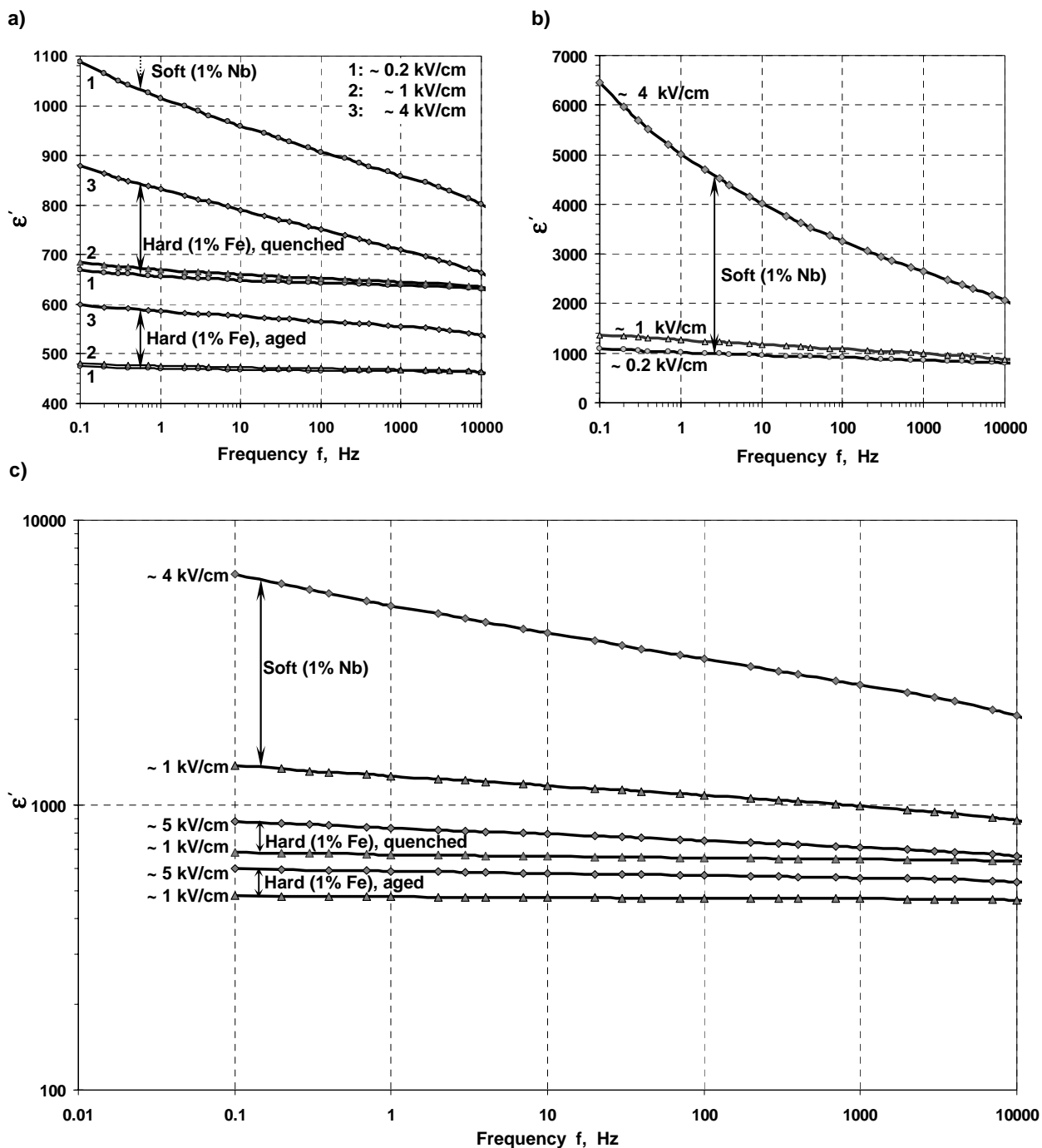
Figure 6.11. *The real part of dielectric permittivity as a function of frequency for 1.0 at.% Fe-doped hard (in aged and thermally quenched states) and 1.0 at.% Nb-doped soft PZT (58/42) ceramics for 3 different amplitudes of driving field plotted on semi-logarithmic (a,b) and logarithmic (c) scales.*
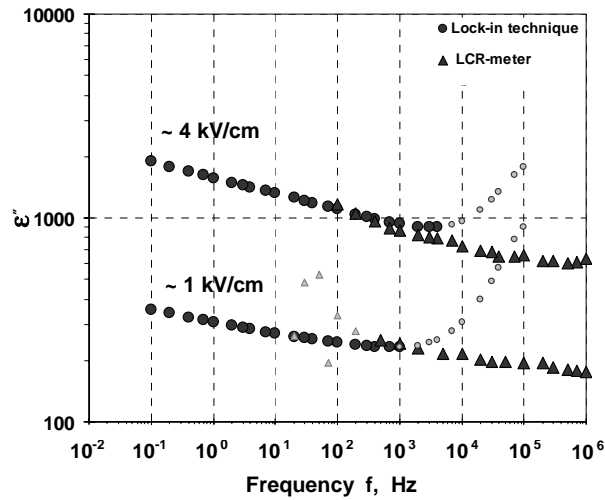
Figure 6.12. *The dispersion of the imaginary part of dielectric permittivity in a broad-band frequency range for 1.0 at.% doped soft PZT (58/42) ceramics*
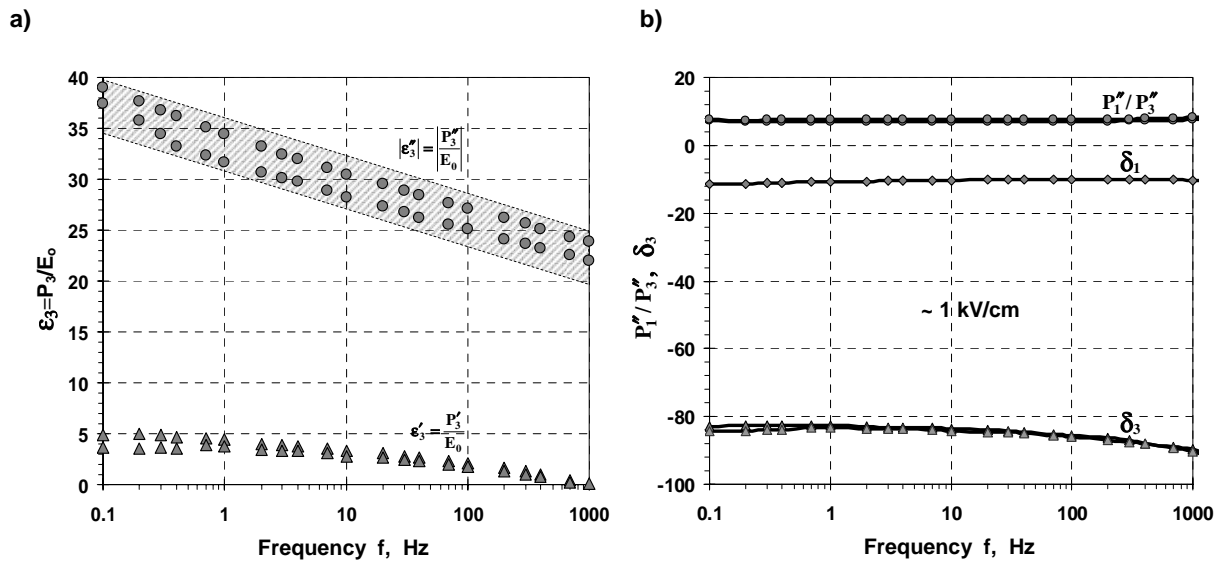
Figure 6.13. *Frequency dispersion of some nonlinear parameters of Rayleigh model for 1.0 at.% doped soft PZT (58/42) ceramics: (a) parameters with a pronounced frequency dependence; (b) parameters with an insignificant frequency dependence*

An attempt to make a unified description of the nonlinear and frequency dependent response is described in [148]. In that article, the frequency dependent response is assumed to arise from pure rate-dependent process while the field independent Rayleigh relations are considered as the high frequency and rate-independent limit of the rate-dependent process. Also

assuming that rate dependent and rate independent losses couple, i.e. are not simply additive, the unified description of nonlinearity and frequency dispersion has been formulated as an additive combination of Rayleigh relations with the frequency dispersion of the complex susceptibility based on the power law. This paper, however, does not describe the details of higher harmonic response since the frequency dispersion of material susceptibility is developed for the first harmonic only. The frequency dependence of the out-phase component of the third harmonic of the polarization response (Fig. 6.13,a) with the same slope as the out- phase component of the first harmonic (Fig.6.13,b), i.e. not deviating from the Rayleigh formalism, gives rise to the assumption that the effective Rayleigh coefficient α in (5.14) is frequency-dependent. The derivation of Rayleigh coefficient from statistical theory of Rayleigh's law proposed in [42] (See Eqs. (2.14) - (2.18)) does not take into account any relaxation effect of the domain wall movement. The concept of waiting time distribution for stochastic motion of a domain wall and its relation to the energy landscape of the domain wall in disordered medium is introduced in [152]. In another work, [159], the waiting time distribution that control the domain wall motion is related to the distribution of the energy barriers. In these models considering irreversible hopping or creep-like domain wall dynamics, the power law equations for the relaxation processes are derived.

The frequency dependent behaviours of aged and thermally quenched hard ceramics (Fig.6.11) are in a good agreement with the concept of waiting time distribution related to the randomness of energy landscape for a domain wall. Demonstrating the transition from quasi-linear anhysteretic response in aged state to the hysteretic Rayleigh-type polarization response in thermally quenched state, the hard PZT ceramics, in the quenched state, also reveal an increase of the slope in the frequency dispersion of the dielectric permittivity. Similarly to the change in nonlinearity, the frequency dispersion of the dielectric permittivity in quenched hard ceramics is in between the properties of aged hard and soft ceramics. Both phenomena (nonlinearity and frequency dispersion) may be attributed to randomization of the energy landscape of domain wall after quenching. The domain wall motion in a random potential profile is irreversible and thus its creep-like dynamics become apparently frequency dependent.

The power law frequency dependence is found to be very broad. For the hard ceramics it is indistinguishable from the logarithmic function (Fig.6.11,a), while for the soft ceramics the difference from the logarithmic function becomes apparent at higher field amplitudes (Fig.6.11,b).

6.2.3. **Frequency dispersion at higher temperatures**

The analysis of frequency dispersion at various temperatures is a tool to study the thermally activated processes in solids, which may manifest themselves in the dielectric response. Dynamical processes in condensed matter often involve motion of charges, e.g. dielectric polarization or ionic conductivity. The dispersion of dielectric permittivity of hard and soft ceramics in a wide frequency range, and at the room temperature, does not reveal any peak of dielectric losses (Fig.6.11 and Fig.6.12). The behaviour of hard ceramics at higher temperatures is shown in Fig.6.14. According to Jonscher's classification of dielectric responses in solids (Fig.6.10), the response of hard ceramics can be attributed to the hopping charge contribution, which dominates at lower frequencies (third column in Fig.6.10). There is a well pronounced transition from the dielectric response of dipole system to dielectric response of hopping charges, when the exponent **n** of power function ω^{-n} changes dramatically. The frequency of this transition increases with an increase of temperature. Therefore, thermally activated charge hopping may take place.
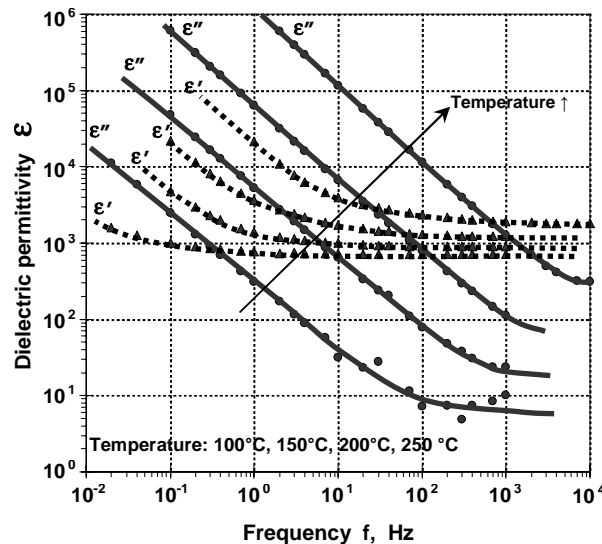

Figure 6.14. *The real and complex part of dielectric permittivity versus frequency of driving field measured at various temperatures for 1 at.% Fe-doped hard PZT (58/42) ceramics.*

Hopping charge carriers are characterized as species that spend most of the time in localized sites where they are subject only to relatively small vibrations, but occasionally they make a big jump or hopping transition to some neighbouring localized sites which may be one or many atomic spacings away. The concept of hopping movement is traditionally considered for ionic conduction, since ions move essentially only by hopping, whether by the interstitial or vacancy mechanism. A relatively more recent extension of this concept accounts also for electronic charges and has found particular application in amorphous and disordered non-metallic solids, such as glasses, amorphous semiconductors, etc. [146,159,160].

The fact that ionic and electronic conducting solids show similar behaviour, apparently, means that one cannot learn much about the details of the conduction mechanism focusing only on measurements of the frequency or temperature dependence of the conductivity. A brief review of ac conduction in disordered solids followed by a detailed discussion of the random free-energy model is given in [161]. In that model the hopping charge carriers are subjected to spatially randomly varying energy barriers.

The activation energy of the hopping charges contribution to dielectric response can be evaluated by plotting the transitional frequency versus temperature in the Arrenius scales. However, the main difficulties of such analysis, using directly the response characterization shown in Fig.6.14 lies in the difference between the transition frequencies of $\varepsilon'(\omega)$ and $\varepsilon''(\omega)$. In addition, these transitional frequencies are located at the limits of the characterized region. The expansion of the frequency measurement range is difficult because of the instrument limits and it would also considerably increase the time of characterization. The alternative solution is to use the frequency dispersion of the absolute dielectric permittivity $|\varepsilon^*(\omega)|$ (Fig.6.15,a) that demonstrates similar dispersion with only one transitional frequency, located somewhere in between ones of $\varepsilon'(\omega)$ and $\varepsilon''(\omega)$. Another parameter widely used for this type of analysis is the dielectric modulus $\mathbf{M}^* = \mathbf{1/\varepsilon^*}$ [155,156,158]. The imaginary part of this parameter $\mathbf{M''(\omega)}$ demonstrates maxima at transitional frequencies for various temperatures (Fig.6.15,b) and may be used for analysis as well. However, the use of $\mathbf{M(\omega)}$ for analysis has been objected through the fact that the dielectric modulus $\mathbf{M}$ is neither a directly measurable quantity nor directly related to any microscopic physical process, and, as a complex function of ε', ε'', and σ_o, may emphasise the experimental error in one of these quantities thus shading the frequency dispersion in the real physical process [162]. For these

reasons, in the following analysis this criticism will be taken into account and the complementary analysis using directly measured quantities, if possible, will be provided.
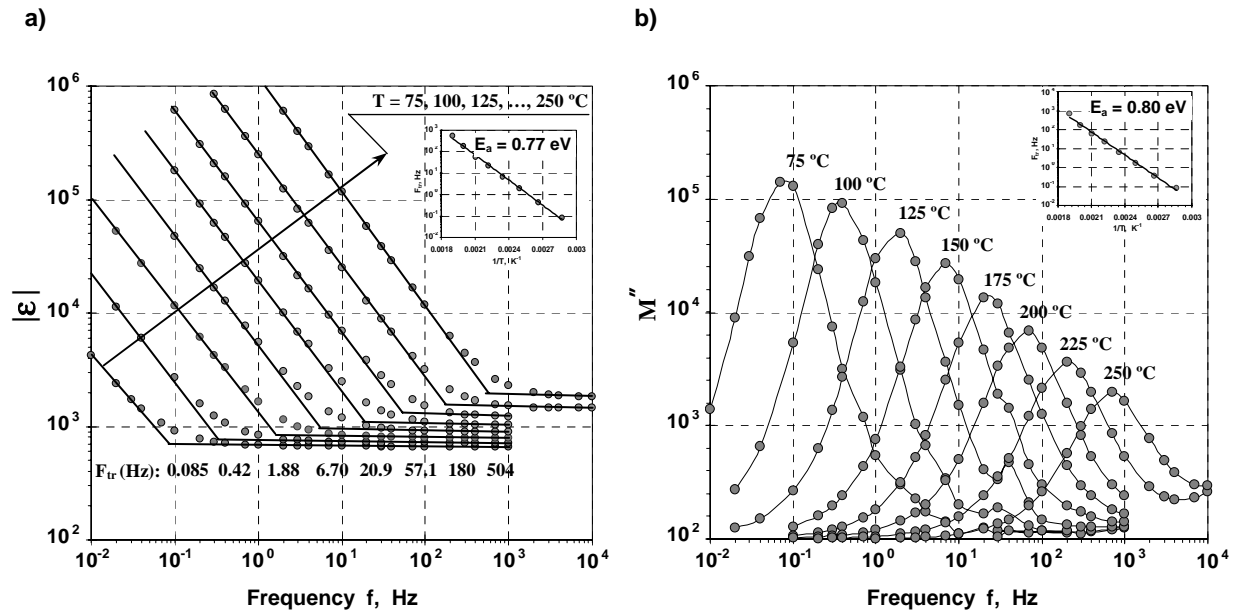
Figure 6.15. *The frequency dispersion of absolute dielectric permittivity (a) and dielectric modulus (b) at various temperatures for 1 at.% Fe-doped hard PZT (58/42) ceramics. The insets show the temperature dependence of transition frequency in the Arrenius scales and corresponding activation energy.*

The material response to the applied electric field is usually characterized by measured ac current parameters with relation to the parameters of the applied ac-voltage. These parameters characterize the form of both generating and detecting signal as well as the delay of the response. For periodic signal, the characterizing parameters include the operating frequency, amplitude, and phase angle of the driving signal, and those of all harmonics for detecting signal. It is stipulated here, that all experimental results presented in this section are measured only at the first harmonic, which is rather a standard practice. The measured current **j** consists of two contributions: mobility of free charges $\sigma_0 E$ (the steady current) and the displacement current **dD/dt**. The displacement current **dD/dt** consists of the polarization current **dP/dt**, and the polarization of vacuum $\varepsilon_0 E$, whose contribution in ferroelectrics is comparatively negligible. As the electric current involves two processes (the conduction, which arises from a finite average velocity of charges motions in a steady electric field, and the polarization, which arises from a finite displacement of charges in a

steady electric field), the material response is characterized by two independent main characteristics: the dc conductivity σ_0, and the dielectric susceptibility χ. The total dielectric contribution also includes polarization of vacuum, and it is denoted by dielectric permittivity $\varepsilon = 1 + \chi$, characterizing the true dielectric response.

Since dielectric measurements are concerned, for the most part, with the movement of charge, i.e. with the electric current, the dc contribution σ_0 also appears in the results of the effectively measured dielectric response because measuring instruments cannot discriminate between true dielectric response which does not contain σ_0 and the effective which does. To represent the results of effective measurements adequately, usually, the effective dielectric permittivity $\tilde{\varepsilon}$ is usually introduced as follows [146]:

$$\mathbf{I(\omega) = i\omega\varepsilon_0\tilde{\varepsilon}(\omega)E(\omega)} \tag{6.5}$$

$$\tilde{\varepsilon}(\omega) = \tilde{\varepsilon}'(\omega) - \tilde{\varepsilon}''(\omega) = \varepsilon'(\omega) - i\left\{\varepsilon''(\omega) + \frac{\sigma_0}{\varepsilon_0\omega}\right\} = 1 + \chi'(\omega) - i\left\{\chi''(\omega) + \frac{\sigma_0}{\varepsilon_0\omega}\right\} \tag{6.6}$$

The true conductive contribution is out-of-phase with respect to the true dielectric response. That is why it manifests itself in effective dielectric losses in a measured response. The real phase angle δ_1, whose experimental value is defined here as $\tilde{\delta}_1 = -\mathbf{arctan}\dfrac{\tilde{\varepsilon}''}{\tilde{\varepsilon}'}$, lies somewhere in between ideal dielectric response $\delta_1 \to 0°$ (polarization is in-phase with electric field) and true conductive response $\delta_1 \to -90°$ (electric current is in-phase with electric field). The measured values of phase angle dispersion at various temperatures have revealed the difference in responses of various ceramics. If for soft ceramics δ_1 demonstrated insignificant change with frequency and temperatures variation up to 250 °C, for pure, and, especially for hard samples, the phase angle δ_1 demonstrated quite dramatic sensitivity to the frequency and temperature. This sensitivity is dependent on the dopant concentration. The examples are shown in Fig.6.16,a,b. for very hard PZT ceramics doped with 1.0 at.% Fe and slightly hard PZT ceramics doped with 0.1 at.% Fe. Very hard sample demonstrates clear transition from dielectric to conductive type of response with decrease of frequency, and this transition occurs at higher frequencies when temperature is higher. For slightly hard sample this transition looks "incomplete", and reveals a dielectric relaxation process characterized by a small peak.
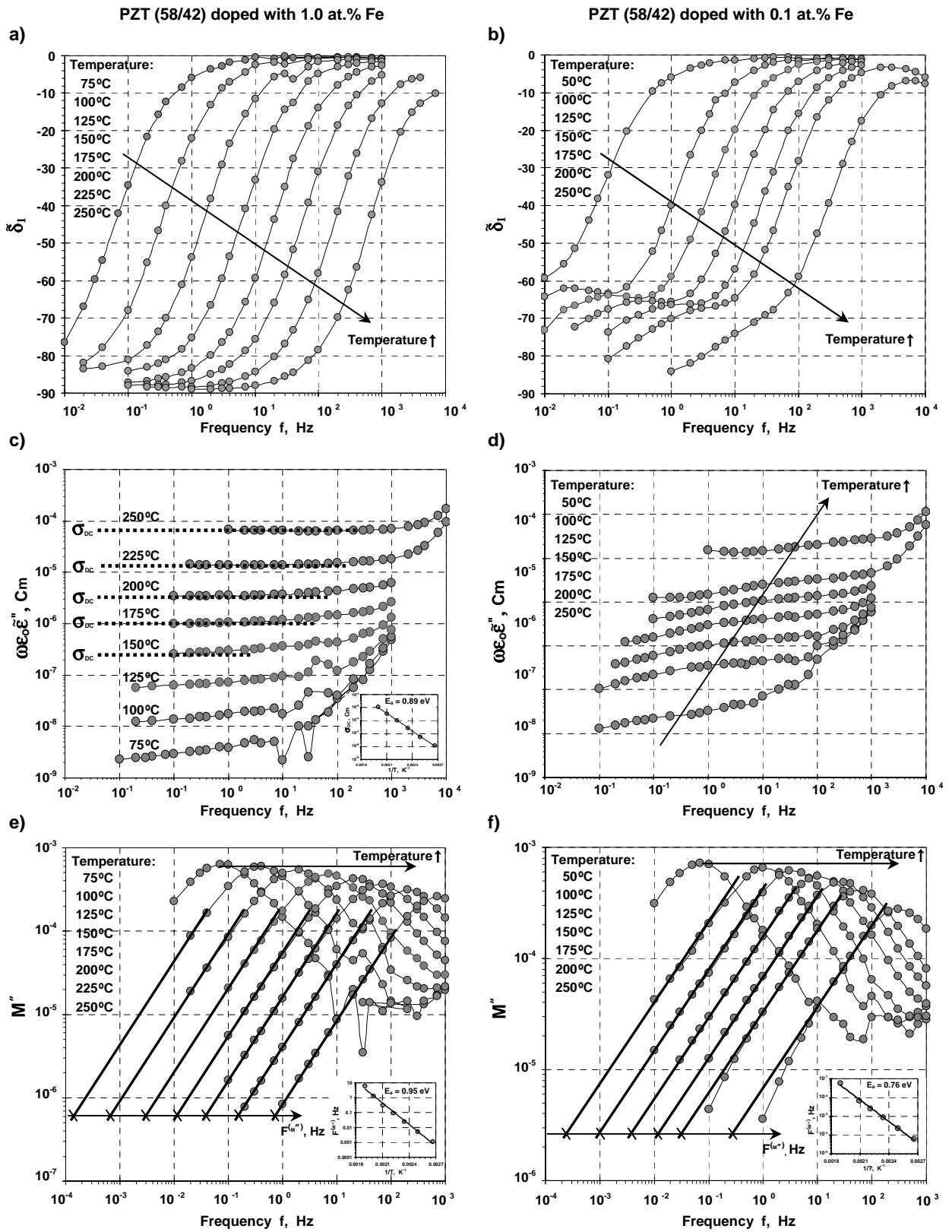
Figure 6.16. *Characterization of two hard PZT (58/42) ceramics doped with 0.1 and 1.0 at.% Fe. The frequency and temperature dependences of various parameters. (See also comments in the text)*

The frequency dispersion of $\omega\varepsilon_0\tilde{\varepsilon}'' = \sigma_0 + \omega\varepsilon_0\varepsilon''(\omega)$ (Fig.6.16, c and d), considered in some publications as the real part of complex ac conductivity, reveals that at low frequencies and high temperatures the response of a very hard sample is strictly conductive so that the frequency dispersion of $\omega\varepsilon_0\tilde{\varepsilon}''$ is saturated by frequency independent dc conductivity σ_o. For slightly hard ceramics, the dc conductive "flat region" of the frequency dispersion of $\omega\varepsilon_0\tilde{\varepsilon}''$ is observed only at very high temperature, but at lower temperatures, the frequency dispersion takes place. The dc conductivity evaluated by this method exhibits a linear dependence in the Arrenius scales and is characterized as an activated process with distinctive activation energy (e.g. the inset in Fig.6.16,c). The $\omega\varepsilon_0\tilde{\varepsilon}''$ parameter, associated with ac conductivity, increases with increasing frequency. This is a feature of any hopping model [161,163], considering non-interacting quasi-particles hopping backwards and forwards at places with high jump probability and sizably contributing to ac-conductivity, while dc conductivity is determined by overcoming of unfavourable places in the solid for formation of continuous "percolation" path between the electrodes [161]. In addition, the dc conduction may also originate in transport of free charge, i.e. electrons and holes.

Another parameter used for complementary analysis of dispersion is the imaginary part of dielectric modulus $\mathbf{M}''(\omega)$ (Fig.6.16, e and f). Even if the advantages and disadvantages of such data representation remain disputable, the log-log plot of this parameter apparently reveals the same transitional process that manifests itself in other representations. For the interpolation by power functions in the log-log scales, this representation, if it does not gain in precision, at least, makes visible some regularities in the dispersion curves plotted for various temperatures. The data points from the left of the $\mathbf{M}''(\omega)$ peak are interpolated by the straight lines parallel to each other, and the corresponding distances between the lines, measured on the frequency scale, also reflect an activation process characterized by distinctive activation energy (shown in the insets in Fig.6.16, e and f).

However, the analysis described above is hampered in some cases. For example, undoped sample of PZT (58/42) ceramics has demonstrated an ambiguous dispersion of absolute dielectric permittivity (Fig.6.17,a). The fact is that the transition from one power law (the pseudo-logarithmic one at very high frequency) to another power law of nearly-conductive response (characterized as $\sim 1/\omega^{-1}$) is passing through the third relaxation process vanishing at higher temperatures. The origin of this process is unknown and available

experimental data in characterized frequency and temperature ranges are not enough to study it in detail. Another sort of difficulty in interpretation arises from the proximity of ferroelectric phase transition when transitional frequencies are observed near the Curie temperature. This is a case in soft ceramics, an example is shown in Fig.6.17,b. At the frequencies where response is mostly dielectric, the temperature influence is more significant when approaching the phase transition point. As a result, the activation of the transitional process gives a high value of activation energy as much as ~3.28 eV for 1% Nb doped soft PZT (58/42) ceramics, which might be incorrect. Note, also, that relevant points in the Arrenius scale are not well fitted by the straight line (see the inset in Fig.6.17,b). The low frequency part of responses, nevertheless, demonstrates behaviour of nearly conductive type. The transitional frequency obtained from $\mathbf{M}''(\omega)$ analysis and evaluated dc conductivity have revealed an activation processes characterized by the same activation energy value (~ 1.76 eV) (Fig.6.18).

Figure 6.17. *Characterization of the undoped (a) and 1.0 at.% Nb-doped soft (b) PZT (58/42) ceramics. The frequency dispersion of dielectric permittivity for various temperatures. Insets show the temperature dependence of transition frequency in the Arrenius scales.*

It is interesting to compare the frequency and temperature dependence of the $\omega\varepsilon_0\tilde{\varepsilon}''$ parameter, associated with ac conductivity, for hard (Fig.6.16,c,d) and soft (Fig.6.18,b)

ceramics. In hard ceramics, the frequency dependent conductive-like process takes place and manifests itself as "plateau" in the frequency dispersion plot, which is almost (but not perfectly) a horizontal line (e.g. Fig.6.16,d). In soft ceramics, this horizontal segment appears sharply and has no slope (e.g. Fig.6.18,b), which means that in soft ceramics the frequency dependent process of hopping charge carriers does not occur most likely, and the dc conductivity originates in transport of faster charge carriers, most probably, electrons emitted by ionization of donor levels associated with Nb dopants in PZT.

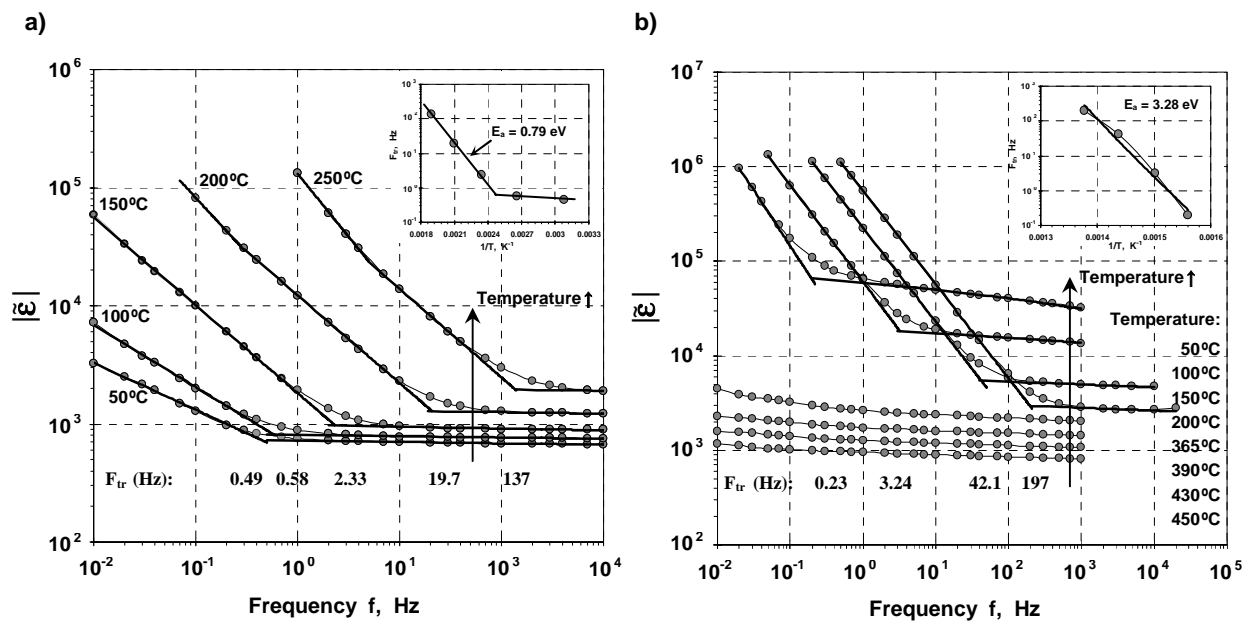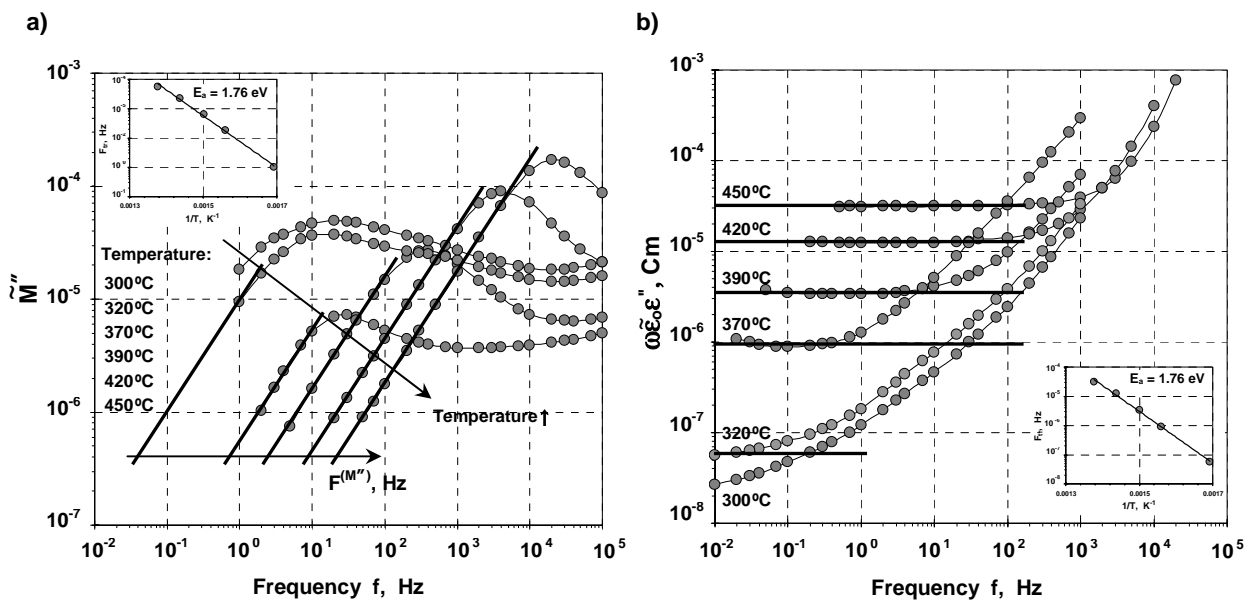**Figure 6.18.** *Characterization of the 1.0 at.% Nb-doped soft PZT (58/42) ceramics. The frequency dispersion of dielectric modulus (a) and conductivity (b) for various temperatures. Insets show the temperature dependence of transition frequency in the Arrenius scales.*

The study of the frequency dispersion of the material response is summarised in Fig.6.19 that shows the curves corresponding to conduction processes in the investigated ceramics and related activation energies. Arrenius plots for σ_0 and for hopping conduction transitional frequencies are shown in Fig.6.19,a,b. The corresponding activation energies as functions of the dopant concentration are shown in Fig.6.19,c,d.

The dc conduction activation energy of soft ceramics is found to be about two times higher than the one in hard ceramics. The activation energy of dc conduction decreases slightly with increase of dopant concentration in both cases. In hard ceramics, the activation

processes resulting in transition of frequency dispersion from dielectric type to the hopping conduction are slightly dependent on dopant concentration; the activation energy increases with increase of dopant concentration and is found to be smaller than activation energy of dc conduction. It is in agreement with the general statement that ac conduction must have smaller activation energy than dc conduction, as concluded in the review paper [161].
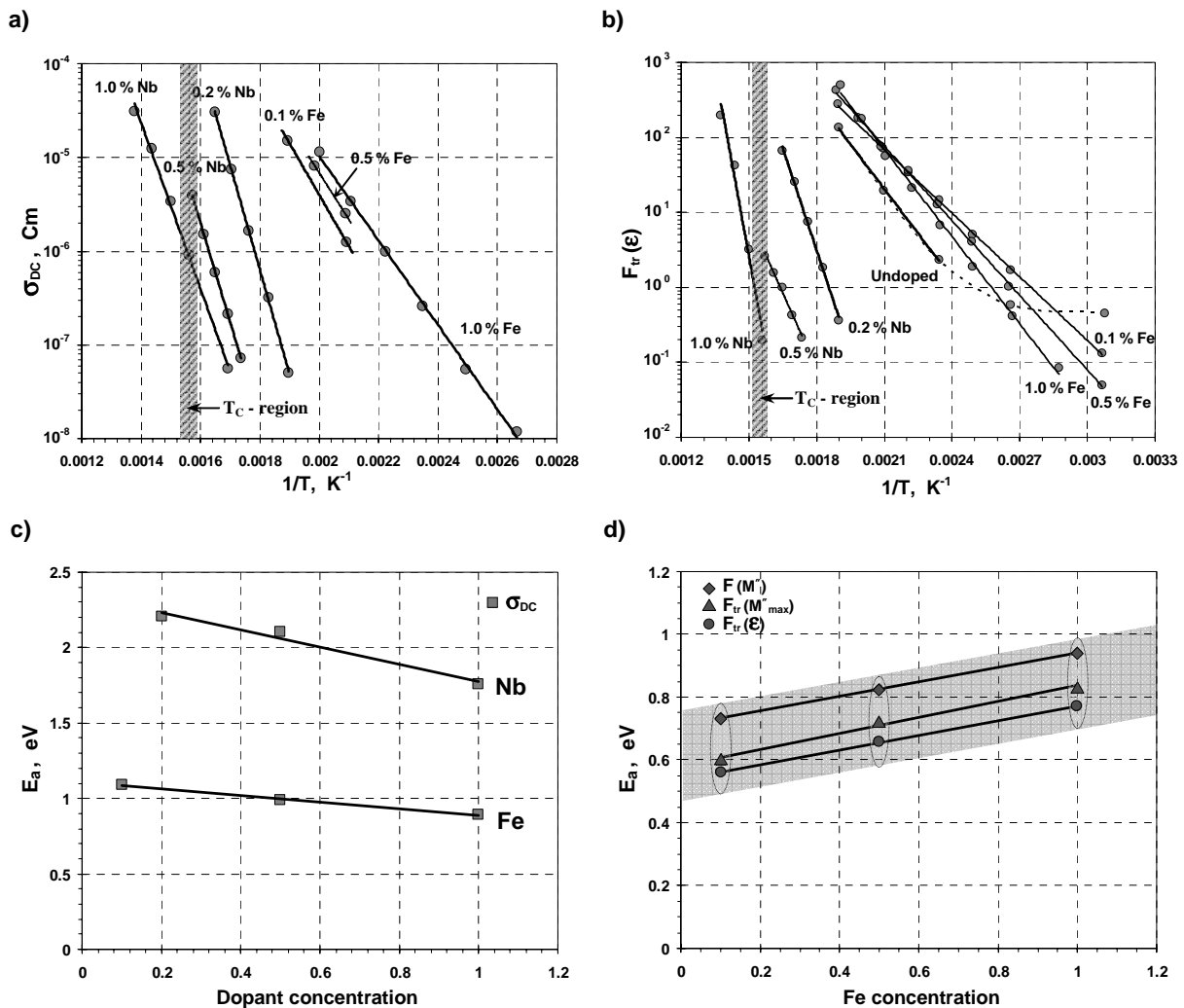
Figure 6.19. *Summary of dielectric relaxation processes in hard and soft PZT (58/42) ceramics: (a) temperature dependence of evaluated dc-conductivity; (b) transition frequency determined from $|\varepsilon|(\omega)$ curves; (c) activation energy of dc conductivity versus dopant concentrations in hard and soft ceramics; (d) activation energy of transition frequencies evaluated by various methods versus dopant concentrations in hard ceramics.*

The presence of charge carriers hopping mechanism in the hard ceramics and its absence in the soft ceramics in the near-room temperature region (50…150 °C) is a very significant feature of these materials, which may explain other phenomena coming in different ways for hard and soft ceramics such as ageing [101,164]. The direct establishment of the exact type and origin of hopping charge carriers cannot be based on this analysis and requires additional study. There is relatively little information in the literature that would be helpful in this issue. In some studies of conduction mechanisms, in particular ferroelectrics, the conducting carriers are specified. In the early study of conduction mechanisms in $BaTiO_3$ single crystal and ceramic [165], the conduction transport is specified as following: ionic conduction occurs near 100°C in single crystals containing Fe_2O_3 while electronic conduction predominates in "pure" crystals from 100°C to 600°C; ceramic samples conduct ionically at 100°C and electronically at 500°C. Similar behaviour is reported for modified strontium titanate. The acceptor-doped (Ni) $SrTiO_3$ ceramic quenched from high-temperature equilibria, investigated in [166], has shown strong indication for a predominant ionic conduction based on oxygen vacancies as mobile species for a broad range of oxygen partial pressure (10^{-11} – 10^5 Pa); the temperature dependence of the ionic conductivity reveals an activation energy of 1.0 to 1.1 eV for the diffusion of oxygen vacancies. Similar analysis made on single-crystal of $Ba_{0.03}Sr_{0.97}TiO_3$ with no detectable impurities revealed the electronic transport behaviour [167]. Those examples cannot, a priori, be assumed to be valid for modified PZT ceramics; however, representing the perovskite ferroelectrics, they can serve as a relevant reference.

6.3. **Summary**

The dielectric properties of hard and soft PZT ceramics have been studied in detail under subswitching conditions using frequency scanning dielectric spectroscopy and harmonic analysis methods. It was shown that the polarization response of soft ceramics can be approximated by the model based on Rayleigh relations. The polarization response of hard ceramics approaches the nonlinear anhysteretic behaviour predicted by the model based on a V-potential profile for the domain wall energy. With higher concentration of iron dopant, when the displacement of domain wall is small, the polarization response is almost linear, which may also be described by V-potential in the smeared region. Analysis of the

polarization nonlinearity and subswitching hysteresis suggests that soft materials can be described by a relative disorder of pinning centres for the domain wall, while behaviour of very hard material indicates strong ordering of pinning centres. The polarization nonlinearity and hysteresis are very sensitive to the state of ordering of pinning centres as demonstrated by quenching experiment. Hard ceramics with thermally disordered state of pinning centres behave qualitatively as soft material.

The frequency dispersion of the dielectric permittivity in thermally quenched hard ceramics is found to be intermediate between ones in an aged hard ceramic and in a soft ceramic. This suggests that the frequency dispersion of the dielectric permittivity in PZT ceramics is mostly of extrinsic origin and becomes more apparent when the irreversibility of domain wall movement increases. This is also consistent with the theoretical description of an irreversible creep-like viscous motion of domain wall given in the literature.

Analysis of the dielectric frequency dispersion in hard and soft PZT ceramics over a wide range of temperatures has revealed the profound presence of hopping conductivity in iron doped PZT ceramics below the Curie temperatures and its absence in niobium doped PZT ceramics. Investigations of bulk conductivity in other ferroelectric ceramics reported in literature strongly indicate the presence of mobile oxygen ions in acceptor-doped ferroelectrics. This and other observations mentioned above permit one to suggest that hopping charged species revealed in PZT ceramics are mobile oxygen ions which play a major role in hardening of ferroelectric by a collective electrostatic interaction with the domain walls. The concept of the ordering-disordering of charged defects interacting with the domain wall is in a good agreement with the experimental results.

Chapter 7

Study of polarization hysteresis at switching conditions.

In this chapter, the detailed study of polarization response to electric field of amplitudes close to or higher than the macroscopic switching field is provided for hard and soft PZT ceramics. The systematic study through analysis of the variety of distinctive effects leading to the specific forms of ferroelectric hysteresis loop has been performed in order to understand better the distinguishing factors leading to harder and softer ferroelectric response. The study is subdivided into sections in accordance with the factors governing transformation of the hysteresis loop.

7.1. Hysteresis in hard and soft ceramics – effect of composition

The effects of dopants and modifiers on switching properties of PZT ceramics has been reported since the beginning of their piezoelectric and other applications [8]. As a matter of fact, many experimental studies indicate that donor-type impurities, causing formation of vacancies in cation sites of the crystal lattice, transform the switching properties of material towards lower coercive fields and higher remanent polarization, i.e. lead to relatively rectangular form of polarization loop. Contrary, acceptor-type impurities, causing creation of oxygen vacancies, depress the polarization loop [8]. These effects of modifiers have very significant importance for the ceramics applications since they offer means for improving the properties of materials in a desirable way – either to soften the

switching, or, contrary, by hardening, to reduce hysteresis and nonlinearity. The latter, hardening, effect is usually considered as a result of ageing, whose mechanisms are still disputable and reviewed in sections 2.4 and 2.5, while the detailed mechanisms of softening effect are still not well understood.

The $Pb(Zr_{0.58}Ti_{0.42})O_3$ ceramics doped with iron or niobium as hardening and softening modifiers demonstrate a profound effect of dopants (depending on their type and concentration) on the shape of the P-E hysteresis loop (Fig.7.1). The changes in response are well pronounced already with very small concentration of modifiers (Fig.7.1,b). The response of samples doped with 0.5 at.% and with 1.0 at.% of Fe or Nb, in both cases are almost indistinguishable (not shown), so the effect of compositions is localized mainly in 0.0 to 0.5 at.% of dopants, the higher concentrations do not enhance the effect.
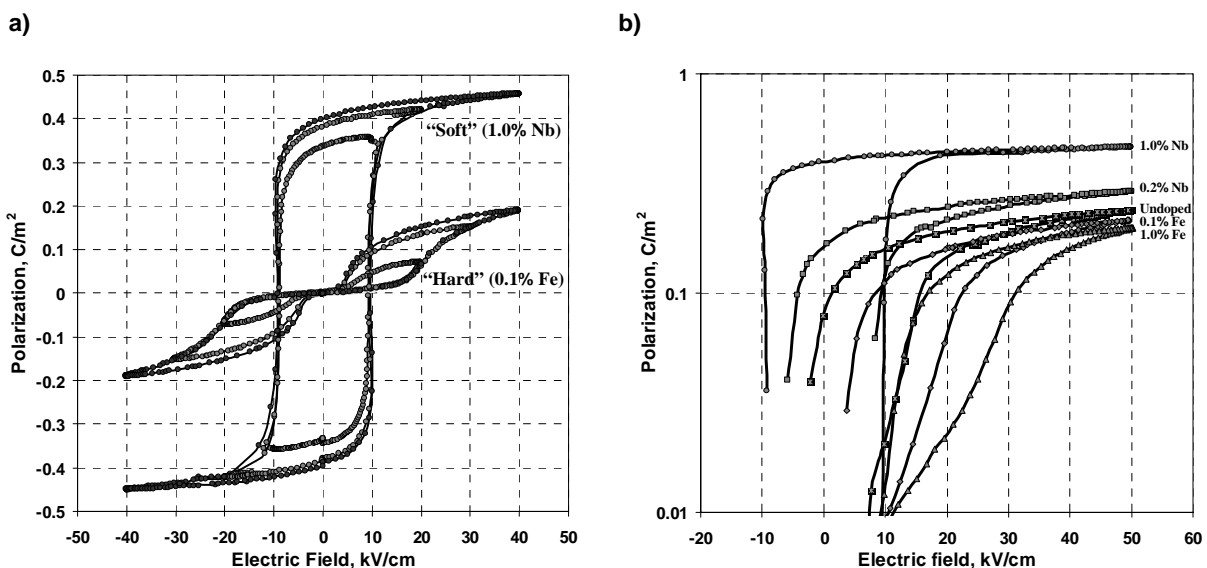
Figure 7.1. *Ferroelectric hysteresis loops for hard and soft PZT (58/42) ceramics.*

The effect of hardening also changes with the change of the Zr/Ti ratio (Fig.7.2). Two effects occur here: one is the decrease of the remanent polarization of PZT ceramics with increase of titanium concentration near the morphotropic phase boundary in general, with or without dopants [8,112], and the second is hysteresis loop constriction that is more pronounced in the rhombohedral phase. In the view of ageing and deageing mechanism of hard ceramics due to electrostatic arrangements of charged carriers and the hopping mechanism of their mobility (discussed in section 6.2), it is interesting to note, through

comparison Fig.4.10 and Fig.7.2, the correlation between the shape of the hysteresis loop and the frequency dispersion of the dielectric permittivity of hard ceramics in various regions of the PZT phase diagram near the morphotropic phase boundary. The higher mobility of charge carriers in tetragonal ceramics is accompanied with weaker constriction of the hysteresis loop. Another effect that may also play a role is the difference in mutual orientations of the dipoles formed by charged defects and the direction of polarization in domains. In tetragonal and rhombohedral phases of PZT the polarization vectors are oriented along different crystallographic directions (**[001]**[*] in tetragonal and **[111]**[**] in rhombohedral), while possible orientations of dipoles are defined only by positions of defects in the crystal lattice (e.g. **[001]**[*] for **[Fe$_{Ti}$-V$_O$¨]** dipole associate). Therefore, the mutual orientations of polarization and dipole vectors are different in the rhombohedral and tetragonal phases as well as the interactions between them. The effect of domain wall pinning by collectively oriented microdipoles, if one dominates, should principally depend on the mutual orientations of domain polarization and polarization of dipoles.
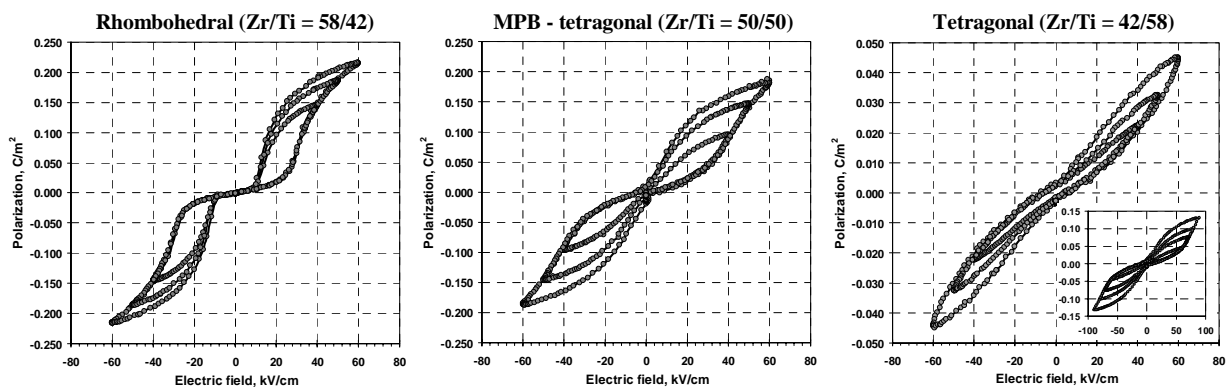

Figure 7.2. *Ferroelectric hysteresis loops of the hard (0.5 at.% Fe doped) PZT ceramics with various Zr/Ti ratios near the morphotropic phase boundary.*

---

[*] i.e. one of six equivalent cubic directions
[**] i.e. one of eight equivalent cubic directions

7.2. Hysteresis activation – effect of electric field amplitude

Hysteretic responses of hard and soft ferroelectrics under the switching conditions are well known and widely described in the literature, while there are very little experimental results distinguishing behaviour of hard and soft materials under subwitching conditions, especially at transitional fields linking the subswitching and switching properties of materials [40,72,168]. In this section the analysis of polarization response in hard and soft PZT ceramics will be focused on the region of electric fields where transition to macroscopic switching occurs.

An application of electric field of altering polarity to ferroelectric material causes the polarization response which becomes hysteretic when the field amplitude overcomes some threshold level and domain walls perform irreversible movements. The hysteresis loop formation and its further development with an increase of the electric field amplitude is very different for soft and hard ceramics. Some examples are shown in Fig.7.3. The first and apparent difference is the amplitude of threshold field of hysteresis opening. For very soft ceramics this field is below 1 kV/cm while for very hard one it is about 10 kV/cm (Fig.7.3, a and b). For intermediate compositions this difference is vanishing though (Fig.7.3, c and d).

The macroscopic switching in very soft ceramics occurs drastically at electric field amplitude 8...10 kV/cm; at this field polarization response transforms from Rayleigh-like to almost rectangular hysteresis loop shape (Fig.7.3,e). In very hard ceramics the development of hysteresis loop is not that dramatic with increasing applied electric field amplitude; the threshold field is about 20…30 kV/cm (Fig.7.3,e). Interestingly, in example, shown in Fig.7.3, d and f, the hysteresis nucleates at the edges of the loop but not in the middle, and the loop constriction has remained at all range of applied fields up to the breakdown amplitudes. In the following the experimentally observed results are briefly discussed considering the models and approaches outlined in chapters 2 and 3.
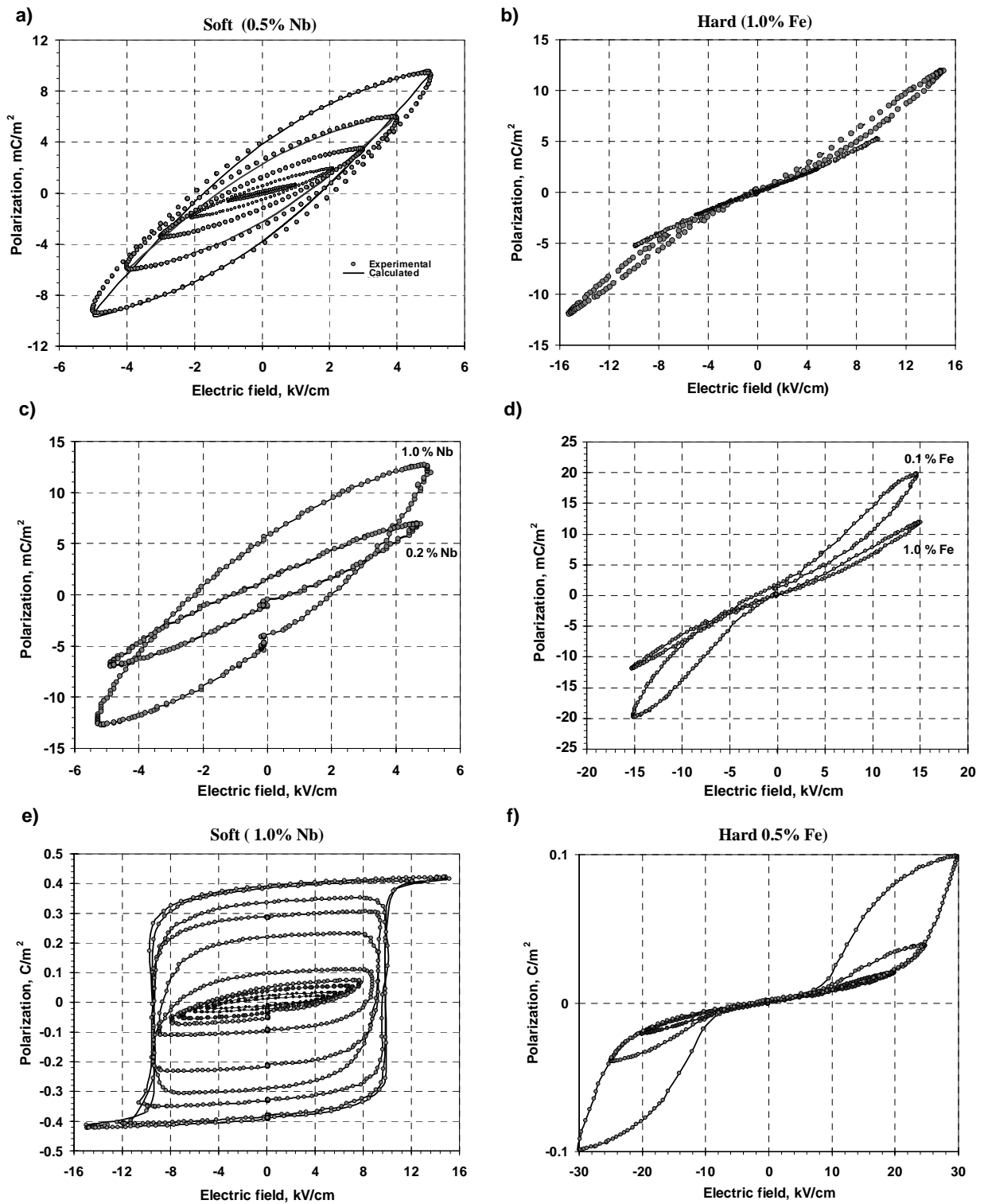
Figure 7.3. *Ferroelectric hysteresis loops for hard and soft PZT (58/42) ceramics – hysteresis loop formation at switching and subswitching conditions.*

The hysteretic response of soft and hard ferroelectric system can be analyzed using the Preisach approach described in section 2.2. However the current states of descriptive models for hard and soft phenomena are not equal in the levels of understanding. As it was mentioned above, the phenomenon of softening is still not well understood in the aspect of stronger nonlinearity and hysteresis of polarization response with respect to the idealistic Rayleigh model. However, the observed deviations are rather insignificant and qualitative agreement of subswitching polarization response in soft ferroelectrics with the Rayleigh relations holds (see chapter 6). The complete phenomenological model of transition from Rayleigh response to rectangular form of hysteresis loop has been developed in terms of Preisach formalism first for ferromagnets [40] and then adapted to ferroelectric systems [19-21]. In these models the evolution of hysteresis loop with a rise of driving field amplitude is described by high order terms of polynomial development of distribution function (2.11) or (2.12). For a pinched hysteresis loop inherent to some hard ferroelectric material, the shape of distribution function outlined in [19] or a forth order polynomial (2.13) proposed in [24] serves as possible and appropriate mathematical model matching both experimentally observed hysteresis loops and one of ageing scenarios considering the pinching effect due to oriented dipoles. Use of a more realistic distribution function such as one combining two superimposed Gaussian functions does not easily yield an analytical result of polarization response. The use of this approach for building a model that would describe also the evolution of hysteresis loop is outlined in [19,24] but not yet developed.

Approaches to develop an improved ageing model for hard ferroelectrics by the harmonic analysis proposed in [141,142] and briefly outlined in section 5.2., can be considered only as an informative tool of detailed analysis of the response aspects. One of the main difficulties of this approach is inadequate fitting of real response by a limited number of low term harmonics. It is possible to show that limited number (**2n-1**) of terms in polynomial expansion (5.16), representing an arbitrary polarization response, gives in corresponding Fourier series **n** odd in-phase components (up to **2n-1**[st] harmonic), describing the anhysteretic core of the loop, and infinite number of out-phase odd harmonics, entirely describing the hysteretic part. Thus, monitoring the behaviour of in-phase and out-phase components is useful for analysis of nonlinearity and hysteresis evolutions. Fitting of ascending and descending branches of real pinched hysteresis loop by 6-order polynomial gives two branches quantitatively very close to the structure of polynomial (5.16), but,

apparently, the order of used polynomial is still not high enough to provide requisite curving to match well the experimental data (Fig.7.4).
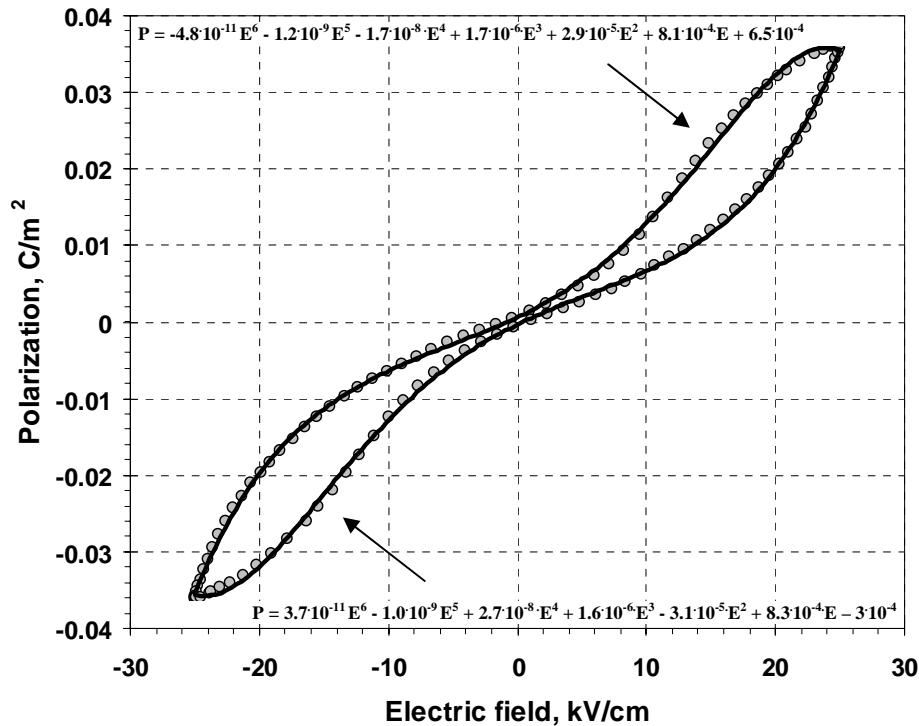
Figure 7.4. Ferroelectric hysteresis loop of hard sample: experimental data obtained on aged Pb(Zr$_{0.58}$Ti$_{0.42}$)$_{0.99}$Fe$_{0.01}$O$_3$ ceramics (dots) and polynomial interpolation of the ascending and descending branches (solid lines and equations).

The model considering the randomisation of V-potential energy profile with applied electric field by trapping the wall in some local potential minima (see chapter 3) is in a good qualitative agreement with observed experimental results. The nucleation of hysteresis on the edges of loop indicates that the randomisation of potential energy profile begins not from the minimum of the V-potential, but somewhere at periphery (Fig.3.3). It corresponds to the following scenario: in hard ferroelectric, the domain wall pinned by defects performs the reversible movements under applied electric field unless the amplitude of the field is enough to displace domain wall as far as the nearest trapping centre location, which results in a local irreversibility of domain wall. When the applied field is removed, the domain wall returns back to its initial position by the restoring force exerted by electrostatically arranged charge carriers. The presence of nearest trapping centers located on hearabout the path of the

domain wall can be attributed either to regular defects distribution or to introduced randomness by perturbing influence of ac field on electrostatic arrangement of charged defects or microdipoles associated with them.

In summary, the difference of hysteresis loop formations in the form and threshold fields are shown for hard and soft PZT ceramics. The activation of hysteresis at periphery of the loop in hard PZT ceramics is consistent with the concept of field activated transition for the domain wall motion from movement in a medium of pinning centres with the global order to movement in a medium of pinning centres with a partial disorder.

7.3. Hysteresis in thermally quenched ceramics – effect of thermal treatment.

The effect of thermal quenching of hard ferroelectric ceramics on polarization nonlinearity and subswitching hysteresis has been discussed in section 6.1. It was shown that thermally quenched hard ceramic behaves qualitatively as soft material. That transition can be interpreted as disordering of pinning centres resulting in randomization of the energy profile for a domain wall motion. Further investigation revealed the presence of charge carriers whose current is thermally activated and results in a jumping conduction in the hard PZT ceramics. Yet, in soft PZT ceramics no conduction was detected almost up to the Curie temperature. Apparently, the stabilization of domain wall pattern in the hard PZT ceramics can be caused namely by those charge carriers who provide the hopping conductivity in the hard ceramics. This, in combination with other observations, including experimental results reported in the literature, permits one to attribute the transition in hysteresis response to the effect of oxygen vacancies disordering caused by thermal quenching. It is also known from the literature that the thermal quenching effect manifests itself similarly under switching conditions, i.e. the hysteresis loop of a hard ceramics cooled from above [77,107,169] or even below [170] the Curie temperature is qualitatively similar to one of a soft ferroelectric. In the following experiment, it will be shown, that gradual transformations of the hysteresis loop between the hard and soft states in the iron-doped PZT can be controlled by the rate of cooling from above the Curie temperature down to the room temperature.

Owing to fast cooling, some diffusion processes, whose rates significantly depend on temperature, are hindered; hence, the quenched ceramics will be in metastable state during the certain period of time that is necessary for diffusion at room temperature. Below the Curie temperature, in the ferroelectric state, the domain pattern is established, and the mobile charge carriers or their dipole associates occupy the most favourable positions according to electrostatic charges and field distributions within the domains. The various degrees of domain pattern stabilization and, as a result, degrees of the hysteresis loop constriction in hard ceramics with respect to different rates of samples cooling are shown in Fig.7.5,a. The cooling rate has been controlled by using various substances in contact with the sample preheated up to 480 °C. The fastest cooling was provided by quenching in water (thermal conductivity ~ 0.60 W/Km); a slower cooling rate is expected for quenching in acetone (thermal conductivity ~ 0.19 W/Km); in open air (thermal conductivity ~ 0.02 W/Km); within the furnace (very slow cooling). The experiment clearly demonstrates that slower cooling of hard ceramics results in stronger pinching hysteresis loop. This effect is also observed in the undoped PZT ceramics but it is much less pronounced (Fig.7.5,b), while for the soft ceramics no effect of thermal quenching on the hysteresis loop geometry has been observed (Fig.7.5,c). The latter fact is in a good agreement with the analysis of dielectric response at various temperature and frequency ranges, suggesting that no hopping conductivity occurs in soft PZT ceramics (section 6.2).
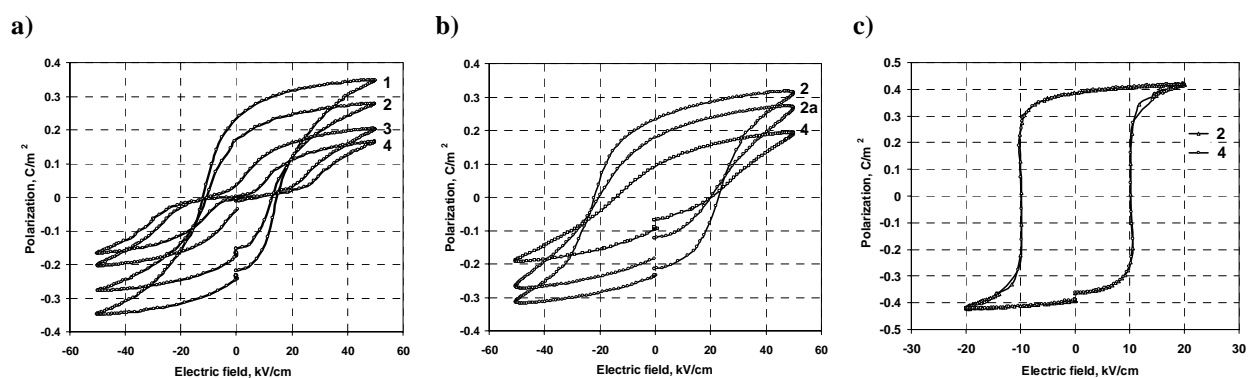
Figure 7.5. Ferroelectric hysteresis loops of (a) hard (doped with 1.0 at.% Fe), (b) undoped, and (c) soft (doped with 1.0 at.% Fe) PZT (58/42) ceramics experienced the thermal treatment at 470 °C and cooling at various conditions: 1 – quenching in hot water (70 °C); 2 – quenching in acetone (at room temperature); 2a – 48 hours after quenching in acetone; 3 – cooling in the open air (at room temperature); 4 – slow cooling within the furnace (down to the room temperature).

The ordered and disordered states of the pinning centres assumed in aged and thermally quenched hard ceramics suggest an approach to build a model of polarization response by considering free energy of a domain wall as a function of its displacement (Fig.7.6). For the domain wall subjected to very strong pinning, the V-potential energy profile or its smeared version described by Eqs. (3.1) - (3.2) can be considered. The effect of the electric field amplitude described in the previous section leads to randomization of potential energy due to one of two possible processes: either domain wall displaces far enough to approach the nearest existing pinning centre that traps it locally and temporary or the trapping pinning centres are formed by electrostatic rearrangement of charged defects and associated dipoles under applied external field. The pinched hysteresis loop corresponds to the described case (Fig.7.6, left). If the collective pinning of domain wall by mobile charge carriers has been prevented by thermal quenching or has never existed due to deficit in mobile charged carriers (suspected in soft PZT ceramics), the random potential profile can be considered for a domain wall in disordered pinning centre media. The Rayleigh-like hysteresis loop corresponds to this case (Fig.7.6, right). Intermediate cases are possible as well (Fig.7.5, a and b). The experimental ferroelectric hysteresis loops are in good qualitative (for aged hard PZT) and quantitative (for quenched hard PZT) agreement with the described model (Fig.7.6, e and f).

In summary, the observed gradual transformation of hysteresis loop in hard PZT ceramics, depending on the rate of their cooling from temperatures above the Curie point, strongly indicates on the link between the state of electrostatic arrangement of defects and the randomness of domain wall potential energy. This link is used in the model considering the hardening – softening transitions in ferroelectric ceramics in terms of the steepness and randomness of the domain wall potential energy profile. The experimental results thus give support to the model's main premise that the degree of order in the electrostatical arrangement of defects, controlled by thermal treatment of PZT ceramics, may, apparently, define the shape of domain wall potential energy.
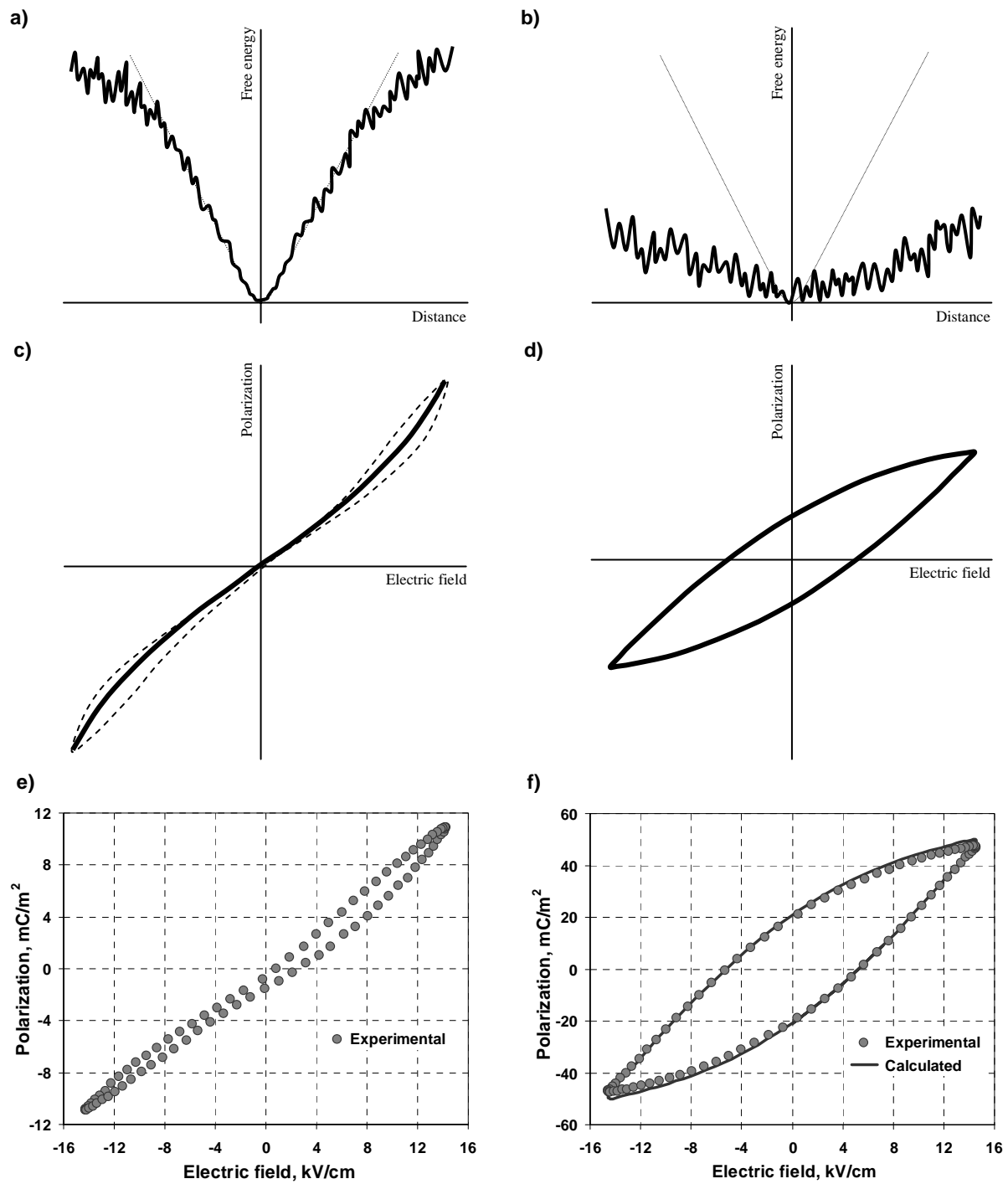
Figure 7.6. *Model of the domain wall contribution to the polarization response in ferroelectrics with ordered (left) and disordered (right) states of pinning centres: (a,b) domain wall free energy versus distance; corresponding P-E loops calculated using (c) model of smeared V-potential (Eq. (3.1) - (3.2)) and (d) Rayleigh model (Eq. (5.14)); experimental hysteresis loops obtained at 1 kHz driving field on (e) aged and (f) thermally quenched $Pb(Zr_{0.58}Ti_{0.42})_{0.99}Fe_{0.01}O_3$ ceramics.*

7.4. Time effects – ageing, "deageing", and fatigue

The effects of continuous disappearance of the hysteresis loop constriction on repeated cycling of unpoled hard aged ceramics is well-known phenomenon. The first detailed study of this effect on hard PZT ceramics has been described in [79]; by analogy with similar phenomenon in ferromagnetic materials [171], the effect is called "hysteresis relaxation". The experimental evidence of this effect is shown in Fig.7.7. At room temperature, a very hard ceramic demonstrates very slow effect of hysteresis loop relaxation; one has been observed after long cycling time (more than 10 hours) at relatively high frequency (1 kHz) and high amplitude (about 25 kV/cm) of driving electric field (Fig.7.7,a). At higher temperatures the rate of hysteresis loop releasing is faster due to the thermally activating nature of the phenomenon [79]. As shown in Fig.7.7,b, the measurement of hysteresis loop performed at 10 Hz frequency reveals (Fig.7.7,b) non-constricted hysteresis loop at higher temperature already at the first minute of measurements, nevertheless, further opening of hysteresis loop towards the rectangular geometry is observed with cycling at 125 °C and 10 Hz (Fig.7.7,c).
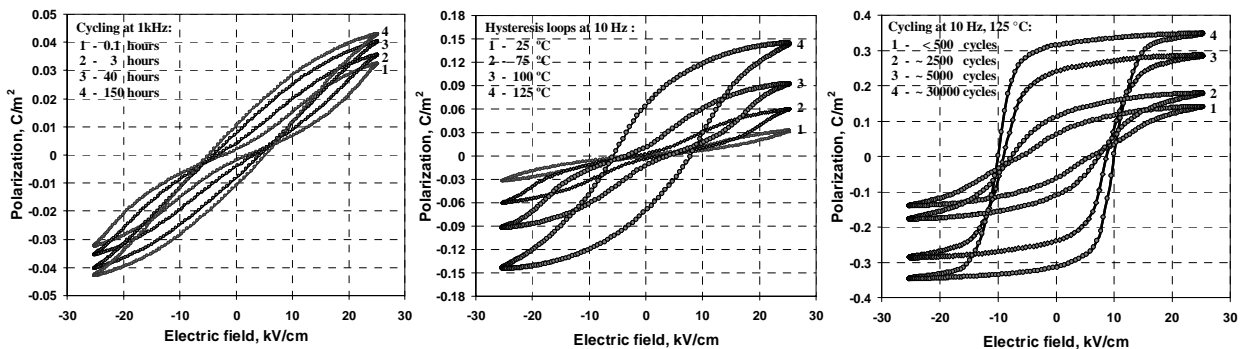
Figure 7.7. *Ferroelectric hysteresis loop relaxation observed in hard (doped with 1.0 at.% Fe) PZT (58/42) ceramics: (a) electric field cycling at high frequency (1kHz); (b) the thermal activation of hysteresis relaxation (characterized at 10 Hz ac field); (c) low frequency field cycling (10 Hz) at 125 °C*

In the discussion of the field amplitude effect on hysteresis loop nucleation in hard ceramics, two mechanisms of domain wall trapping have been assumed: 1) the existence of local pinning centres in a distance with respect to the initial domain wall position so that

under action of a certain threshold field, the domain wall reaches these pinning centres and gets pinned; 2) the formation of pinning centres for the domain wall path by the influence of the external electric field. The latter mechanism assumes either displacement of charge carrier from current pinning position to another one, or reorientation of dipoles associated with charged defects (the possible mechanisms of domain wall pinning are considered in detail in chapter 2). The second mechanism is more likely since the mobility of charge carriers is more evident at higher temperatures and it has been detected in hard ceramics as a hopping conduction with specific frequency dispersion (section 6.2). Hence, the displacement of charge carriers or the reorientation of dipoles associated with them, under an external electric field action may result in a transitional process from the initial electrostatic order, through local disorder, towards the global disorder. An example of possible potential energy profile transformation for this model is shown in Fig.3.3.

The hopping conduction, resulting from average charge carrier mobility, also reveals itself at low-frequency hysteresis characterization as a "leaking" loop with blunt edges (Fig.7.8).
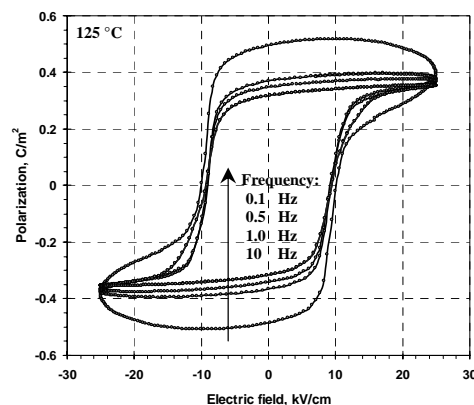
Figure 7.8. *Ferroelectric hysteresis loops of hard (doped with 1.0 at.% Fe) PZT (58/42) ceramics measured at various frequencies of driving field*

Another apparent effect of time is ageing. In the study of thermal treatment effects on polarization response, in the previous section, has been shown that stage of ageing (constriction of hysteresis loop) depends on the cooling rate from temperature above the Curie point. In the following, the effects of time with and without influence of electric field will be analyzed.

124

The ageing of hard ceramics quenched in liquid substances is relatively slow at room temperature (Fig.7.9,a). Therefore, the characterization of properties of ceramics in a quenched state is possible during several hours after quenching.

Figure 7.9. *Ferroelectric hysteresis loop evolution under influence of various factors on hard (doped with 1.0 at.% Fe) PZT (58/42) ceramics: (a) time effect on quenched sample (ageing at room temperature); (b) time and field effects on quenched sample; (c) time and field effects on aged sample. The time passed between first and last measurements is ~10^4 minutes.*

However, the degradation of the hysteresis loop in thermally quenched hard ceramics under continuous cycling by applied electric field at 1 kHz is dramatically stronger (Fig.7.9,b) than one without continuous cycling by ac field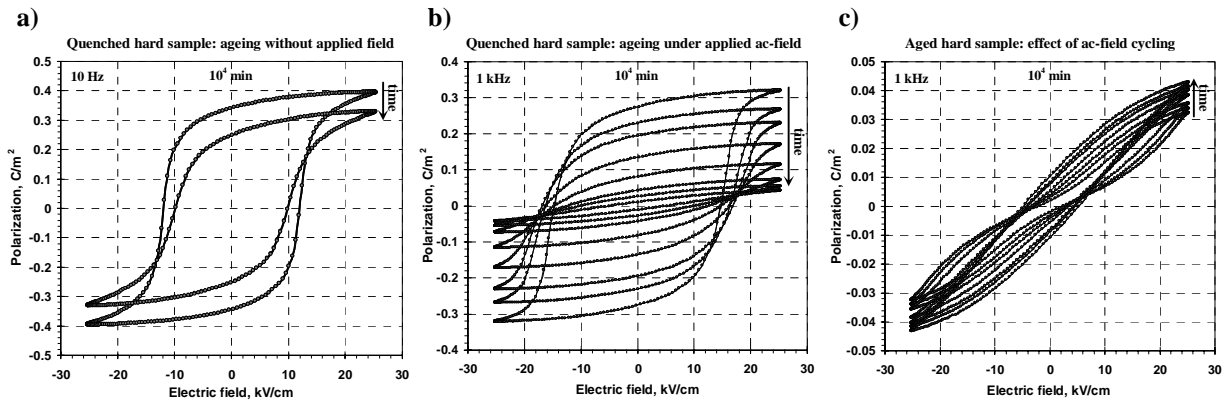 (Fig.7.9,a). For comparison, the results of electric field cycling during the same time period on hysteresis loop of aged hard ceramic sample of the same composition is shown in Fig.7.9,c. The last hysteresis loops measured on aged and quenched hard ceramics cycled under 1 kV/cm during long times are almost indistinguishable. That assumes an equilibrium state to which both ceramics reached after a certain time under electric field cycling, independently of their initial states. Since this state is not the result of only ageing effect for quenched ceramics, it is likely that it is not also the direct result of ac-field cycling effect. In other words, there is a third effect leading to loop degradation when the external ac-field is applied. Taking into account that an ac field at 1 kHz during 10^4 min assumes $6\cdot10^8$ cycles, the well known effect of fatigue [172-174] observed in many ferroelectrics under continuous switching can be considered as a good candidate for that interfering third effect. The deageing effect of electric field cycling without influence of fatigue is anticipated to lead towards the rectangular form of hysteresis loop like has been observed with electric field cycling at lower frequency but higher temperature Fig.7.7,c.

To ascertain the presence of fatigue in studying system of modified PZT, the response of the soft ceramic (known as one subjected to very slow ageing) was analyzed during its continous cycling by ac field of various amplitudes applied for a relatively long time. An example is shown in Fig.7.10.
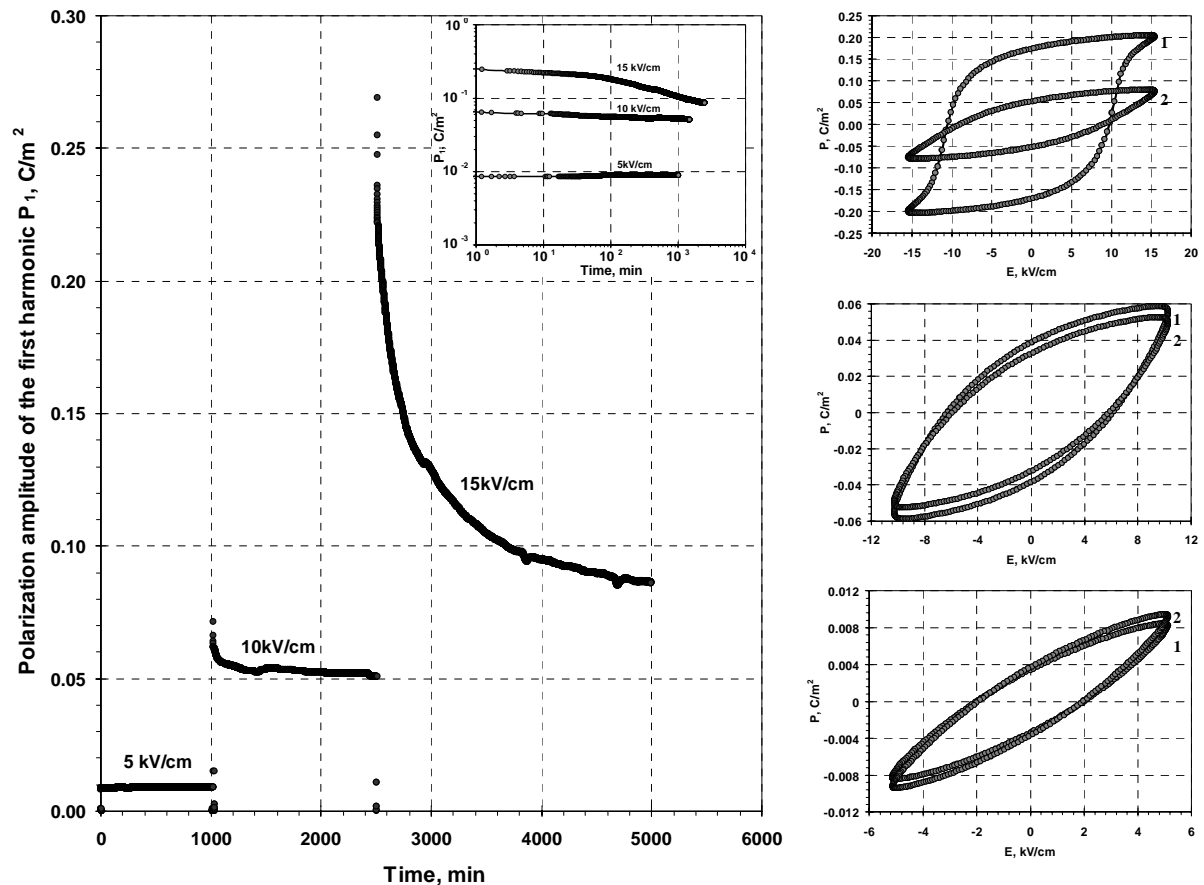
Figure 7.10. *Continuous periodic cycling of soft PZT ceramics by electric ac field at 1 kHz. Polarization response to various field amplitudes as a function of cycling time (left) and corresponding hysteresis loops at the beginning (1) and ending (2) of cycling for each amplitude of cycling field (right).*

The possible origins of the fatigue phenomenon are not discussed here, this brief study is only to establish and distinguish the complementary effect that at certain condition may interfere with experiments directed to study the ageing-deageing processes. As demonstrated by the soft ceramics, fatigue has been observed only in the range of switching fields (10 kV/cm and higher) (Fig.7.10).

It is interesting to compare the hysteresis loop of originally very hard (1.0 at.% Fe-doped) ceramic subjected to ac-field cycling at 125 °C with one of very soft ceramic sample. The difference is mostly apparent in quantitatively difference of 25-30% in the amplitudes of polarization response, while the form and coercive fields are almost equal in both cases (Fig.7.11,a). A relatively closed form of hysteresis loop is demonstrated by thermally quenched ceramics (Fig.7.11,b). It has been shown in the previous section that the form of the hysteresis loop revealed by quenched ceramics is approaching the rectangular shape with increase of the cooling rate.
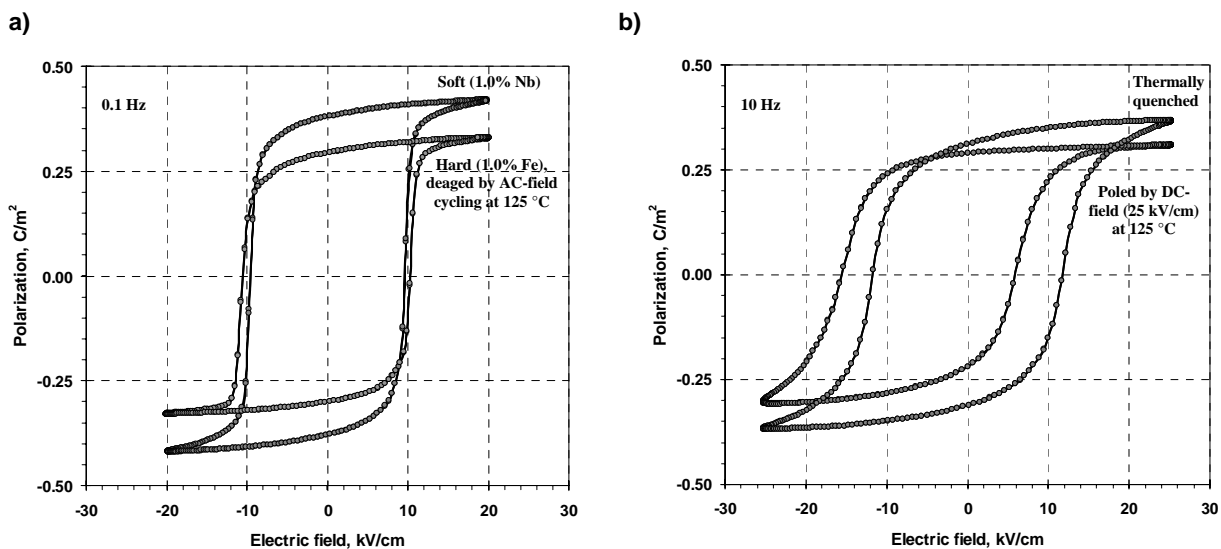
Figure 7.11. *Comparison of ferroelectric hysteresis loops: (a) soft (1.0 at.% Nb-doped)PZT (58/42) ceramics and hard (1.0 at.% Fe-doped) PZT (58/42) ceramics relaxed by ac field cycling at 125 °C; (b) thermally quenched and poled at dc field 25 kV/cm, 125 °C hard (1.0 at.% Fe-doped) PZT (58/42) ceramics. All loops are measured at room temperature.*

Surprisingly, the amplitude of polarization response to the external switching electric field increases about an order of magnitude and hysteresis loop approaches the rectangular form also after thermal poling of hard ceramics (Fig.7.11,b). The sample was poled by application of constant dc field (25 kV/cm) at 125 °C for about 10 minutes and, then, cooled down to the room temperature under the applied field. The experimental difference between poling and field cycling at 125 °C is only the field polarity, which is constant in the first case and alterng in the second case. As the result, the hysteresis loop of poled sample is shifted with respect to the symmetrical loop of quenched sample. There is a good reason to

think that the difference in polarization amplitude between well-aged and deaged ceramics at higher fields is much less than an order of magnitude, i.e. about 40-60 % only (Figures 7.1 and 7.5,a) due to the fact that in the aged ceramics the polarization response is dramatically sensitive to the switching field amplitude in the region of 15-40 kV/cm, while ceramics possessing rectangular-like hysteresis loop do not have this feature (Fig.7.3,e). Higher polarization amplitudes of deaged ceramics than in aged ceramics has also been observed in other aged ferroelectrics [79,169], however, as reported in a recent paper [107], the hysteresis loops in the aged and deaged states of Mn-doped $BaTiO_3$ single crystal have approximately equal amplitudes of polarization response to the same field amplitude. In that paper it is also shown that domain configuration is retained after a cycle of hysteresis loop measurement and is not retained in deaged samples, thus, confirming the bulk scenario of domain wall stabilization. Deageing in that work was provided by quick cooling from temperature above T_C; ageing, was provided by keeping deaged sample for two weeks at 80 °C. The manner of ageing, however, may be a crucial point in the dominating mechanism of domain pattern stabilization by the charged defects. Indeed, among mostly discussed scenarios, the domain pattern stabilization is provided by 1) orientation of dipoles associated with charged defects; 2) diffusion of charged defects towards domain walls; and 3) accumulation of charged carriers on the interfaces (grain boundaries). Considering oxygen vacancies as the charge carrier responsible for the effect, it is evident that only the first of the mentioned mechanisms assumes the jump distance of about one lattice parameter, others assume more extended diffusion. Hence, kinetically, these processes are not equal, and for arbitrary temperature, these processes occur with different rate that have an activated nature. The EPR observations of dipole alignment along the electric field direction in perovskite ferroelectrics made at 65 °C [93-95] and calculations of oxygen migration distances in PZT for room temperature in [100] confirms the "dipoles" scenario. However, other mechanisms can not be decisively rejected in all instances. When a sample is aged naturally at the processing stage during the slow cooling from sintering temperature, the diffusion processes at higher temperatures may extensively support other mechanisms of domain wall stabilization. Moreover, the higher Curie temperature is, the higher is the probability for diffusive process to dominate. From this point of view, the ageing mechanisms in $BaTiO_3$ and $Pb(Zr,Ti)O_3$ ceramics may be different but manifest themselves similarly.

One of the indications on the ambiguity of charge's role in ageing, fhich does not allow attributing the ageing process in favour of only one mechanism, is the discrepancy

between bias field revealed by aged unpoled and aged poled hard ceramics. The anticipated biased hysteresis loops for the poled and unpoled samples are shown in Fig.7.12 in comparison with the experimental result. The field-axis biasing of pinched hystereses of unpoled sample is as much as twice higher than one of poled sample. It means, at least, that not all the species participated in hystereses biasing in aged ceramic, manifest in loop biasing in poled ceramic. The detailed analysis of this phenomenon is complicated as the number of domain walls is changing with poling and, as a result, the depolarizing fields in ceramic are changing as well. In [79] this discrepancy between apparent biasing in hysteresis loops of aged and poled ceramics is attributed to a smaller number of domains and domain walls in poled sample, i.e. the reduction of non-180° domain walls being presumably decisive factor. On other hand, in the recent work [170] the autors, following their analysis of ferroelectric hysteresis loops obtained on $Pb[(Zr,Ti),(Mn,Nb)]O_3$ ceramics with various state of quenching, concluded that different mechanisms are expected to explain the aparent internal bias and the constriction of hysteresis loop.
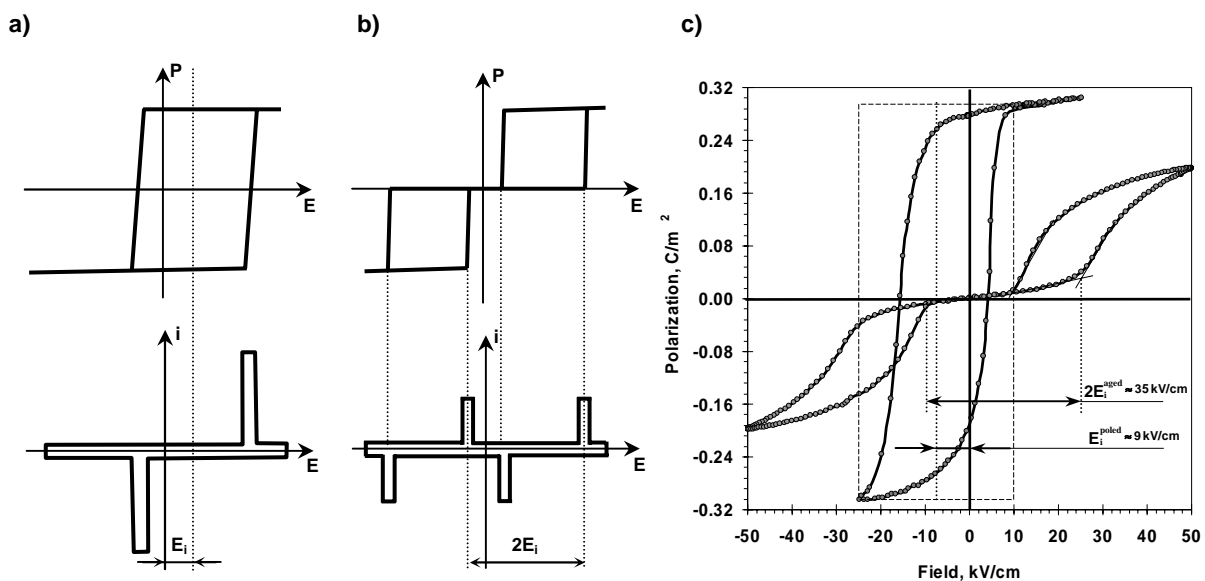
Figure 7.12. *Definition of the internal bias [79] : hysteresis loops and corresponding current curves for (a) poled aged and (b) unpoled aged ceramics; (c) the experimental hysteresis loops of hard (1.0 at.% Fe-doped) PZT (58/42) ceramics: in aged state and poled at 120 °C, 10 min, cooling down to the room temperature under applied dc field.*

The deageing process in hard PZT ceramics under cycling by electric field as well as its activation nature was shown in [79] by analysis of time that is necessary for apparent

disappearence of the initial constriction of the hysteresis loop at various temperatures. In practice, the main criterium for determining this time in [79] was the disappearence of four peaks in the current curves (they are shown schematically in Fig.7.12,b), and their merging into two peaks. This method, however, is not always convenient because the current peaks may not be well pronounced, especially in the merging region. In the following, the alternative criteria for monitoring the deageing process using the advantage of harmonic analysis will be proposed.

The evolution of the phase angles of the first nine harmonics of the polarization response is shown in Fig.7.13,a. It is remarkable that the entire evolution of the polarization response during cycling has manifested itself very distinctly in the third harmonic whose phase angle during certain transition time made a turn about 180°. Interestingly, the out-phase ratio between the first and third harmonics approaches with cycling value close to five as in the case of Raleigh behaviour (Fig.7.13,b). Whether this is a coincidence or a property of more general irreversible process has not been established yet.
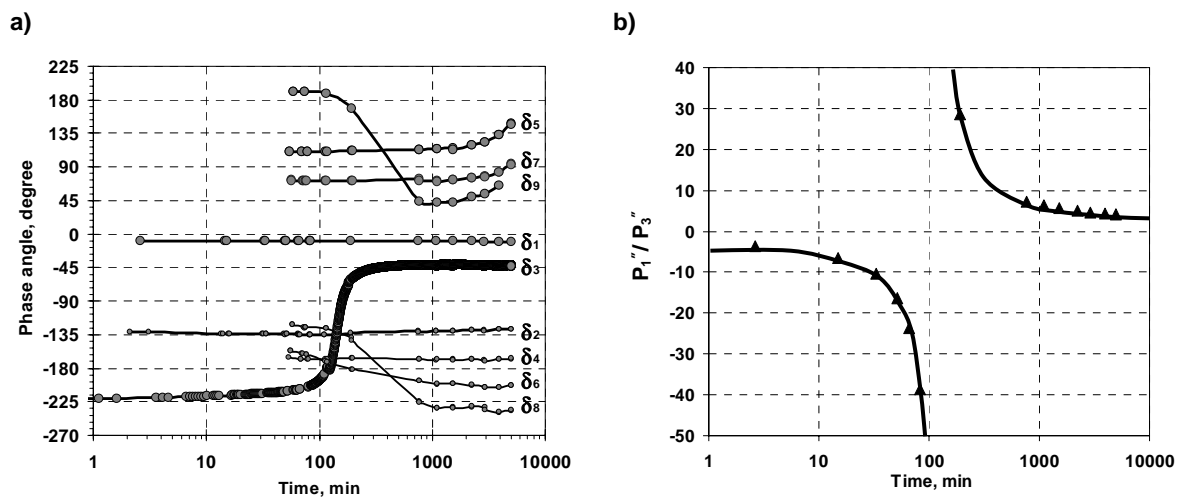
Figure 7.13. *Evolution of nonlinear parameters of polarization response during electric ac field cycling 1.0 at.% Fe-doped hard PZT (58/542) ceramics at 25 kV/cm, 1kHz: (a) phase angles of first 9 harmonics; (b) out-phase amplitude ratio between first and third harmonic*

The meaning of the third harmonic phase angle behaviour can be realized using illustrations shown in Figures 5.2 and 7.14. The relations between the geometry of hysteresis loop and the in-phase and out-phase components are discussed in section 5.2. For a pinched hysteresis loop, the out-phase component of the third harmonic is positive which contributes

to the compression of loop at zero field (Eq. (5.13)). When loop is depinched, the out-phase component of the third harmonic changes sign and corresponds to enhancing of the loop as shown in Fig.7.14. While evolution of the first harmonic (whose phase angle almost does not change during field cycling, Fig.7.13) corresponds to the expansion of the main core of the hysteresis loop, the evolution of the third harmonic reveals the "depinching process", as schematically shown in Fig. 7.14. The phase angle of third harmonic of polarization response changes angle from II to IV quadrant of the complex plane, so the contribution of the third harmonic evolves during field cicling in such a way that the geometrical proportions of the loop change in favour of the loop's middle part expansion.
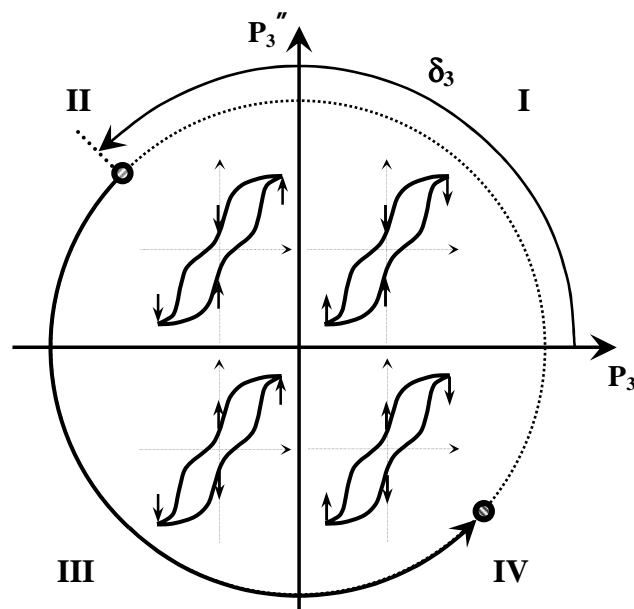
Figure 7.14. Illustration on the third harmonic contribution in total polarization response in different quadrants of the complex plane. Arrows show the suppressing or enhancing effects of the form of hysteresis loop. For details see also Fig.5.2.

The activation nature of deageing process by field cycling is shown in Fig.7.15. The time characterizing transitional process (τ) can be determined as the time when the phase angle δ_3 of the third harmonic of polarization response makes turn of about **180°** (Fig.7.15,a) or as the time corresponding to the crossing point of in-phase and out-phase components plotted as functions of time. In both cases τ strongly depends on temperature.
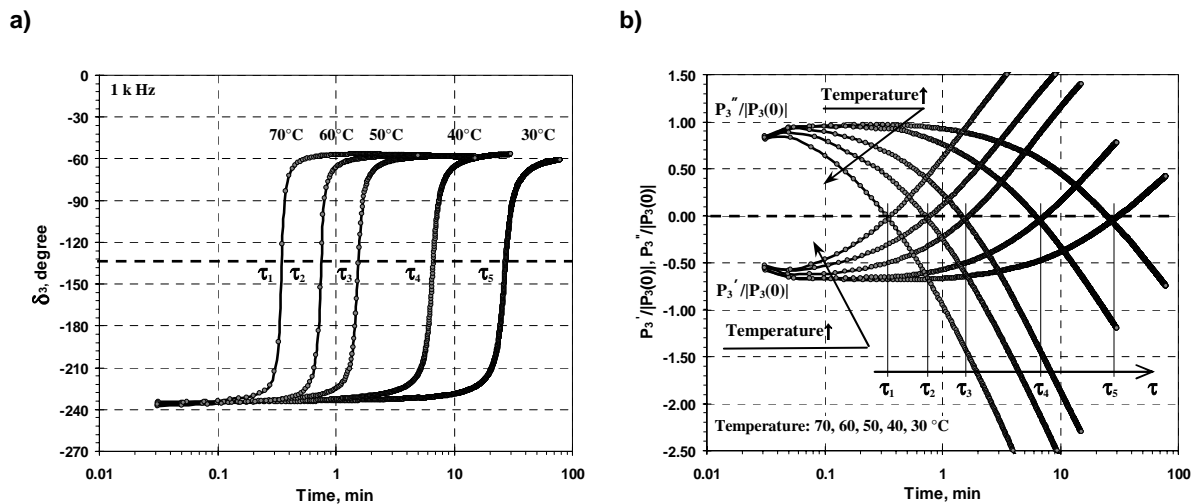
Figure 7.15. *Time dependence of the third harmonic component of polarization response of the hard (0.5 at.% Fe-doped) PZT (58/42) ceramics under ac field cycling (25 kV/cm, 1 kHz) at various temperatures: (a) third harmonic phase angle as a function of time and temperature; (b) evolution of the in-phase and out-phase components of the third harmonic of polarization response with respect to their initial values characterized at various temperatures*

The meaning of the cross-point of the in-phase and out-phase components, τ, can be defined as the moment of time at which the contribution of the third harmonic nonlinear component in total polarization response is switching from "pinching" to "depinching" the hysteresis loop, however, it does not correspond identically to any real physical process and it is used, in the following, as a convenient phenomenological parameter. To ascertain, that it is the time that characterizes the hysteresis relaxation process but not the number of cycles, the experiments have been performed at various frequencies. As shown in Fig.7.16, the effect of frequency and, hence, number of cycles is rather minor. The electric field amplitude has an effect on the relaxation time. As reported in [79], the relaxation time drops exponentially with increasing field. This observation has been made in the range of field examined **25…50 kV/cm**. In addition to that, the linear dependence of relaxation time has been observed in very hard ceramics in the field range **15…23 kV/cm** (Fig.7.17). The mentioned ranges of field amplitudes are relative and may vary depending on ceramic composition and temperature. Moreover, it is very unlikely that linear dependence of relaxation time holds down to zero field amplitude, since the finite relaxation time at zero field has no meaning, contrary, the ageing takes place. Nevertheless, the activation energies determined by temperature dependence of τ plotted in Arrenius scales are found to be different for different field amplitudes (Fig.7.18).
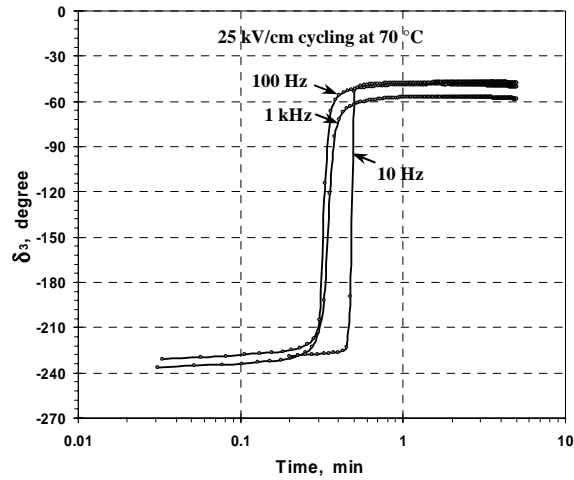
Figure 7.16. *Phase angle of the third harmonic of polarization response versus time for hard (0.5 at.% Fe-doped) PZT (58/542) ceramics cycling by electric field (25 kV/cm) at 72 °C with various frequencies*
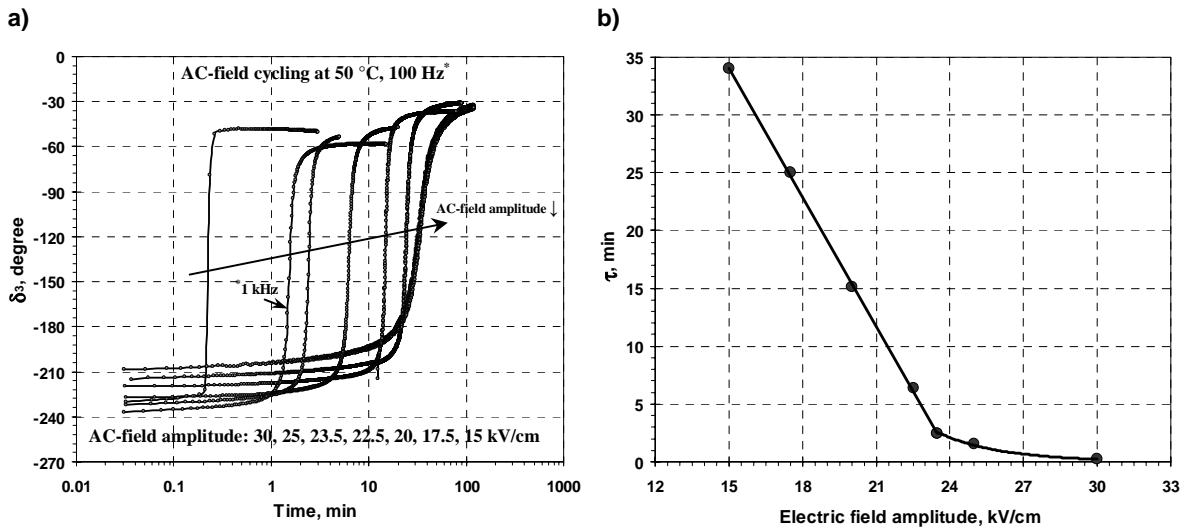
Figure 7.17. . *Phase angle of the third harmonic of polarization response versus time for hard (0.5 at.% Fe-doped) PZT (58/542) ceramics cycling (at 50 °C) by ac electric field of various amplitudes (a) and electric field amplitude dependence of the transition time (b).*
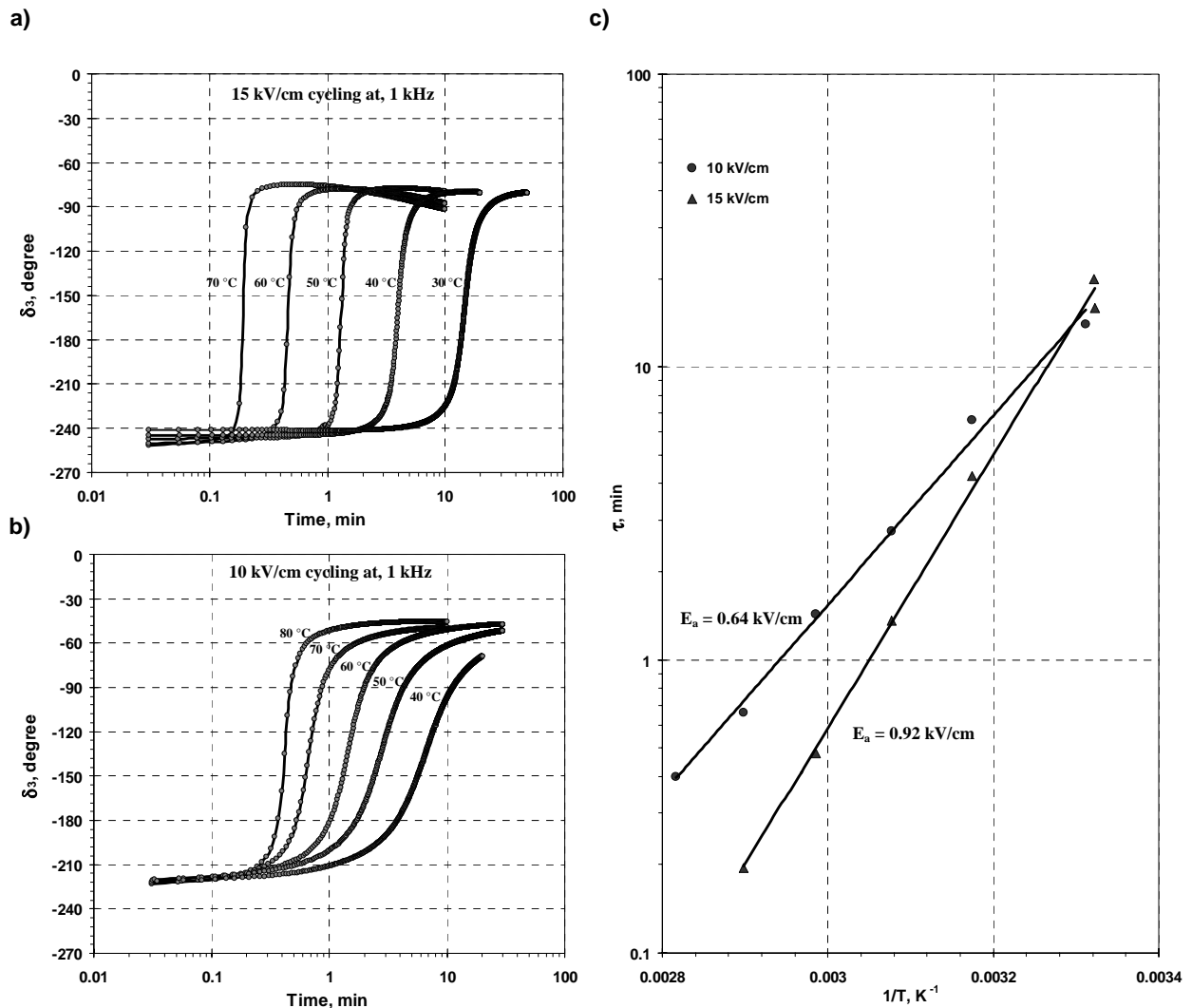
Figure 7.18. *Phase angle of the third harmonic of polarization response versus time for hard (0.1 at.% Fe-doped) PZT (58/542) ceramics cycling at various temperatures at ac electric field amplitudes 15 kV/cm (a) and 10 kV/cm (b); temperature dependences of the corresponding transition times plotted in Arrenius scales (c).*

The comparison of available experimental data obtained by studying relaxation processes in the time and frequency domain reveals the trend of slight increase of activation energy in hard PZT (58/42) ceramics with increasing amount of hardening dopants; however the data have relatively high scattering within the trend depending on the characterizing parameter and the characterization conditions (Fig.7.19).
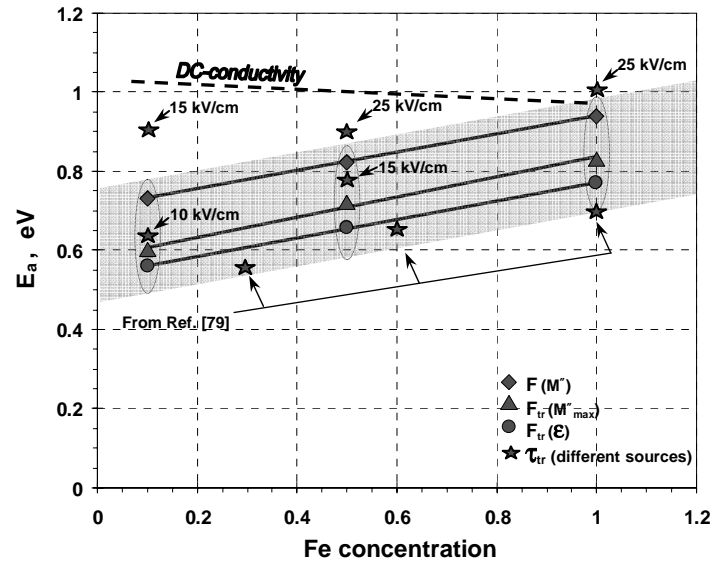
Figure 7.19. *Summary of dielectric relaxation processes in hard PZT (58/42) ceramics. Activation energies obtained by analysis of various manifestations of dielectric relaxations.*

Summarizing the results of this section, there are three different effects that may occur in ferroelectric ceramics with time and under external field. There is ageing, hysteresis relaxation, and fatigue. The two latter effects require continuous application of an electric field. Fatigue occurs under switching conditions; no effect of hysteresis loop degradation has been observed under subswitching conditions, at least, in soft PZT ceramics. The role of third harmonic of polarization response in characterization of hysteresis relaxation process has been shown and the advantages of proposed method of monitoring the relaxation state using nonlinear dielectric parameters have been discussed.

7.5. Summary

Several effects, revealing the hardening-softening transitions, have been analyzed under the switching fields. The results described in this chapter demonstrate that hardening-softening transitions may occur in ferroelectrics under the influence of dopants depending on their type and concentration, thermal treatement, cyclically applied electric field, and time. The most profound effect of hardening-softening was found in the ceramcs of PZT with the rhombohedral structure.

Most of the observed phenomena are in a good agreement with the concept of a model considering hardening-softening in ferroelectrics as a result of order-disorder transitions in electrostatic arrangement of the defects within the bulk. The links between electrostatic processes in defect structure and ferroelectric softening-hardening have been demonstrated by the thermal quenching experiments with controlled cooling rate.

The time effects of ageing, deageing, and fatigue have been investigated systematically. It was shown that under applied electric field, the fatigue effect dominates over ageing in hard quenched ceramics. Experiments performed on soft PZT ceramics that are practically not subjected to ageing effects, have revealed that noticeable fatigue occurs only under switching fields.

Study of hysteresis relaxation in hard PZT ceramics under influence of continuously applied electric field was performed using analysis of third harmonic of polarization response. It has been shown, that the evolution of nonlinear parameters characterizing the third harmonic of polarization response corresponds to the hysteresis relaxation under the electric field cycling and thus the use of harmonic analysis may be convenient for monitoring the deageing state of the hard ceramics.

Summary and conclusions

An attempt to enhance the understanding of softening and hardening phenomena in PZT ceramics has been made by systematic study of various effects revealing the hardening – softening transitions in the ferroelectrics. The main results of work can be formulated as follows:

1) A prototype ferroelectric system exhibiting nonlinear dielectric properties and hardening-softening transitions was obtained and investigated in $Pb(Zr,Ti)O_3$ ceramics doped with a small concentration of Fe and Nb impurities. In an aged state, the iron doped ceramics reveal very profound pinching of the hysteresis loop, especially in PZT with the rhombohedral structure. The niobium doped PZT ceramics is not subjected to a noticeable ageing and demonstrate the rectangular form of hysteresis loop, especially with higher concentrations of Nb dopants.

2) The set of models considering the limiting cases for very hard and soft ceramics as well as the model accounting for hardening – softening transitions were experimentally verified in a prototype system using the method of harmonic analysis of the polarization response to periodic field signal. It has been shown that some nonlinear parameters accounted by the third harmonic of polarization response correlate with the ageing state of ferroelectric system and may serve as the characteristic of ferroelectric hardening-softening transitions

3) The dielectric properties of hard and soft PZT ceramics have been studied under subswitching conditions over a wide range of temperature, frequency and amplitude of driving electric field. A good qualitative agreement is found between the behaviour of a real ferroelectric system and phenomenological models considering various states of order for the domain wall pinning centres.

4) The frequency dispersion of the dielectric permittivity in PZT ceramics with various degree of ageing has been analyzed. The results suggest that frequency dispersion of the dielectric permittivity in PZT ceramics is mostly of extrinsic origins and becomes more apparent with increasing irreversibility of the domain wall motion.

5) Analysis of dielectric frequency dispersion in hard and soft PZT over a wide range of temperature has revealed the profound presence of hopping conductivity in the iron-doped PZT ceramics and its absence in niobium-doped PZT ceramics. This feature permits one to attribute the origin of ferroelectric hardening to electrostatic arrangement of species responsible for the hopping conduction. The oxygen vacancies are prime candidates for this role.

6) Analysis of polarization response in iron-doped PZT ceramics, quenched under various conditions controlling the cooling rate, has revealed the gradual hardening of the ferroelectric with decrease of the cooling rate. This indicates the decisive role of the structural point defects in the mechanisms of ferroelectrics hardening.

7) The processes of dielectric relaxation manifested by iron-doped PZT ceramics under subswitching conditions and in the frequency domain, as well as the processes of ferroelectric relaxation manifested by the same ceramics under switching conditions and in the time domain, revealed the regularity with respect to the dopant concentration, however the scattering in estimated values of the activation energy characterizing the processes was found to be relatively large.

In conclusion, the polarization response of the studied ferroelectric system experiencing the hardening-softening transitions can be described in terms of a phenomenological model linking the structural electrostatic arrangement of the domain wall pinning centres in the ceramic bulk with the randomness, roughness, and steepness of the energy landscape for a domain wall movement.

References

1. Haertling, G.H., *Ferroelectric ceramics: history and technology*. J. Am. Ceram. Soc., 1999. **82** [4]: p. 797-818.

2. Waser, R., *Modeling of electroceramics – applications and prospects*. J. Eur. Ceram. Soc., 1999. **19**: p. 655-664.

3. Haertling, G.H., "*Electrooptic ceramics and devices*" in *Electronic ceramics: properties, devices, and applications*. Ed. by Levinson, L.M. 1988. New York: Dekker. p. 371-492.

4. Vest, R.W., *Metallo-organic decomposition (MOD) processing of ferroelectrics and electrooptic films: A. Review*. Ferroelectrics, 1990. **102**: p. 53-68.

5. Sheppard, L.M., *Advances in processing of ferroelectric thin films*. Am. Ceram. Soc. Bull., 1992. **71** [1]: p. 85-95

6. Schwartz, R.W., Boyle, T.J., Lockwood S.J., Sinclair, M.B., Dimos, D., Buccheit C.D., *Sol-gel processing PZT thin films: A. Review of the state of the art and process optimization strategies*. Integr. Ferroelectr., 1995. **7**: p. 259-277.

7. Auciello, O., Kingon, A.I., Krupanidhi, S.B., Ramesh, R., Keijser, M., Dormans, G.J., Dey, S.K., Alluri, P.V., Tuttle, B.A., Schwartz, R.W., Jones, R.E., Desu, S.B., *Electroceramic thin films, part 1: Processing*. MRS Bull., 1996. **21**: [6]: p. 25-58.

8. Jaffe, B., W.R. Cook, and H. Jaffe, *Piezoelectric Ceramics*. 1971. New York: Academic. p. 1-5.

9. Jaffe, H., Berlincourt, D.A., *Piezoelectric transducer materials*, Proc. IEEE. 1965. **53** [10]: p. 1372-1386.

10. Haertling, G.H., "*Piezoelectric and Electrooptic ceramics*" in *Ceramic materials for electronics: processing, properties, and applications*. Ed. by Buchanan, R.C., 1986. New York; Basel: Dekker. p. 135-225.

11.   Gerson, R., *Variation in Ferroelectric Characteristics of Lead Zirconate Titanate Ceramics due to Minor Chemical Modifications*, J. Appl. Phys., 1960. **31** [1]: p. 188-194.

12.   Ikeda, T., *A few quaternary systems of perovskite type $A^{2+}B^{4+}O_3$ solid solutions*. J. Phys. Soc. Japan. 1959. **14** [10]: p.1286-1294.

13.   Damjanovic, D., Demartin Maeder, M., Voisard, C., Setter, N., *Maxwell-Wagner piezoelectric relaxation in ferroelectric heterostructures*. J. Appl. Phys, 2001. **90** [11]: p. 5708-5712.

14.   Damjanovic, D., *Stress and frequency dependence of the direct piezoelectric effect in ferroelectric ceramics*. J. Appl. Phys., 1997. **82** [4]: p. 1788-1797.

15.   Berlincourt, D., Krueger, H.H.A., *Domain processes in lead titanate zirconate and barium titanate ceramics*. J. Appl. Phys., 1959. **30** [11]: p. 1804-1810.

16.   Preisach, F., *Über die magnetische nachwirkung*. Z. Physik, 1935. **94**: p. 277-302.

17.   Lord Rayleigh, R.S., XXV. *Notes on Electricity and Magnetism-III. On the behaviour of iron and steel under the operation of feeble magnetic forces*. Phil. Mag., 1887. **23**: p. 225-245.

18.   Hall, D.A., *Rayleigh behavior and the threshold field in ferroelectric ceramics*. Ferroelectrics, 1999. **223**: p. 319-328.

19.   Turik, A.V., *Theory of polarization and hysteresis of ferroelectrics*. Soviet Phys.-Solid State, 1963. **5** [4]: p. 885-887.

20.   Turik, A.V., A *statistical method for the investigation of repolarization processes in ferroelectric ceramics*. Soviet Phys.-Solid State, 1964. **5** [9]: p. 1751-1753.

21.   Turik, A.V., *Experimental investigation of the statistical distribution of domains in a ferroelectric ceramic*. Soviet Phys.-Solid State, 1964. **5** [10]: p. 2141-2143.

22.   Boser, O., *Statistical theory of hysteresis in ferroelectric materials*. J. Appl. Phys., 1987. **62** [4]: p. 1344-1348.

23.   Bartic, A.T., Wouters, D.J., H.E.Maes, Rickes, J.T., Waser, R.M., *Presiach model for the simulation of ferroelectric capacitors*. J. Appl. Phys., 2001. **89** [6]: p. 3420-3425.

24. Robert, G., Damjanovic, D., Setter, N., *Preisach modeling of ferroelectric pinched loops*. Appl. Phys. Lett., 2000. **77** [26]: p. 4413-4415.

25. Taylor, D.V., Damjanovic, D., *Evidence of domain wall contribution to the dielectric permittivity in PZT thin films at sub-switching fields*. J. Appl. Phys., 1997. **82** [4]: p. 1973-1975.

26. Taylor, D.V., Damjanovic, D., *Domain wall pinning contribution to the nonlinear dielectric permittivity in Pb(Zr,Ti)O₃ thin films*. Appl. Phys. Lett., 1998. **73** [14]: p. 2045-2047.

27. Taylor, D.V., Damjanovic, D*., Piezoelectric properties of rhombohedral Pb(Zr,Ti)O₃ thin films with (100), (111) and "random" crystallographic orientation*. Appl. Phys. Lett., 2000. **76** [12]: p. 1615-1617.

28. Perrin, V., Troccaz, M., Gonnard, P., *Non linear behavior of the permittivity and of the piezoelectric strain constant under high electric field drive*. J. Electroceramics, 2000. **4** [1]: p. 189-194.

29. Taylor, D.V. Damjanovic, D., Setter, N., *Nonlinear contributions to dielectric and piezoelectric properties in lead zirconate titanate thin films*. Ferroelectrics, 1999. **224**: p. 299-306

30. Pasco, Y., Berry, A., *A hybrid analytical/numerical model of piezoelectric stack actuators using a macroscopic nonlinear theory of ferroelectricity and a Preisach model of hysteresis*. Journal of Intelligent Material Systems and Structures, 2004. **15** (5): p. 375-386.

31. Robert, G., Damjanovic, D., Setter, N., *Piezoelectric hysteresis analysis and loss separation*. J. Appl. Phys., 2001. **90**(9): p. 4668-4675.

32. Robert, G., Damjanovic, D., Setter, N., *Preisach distribution function approach to piezoelectric nonlinearity and hysteresis*. J. Appl. Phys., 2001. **90**(5): p. 2459-2464.

33. Robert, G., Damjanovic, D., Setter, N., Turik, A.V., *Preisach modeling of piezoelectric nonlinearity in ferroelectric ceramics*. J. Appl. Phys., 2001. **89**(9): p. 5067-5074.

34. Damjanovic, D., Demartin M., *The Rayleigh law in piezoelectric ceramics*. J. Phys. D: Appl. Phys., 1996. **29**: p. 2057-2060.

35. Ge, P., Jouaneh, M., *Modeling hysteresis in piezoceramic actuators*. Precision Engineering, 1995. **17**: p. 211-221.

36. Ge, P., Jouaneh, M., *Generalized Preisach model for hysteresis nonlinearity of piezoceramic actuators.* Precision Engineering, 1997. **20**: p. 99-111.

37. Mayergoyz, I.D., *Mathematical Models of Hysteresis.* Phys.Rev.Lett. 56, 1518 (1986)

38. Mayergoyz, I.D., *Mathematical Models of Hysteresis.* 1991, New York: Springer-Verlag. 207.

39. Bertotti, G., *Hysteresis in magnetism.* Electromagnetism, Ed. I. Mayergoyz. 1998, San Diego: Academic Press.

40. Akulov, N.S., Galenko, P.P., *About theory of rectangular hysteresis loops in ferromagnetics.* Dokl. Acad. Nauk BSSR, 1962. **6**(9): p. 551-555.

41. Néel, L., *Théories des lois d'aimantation de Lord Rayleigh.* Cahiers Phys., 1942. **12**: p. 1-20.

42. Kronmüller, H., *Statistical theory of Rayleigh's law.* Z. Angew. Phys., 1970. **30**: p. 9-13.

43. Pfeffer, K.H., *Zur theorie der koerzitivfeldstarke und anfangssuszeptibilitat.* Phys. Stat. Sol. 1967. **21** (2): p. 857.

44. Alessandro, B., Beatrice, C., Bertotti, G., Montorsi, A., *Domain-wall dynamics and Barkhausen effect in metallic ferromagnetic materials. I. Theory.* J. Appl. Phys. 1990. **68**: p.2901-2907.

45. Alessandro, B., Beatrice, C., Bertotti, G., Montorsi, A., *Domain-wall dynamics and Barkhausen effect in metallic ferromagnetic materials. II. Experiments.* J. Appl. Phys. 1990. **68**: p.2908-2915.

46. Magni, A., Beatrice, C., Gurin, G., Bertotti, G., *Stochastic model for magnetic hysteresis.* J. Appl. Phys., 1999. **86**(6): p. 3253-3261.

47. Bertotti, G., Basso, V., Durin, G., *Random free energy model for the description of hysteresis.* J. Appl. Phys., 1996. **79**(8): p. 5764-5766.

48. Bertotti, G., *Energetic and thermodynamic aspects of hysteresis.* Phys. Rev. Lett., 1996. **76**(10): p. 1739-1742.

49. Bertotti, G., Mayergoyz, I. D., Basso, V., Magni, A., *Functional integration approach to hysteresis.* Phys. Rev. E. 1999. 60 (2): p. 1428-1440.

50. Träuble, H., in "Moderne Probleme der Metallphysik". Ed. Alfred Seeger. 1966. Bd. 2. Berlin – Heidelberg – New York: Springer.

51. Gardiner, C.W., *Handbook of stochastic methods: for physics, chemistry and the natural sciences*. Third edition. 2004. Berlin: Springer.

52. Barkhausen H., *Zwei mit Hilfe der neuen Verstarker entdeckte Erscheinunften*. Phys. Zeits. 1919. 20 [17]: p. 401.

53. Newton, R.R., Ahearn, A.J., McKay, K.G., *Observation of the Ferro-Electric Barkhausen Effect in Barium Titanate*. Phys. Rev. 1949. **75** [1]: p. 103-106

54. Chynoweth, A.G., *Barkhausen pulses in barium titanate*. Phys. Rev. 1958. **110** [6]: p. 1316-1332

55. Merz, W.J., *Domain formation and domain wall motions in ferroelectric BaTiO₃ single crystals*. Phys. Rev. 1954. **95** [3]: p. 690-698.

56. Little, E.A., *Dynamic Behavior of Domain Walls in Barium Titanate*. Phys Rev. 1955. 98 [4]: p. 978-984.

57. Miller, R.C., *Some experiments on the motion of 180ºdomain walls in BaTiO₃*. Phys Rev. 1958. **111** [3]: p.736-739.

58. Plessner, K.W., *Ageing of the dielectric properties of barium titanate ceramics*. Proc. Phys. Soc. of London. 1956. **B 69** (12): p. 1261-1268.

59. Lines, M.E., Glass, A.M., *Principles and Applications of Ferroelectrics and Related Materials*. 1979. Oxford: Clarendon.

60. Stemmer, S., Streiffer, S.K., Ernst, F., Rühle, M., *Atomistic structure of 90° domain walls in ferroelectric PbTiO3 thin films*. Phil. Mag. A, 1995. **71**(3): p. 713-724.

61. Foeth, M., Sfera, A. Stadelmann, P. Buffat, P.A., *A comparison of HREM and weak beam transmission electron microscopy for the quantitative measurement of the thickness of ferroelectric domain walls*. J. Electron. Microsc., 1999. **48**(6): p. 717-723.

62. Kittel, C., *Domain boundary motion in ferroelectric crystals and the dielectricconstant at high frequency*. Phys. Rev. Lett. 1951. **83**: p. 458.

63. Arlt, G., Dederich, H., *Complex elastic, dielectric and piezoelectric constants by domain wall damping in ferroelectric ceramics.* Ferroelectrics. 1980 **29**: p. 47-50.

64. Kröner, E., O*n the calculation of the strain energy associated with the nucleation of a new phase within a* crystal. Acta Metalurgica. 1954. **2** [2]: p.302-309

65. Nowick A.S., Heller W.R. *Dielectric and anelastic relaxation of crystals containing point defects.* Adv. in Phys. 1965. **14** [54]: p.101.

66. Arlt, G., Dederichs, H., Herbeit, R., *90°-domain wall relaxation in tetragonally distorted ferroelectric ceramics.* Ferroelectrics, 1987. 74: p. 37-53.

67. Fousek, J., B ezina, B., The movement of single *90° domain walls of BaTiO₃ in an alternating electric field.* Czech J. Phys. 1960. **B 10**: p. 511-528.

68. Fousek, J., B ezina, B., The motion of *90° wedge domains in BaTiO₃ in an alternating electric field.* Czech J. Phys. 1960. **B 10**: p. 511-528.

69. Fousek, J. and B. Brezina, *Relaxation of 90° domain walls of BaTiO3 and their equation of motion.* J. Phys. Soc. Jap., 1964. **19**(6): p. 830-838.

70. Tikhomirov, O.A., Red'kin, B.S., *Direct optical investigation of the domain wall oscillations in ac field.* Ferroelectrics, 1996. **189**: p. 73-80.

71. Tikhomirov, O.A., *Vibrations of domain walls in ac field and the low frequency permittivity of ferroelectrics.* Ferroelectrics, 1997. **190**: p. 37-42.

72. Li, S., Cao, W., Cross, L.E., *The extrinsic nature of nonlinear behavior observed in lead zirconate titanate ferroelectric ceramic.* J. Appl. Phys., 1991. **69** (10): p. 7219-7224.

73. Shur, V., Rumyantsev, E., Batchko, R., Miller, G., Fejer, M., Byerb, R., *Physical basis of the domain engineering in the bulk ferroelectrics* Ferroelectrics. 1999. **221**: p. 157-167.

74. Yang, T.J., Gopalan, V., Swart, P.J., Mohadeen, U., *Direct observation of pinning and bowing of a single ferroelectric domain wall.* Phys. Rev. Lett, 1999. **82**(20): p. 4106-4109.

75. Ma, H.Z., Kim, W. J. Horwitz, J.S., Kirchoefer, S.W., Levy, J., *Lattice-scale domain wall dynamics in ferroelectrics.* Phys. Rev, Lett. 2003. **91** (21): 217601.

76. D. Damjanovic, "*Hysteresis in piezoelectric and ferroelectric materials*", in *Science of Hysteresis*, edited by G. Bertotti and I. Mayergoyz, 2005. Elsevier – Academic press, Vol. III, Ch.4, p. 337-465.

77. Jonker, G.H., *Nature of Aging in Ferroelectric ceramics.* J. Am. Ceram. Soc, 1972. **55**: p. 57-58.

78. Lambeck, P.V., Jonker, G.H., *Ferroelectric domain stabilization in BaTiO3 by bulk ordering of deffects.* Ferroelectrics, 1978. **22**: p. 729-731.

79. Carl, K., Härdtl, K.H., *Electrical after-effects in Pb(Ti,Zr)O3 ceramics.* Ferroelectrics, 1978. **17**: p. 473-486.

80. Okada, K., *Ferroelectric properties of X-ray damaged Rochelle Salt*. J. Phys. Soc. Japan. 1961. **16** (3): p. 414-423.

81. Muser, H.E., *Die auswirkung des eingepragten nachwirkungsfeldes auf die bewegung ferroelektrischer domanenwande in seignettesalzkristallen*. Z. Physik. 1965. **184** (1): p. 105.

82. Unruh H.G., Sailer E., Dielectric relaxations and crystal water stoichiometry of Rochelle salt. Z. Physik. 1965. **224** (1-3): p. 45.

83. Keve, E.T., Bye, K.L., Annis, A.D., Whipps, P.W., *Structural inhibition of ferroelectric switching in triglycine sulfate. 1. Additives*. Ferroelectrics. 1971. **3** (1): p. 39.

84. Wieder, H.H., Parkerson, C.R., *External habit modification + ferroelectric properties of TGS*. J. Phys. Chem. Solid. 1964. **25** (2): p. 241.

85. McQuarrie, M.C., *Time Effects in the Hysteresis Loop of Polycrystalline Barium Titanate*. J. Appl. Phys. 1953. **24** (10): p. 1334-1335.

86. Griffith, C.R., Russell, R., *Time effects in hysteresis loop of (Pb,Sr)TiO₃*. J. Amer. Ceram. Soc. 1972. **55** (2): p. 110.

87. Glower, D. D., Hester, D. L. *Hysteresis studies of reactor-irradiated single-crystal barium titanate*. J. Appl. Phys. 1965. **36** (7): p.2175-2180.

88. Glower, D.D., Hester, D.L., Warnke, D.F., *Effects of radiation-induced damage centers in lead zirconate titanate ceramics.* . J. Amer. Ceram. Soc. 1965. **48** (8): p. 417.

89. Misarova, A. *Aging of barium titanate single crystals*. Soviet Phys. - Solid State, 1960. **2** (6): p. 1160-1165.

90. Gopalan, V., Gupta, M. C. *Origin of internal field and visualization of 180° domains in congruent LiTaO₃ crystals*. J. Appl. Phys. 1996. **80** (11): p.6099-6106.

91. Gopalan, V., Gupta, M.C., *Observation of internal field in LiTaO₃ single crystals: its origin and time-temperature dependence*. Appl. Phys. Lett. 1996. **68** (7): p.888-890.

92. Kitamura, K., Furukawa, Y., Niwa, K., Gopalan, V., Mitchell, T.E., *Crystal growth and low coercive field 180 degrees domain switching characteristics of stoichiometric LiTaO₃*. Appl. Phys. Lett. 1998. **73** (21): p.3073-3075.

93. Warren, W.L., Dimos, D., Pike, G.E., Vanheusden, K., Ramesh, R., *Alignment of defect dipoles in polycrystalline ferroelectrics*. Appl. Phys. Lett., 1995. **67**(12): p. 1689-1691.

94. Warren, W.L., Pike, G.E., Vanheusden, K., Dimos, D., Tuttle, B.A., Robertson, J., *Defect-dipole alignment and tetragonal strain in ferroelectrics*. J. Appl. Phys., 1996. **79**(12): p. 9250-9257.

95. Warren, W.L., Vanheusden, K., Dimos, D., Pike, G.E., Tuttle, B.A., *Oxygen vacancy motion in perovskite oxides*. J. Amer. Ceram. Soc. 1996. **79** [2]: p.536-538.

96. Schulze, W.A., Ogino, K., *Review of literature on aging of dielectrics*. Ferroelectrics. 1988. **87**: p. 361-377.

97. Lambeck, P.V., Jonker, G.H., *The nature of domain wall stabilization in ferroelectric perovskites*. J. Phys. Chem. Solids. 1986. **47** (5): p. 453-461.

98. Postnikov, V.S., Pavlov, V.S., Turkov, S.K., *Interacton between 90º domain walls and point defects of the crystal lattice in ferroelectric ceramics*. Soviet Phys. - Solid State. 1968. **10** (6): p. 1267-1270.

99. Postnikov, V.S., Pavlov, V.S., Turkov, S.K., *Internal friction in ferroelectrics due to interaction of domain boundaries and point defects*. J. Phys. Chem. Sol., 1970. **31**: p. 1785-1791.

100. Yoo, I.K.. Desu, S.B., *Mechanism of fatigue in ferroelectric thin films*. Phys. Stat. Sol. (a), 1992. **133**: p. 565-573.

101. Arlt, G., Neumann, H., *Internal bias in ferroelectric ceramics: origin and time dependence.* Ferroelectrics, 1988. **87**: p. 109-120.

102. Robels, U., Arlt, G., *Domain wall clamping in ferroelectrics by orientation of defects.* J. Appl. Phys., 1993. **73**(7): p. 3454-3460.

103. Arlt, G., *Piezoelectric relaxation.* Ferroelectrics, 1982. **40**: p. 149-157.

104. Gridnev S.A., Shuvalov L.A., *The influence of real structure on switching processes and peculiarities of mechanical relaxation in proper ferroelastics $KH_3(SeO_3)_2$ and $KD_3(SeO_3)_2$.* Ferroelectrics. 1983. **48** (1-3): p. 113-129.

105. Balke, N., Genenko Yu., Rauh, Lupascu, D., H. Rödel, J., Ferroelectric a*ging by drift of charge carriers.* In Programme and abstracts of 9th *International Conference on electroceramics and their applications.* Electroceramics IX. May 2004, Cherbourg, France. p. 370.

106. Klie, R.F., Ito, Y., Stemmer, S., Browing, N.D., *Observation of oxygen vacanciy ordering and segregation in perovskite oxides*. Ultramicroscopy. 2001. **86**: p. 289-302.

107. Zhang, L.X., Ren, X., *In situ observation of reversible domain switching in aged Mn-doped $BaTiO_3$ single crystals*. Phys.Rev. 2005. **B 71**: 174108.

108. Arlt, G., Pertsev, N.A. *Force constant and effective mass of 90° domain walls in ferroelectric ceramics.* J. Appl. Physics., 1991. **70**(4): p. 2283-2289.

109. Smyth, D.M., *Charge motion in ferroelectric thin films.* Ferroelectrics, 1991. **116**: p. 117-124.

110. Waser, R., *Bulk conductivity and defect chemistry of acceptor-doped strontium tianate in the quenched state.* J. Am. Ceram. Soc., 1991. **74**(8): p. 1934-40.

111. Schaffrin, C., *Oxygen diffusion in $BaTiO_3$ ceramic.* Phys. Stat. Solidi A. 1976. **35**: p. 79.

112. Weston, T.B., A.H. Webster, and V.M. McNamara, *Lead zirconate-lead titanate piezoelectric ceramics with iron oxide additions.* J. Am. Ceram. Soc., 1969. **52**(5): p. 253-257.

113. Noheda, B., Cox, D.E., Shirane, G., Gonzalo, J.A., Cross, L.E., Park, S.E., *A monoclinic ferroelectric phase in the $Pb(Zr_{1-x}Ti_x)O_3$ solid solution.* Appl. Phys. Lett., 1999. **74**(14): p. 2059-2061.

114. Noheda, B., et al., *Stability of the monoclinic phase in the ferroelectric perovksite PbZr1-xTixO3*. Phys. Rev. B, 2000. **63**: 014103.

115. Гориш, А.В., Дудкевич, В.П., Куприянов, М.Ф., Панич, А.Е., Турик, А.В., *Пьезоэлектрическое приборостроение. Т.1. Физика сегнетоэлектрической керамики.* – М.: ИПРЖР. 1999.

116. Noheda, B., *Structure and high-piezoelectricity in lead oxide solid solutions*. Curr. Opinion Solid State Mat. Sci., 2002. **6**: p. 27-34.

117. Cross, L.E., *Boundary conditions for shape memory in ceramic material systems*. Journal of Intelligent Material System and Structures. 1995. **6**: p. 55-61.

118. Okuyama, M., Asano, J.-J., Hamaka, Y. *Electron emission from PZT ceramic thin plate by pulsed electric field*. Integrated Ferroelectrics. 1995. **9**: p. 133-142.

119. Glazer, A.M., Mabud, S.A., R. Clarke, R., *Powder profile refinement of lead zirconate titanate at several temperatures. I. $PbZr_{0.9}Ti_{0.1}O_3$*. Acta Cryst. 1978. **B34**: p. 1060-1065.

120. Darlington, C.N.W., *Transitions in the glassy ferroelectric PLZT (8.7/65/35)*. J. Phys. C.: Solid State Phys. 1988. **21**(21): p. 3851-3861.

121. Cross, L.E., *Ferroelectric Materials for Electromechanical Transducer Applications*. Japan. J. Appl. Phys. 1995. **34**: p.2525-2532

122. Turik, A.V., Topolov, V.Yu., *Ferroelectric ceramics with a large piezoelectric anisotropy*. J. Phys. D : Appl. Phys. 1997, **30**, p.1541-1549

123. Tashiro, S., Oikawa, Y., Igarashi, H., Okazaki, K., *Piezoelectric anisotropy in lead titanate system ceramics*. Jpn. J. Appl. Phys. Suppl. 1987. **26**: p. 61-64.

124. Kingery, W.D. (Ed.), *Ceramic fabrication processes*. 1956. [Boston] : Technology Press of Masachusetts Institute of Technology, 1956.

125. Kahn. M., Burks, D., Burn, I., Schulze, W., *Ceramic capacitor technology*. in *Electronic ceramics: properties, devices, and applications*. Ed. by Levinson, L.M. 1988. New York: Dekker. p.191-274.

126. Chandratreya, S.S., Fulrath, R.M., Pask, J., *Reaction mechanisms in the formation of PZT solid solutions*. J. Am. Ceram. Soc. 1981. **64** [7]: p. 422-425 .

127. Härdtl, K.H., Rau, H., *PbO vapour pressure in the Pb(Ti$_{1-x}$Zr$_x$)O$_3$ system*. Solid State Commun. 1969. **5**: p. 41-45

128. Holman, R.L., Fulrath, M., *Intrinsic nonstoichiometry in the lead zirconate – lead titanate system determined by Knudsen effusion*. J. Appl. Phys. 1973. **44** (12): p. 5227-5236

129. Kingon, A.I., Clark, J.B., *Sintering of PZT ceramics: I, Atmosphere Control*. J. Am. Ceram. Soc. 1983. **66** (4): p.253-256.

130. Kingon, A.I., Clark, J.B., *Sintering of PZT ceramics: II, Effect of PbO content on densification kinetics*. J. Am. Ceram. Soc. 1983. **66** (4): p.256-260.

131. He, Z., Ma, J., *Constitutive modelling of the densification of PZT ceramics*. J. Phys. Chem. Solids. 2003. **64**: p.177-183.

132. Hammer, M., Hoffmann, M.J., *Sintering model for mixed-oxide-derived lead zirconate titanata ceramics*. J. Am. Ceram. Soc. 1998. **81**: p. 3277–3284.

133. Yoshikawa, Y., Tsuzuki, K., *Fabrication of transparent lead lanthanum zirconate titanate ceramicd from fine powders by two-stage sintering*. J. Am. Ceram. Soc. 1992. **75**: p. 2520–2528.

134. Lucuta, P.G., Constantinescu, F., Barb, D., *Structural dependence on sintering temperature of lead zirconate–titanate solid solutions*. J. Am. Ceram. Soc. 1985. **68**: p. 533–537.

135. Ryu, J. Choi, J.J., Kim, H.E., *Effect of heating rate on the sintering behavior and the piezoelectric properties of lead zirconate titanate ceramics*. J. Am. Ceram. Soc. 2001. **84**: p. 902–904.

136. Ghosh, V.J., Nielsen, B., Friessnegg, T., *Identifying open-volume defects in doped and undoped perovskite-type LaCoO$_3$, PbTiO$_3$, and BaTiO$_3$*. Phys. Rev. 2000. **B61**: p. 207-212.

137. Krause-Rehberg, R., Leipner, H.S. *Positron annihilation in semiconductors*. Berlin: Springer-Verlag. 1999.

138. Gottschalk, S., Hahn, H., Balogh, A.G., Puff, W., Kungl, H., Hoffmann, M.J., *A positron lifetime study of lanthanum and niobium doped Pb(Zr$_{0.6}$Ti$_{0.4}$)O$_3$*. J. Appl. Phys. 2004 **96** (12): p. 7464-7470.

139. Puska, M. J., Jepsen, O., Gunnarsson, O., Nieminen, R.M., *Electronic structure and positron states at vacancies in Si and GaAs*. Phys. Rev. 1986. **B 34** [4]: p. 2695-2705.

140. Puska, M.J., Corbel, C., Nieminen, R.M., *Positron trapping in semiconductors*. Phys. Rev. 1990 **B 41**: p. 9980-9993.

141. Leary, S.P. and S.M. Pilgrim, *Harmonic analysis of the polarization response in Pb(Mg1/3Nb2/3)O3-based ceramics - a study in aging.* IEEE Trans. UFFC, 1998. **45**(1): p. 163-169

142. Srilomsak, S., Schulze, A., Pilgrim, S.M., William, F.A., *Harmonic analysis of polarization hysteresis of aged PZTs*, J. Am. Ceram. Soc., 2005. **88**[8]: p. 2121-2125.

143. DiAntonio, C.B., Williams F.A., Pilgrim, S.M. *The use of harmonic analysis of the strain response in Pb(Mb$_{1/3}$Nb$_{2/3}$)O$_3$-based ceramics to calculate electrostrictive Coefficients*, IEEE Trans. Sonics Ultrason., 2001. **48** [6]: p. 1532-1538.

144. Sjöström, M., *Frequency analysis of classical Preisach model.* IEEE Transactions on magnetics, 1999. **35**(4): p. 2097-2103.

145. Yamaguchi, T., Hamano, K., *Piezoelectric relaxation in ferroelectric AgNa(NO$_2$)$_2$.* J. Phys. Soc. Japan., 1981. **50**(12): p. 3956-3963.

146. Jonscher, A.K., *Dielectric relaxation in solids*. 1983, London: Chelsea Dielectric Press.

147. Damjanovic, D., *Logarithmic frequency dependence of the piezoelectric effect due to pinning of ferroelectric-ferroelastic domain walls.* Phys. Rev. B, 1997. **55** (2): p. R649-R652

148. Damjanovic, D., Bharadwaja, S.S.N., Setter, N., *Toward a unified description of nonlinearity and frequency dispersion of piezoelectric and dielectric responses in Pb(Zr,Ti)O$_3$.* Material Science and Engineering. B., 2005. **B 120**: p. 170-174.

149. Nattermann, T., Y. Shapir, Vilfan, I., *Interface pinning and dynamics in random systems.* Phys. Rev. B, 1990. **42**(13): p. 8577-8586.

150. Nattermann, T., V. Pokrovsky, Vinokur, V.M., *Hysteretic dynamics of domain walls at finite temperatures.* Phys. Rev. Lett., 2001. **87**(19): p. 197005.

151. Braun, Th., Kleemann, W., Dec, J., Thomas, P. A., *Creep and relaxation dynamics of domain walls in periodically poled KTiOPO$_4$*, Phys. Rev. Lett., 2005. **94**: 117601.

152. Fedorenko, A.A., Mueller, V., Stepanow, S., *Dielectric response due to stochastic motion of pinned domain walls*, Phys. Rev. B, 2004. **B 70**: 224104 (2004)

153. Kleemann, W., Dec, J., Miga, S. Woike, Th., Pankrath, R., *Non-Debye domain wall induced dielectric response in Sr0.61-xCexBa0.39Nb2O6.* Phys. Rev. B, 2002. B **65**: p. 220101.

154. Kremer, F., *Dielectric spectroscopy – yesterday, today and tomorrow*, J. Non-Cryst. Solids, 2002. **305**: p. 1-9.

155. *Impedance Spectroscopy : Emphasizing Solid Materials and Systems*, Ed.: MacDonald, J. R., 1987. New York: Wiley.

156. Richert, R., *The modulus of dielectric and conductive materials and its modification by high electric field,* J. Non-Cryst. Solids, 2002. **305**: p. 29-39.

157. Vinokur, V.M., Marchetti, M.C., Chen, L.-W., *Glassy Motion of Elastic Manifolds*, Phys. Rev. Lett., 1996 **77**: p. 1845–1848.

158. Macedo, P.B., Moynihan, C.T., Bose, R., *The role of ionic diffusion in polarization in vitreous ionic conductors,* Phys. Chem. Glasses, 1972. **13**: p. 171-179.

159. Jonscher, A. K., *The 'universal' dielectric response*, Nature, 1977. **267**: p. 673 – 679.

160. N.F. Mott and E.A. Davis. *Electronic processes in non-crystalline materials*, 2nd ed., 1979. Oxford : Clarendon Press.

161. Dyre, J.C., *The random free-energy barrier model for ac conduction in disordered solids*, J. Appl. Phys., 1988. **64**(5): p. 2456-2468.

162. Elliott, S.R., *Use of the modulus formalism in the analysis of ac conductivity data for ionic glasses.* J. Non-Cryst. Solids, 1994. **170**: p. 97-100.

163. Kimball, J.C., Adams, L.W., *Hopping conduction and superionic conductors.* Phys. Rev., 1978. **B18**: p. 5851–5858 (1978)

164. Lohkämper, R., Neumann, H., Arlt, G., *Internal bias in acceptor-doped $BaTiO_3$ ceramics: numerical evaluation of increase and decrease*, J. Appl. Phys., 1990. **68**(8): p. 4220-4224.

165. Glower, D.D., Heckman, R.C., *Conduction – ionic or electronic – in $BaTiO_3$*, J. Chem. Phys., 1964. **41**(3): p. 877-879.

166. Waser, R., *Bulk conductivity and defect chemistry of acceptor-doped strontium tianate in the quenched state.* J. Am. Ceram. Soc., 1991. **74**(8): p. 1934-1940.

167. Choi, G.M., Tuller, H.L., Goldschmidt, D., *Electronic-transport behavior in single-crystalline $Ba_{0.03}Sr_{0.97}TiO_3$*, Phys. Rev. B, 1986. **34**(10): p. 6972-6979.

168. Kugel, V.D. and L.E. Cross, *Behavior of soft piezoelectric ceramics under high sinusoidal electric fields.* J. Appl. Phys., 1998. **84**(5): p. 2815-2830.

169. Ren, X., *Large electric-field-induced strain in ferroelectric crystals by point-defect-mediated reversible domain switching*, Nature mater., 2004. **3**: p. 91-94.

170. Li B.S., Li, G.R., Zhao, S.C., Zhu, Z.G., Ding, A.L., *Reorientation of Defect Dipoles in Ferroelectric Ceramics*, Chinese Phys. Lett, 2005. **22**: p. 1236-1238.

171. Schreiber, F.*, Hysteresis relaxation and permeability of carbon-containing silicon-iron*, Z. Angew. Phys., 1956. **8**: p.539-551.

172. Campbell, D.S., *Some observations on switched single crystal barium titanate*, Philos. Mag., 1962. **7**: 1157-1166.

173. Lupascu, D.C., *Fatigue in Ferroelectric Ceramics and Related Issues*, 2004. Berlin: Springer

174. Tagantsev, A.K., Stolichnov, I., Colla, E.L., Setter, N., *Polarization fatigue in ferroelectric films: Basic experimental findings, phenomenological scenarios, and microscopic features*, J. Appl. Phys., 2001. **90**(3): p. 1387-1402.

Curriculum Vitae

Name:	Maxim
Surname:	Morozov
Date of birth:	21 July 1977
Place of birth:	Saint-Petersburg, Russia
Nationality:	Russian

Education

2001 – 2005   *Ph.D. student* in the Ceramics Laboratory, Swiss Federal Institute of Technology, Lausanne, Switzerland

1998 – 2000   *Graduate student*, Faculty of Electronics, Saint-Petersburg State Electrotechnical University, Russia. *Master's degree* in Techniques and Technologies, spezialization: Semiconductor Materials and Structures in Electronics and Microelectronics

1994 – 1998   *Student*, Faculty of Electronics, Saint-Petersburg State Electrotechnical University, Russia. *Bachelor's degree* in Techniques and Technologies, Electronics and Microelectronics division

Working experience

2001 – 2005   *Research assistant*. Ceramics Laboratory, Swiss Federal Institute of Technology, Lausanne, Switzerland

1999 – 2001   *Research assistant*. Laboratory of Phase Equilibria of Oxide Systems, Institute of Silicate Chemistry of Russian Academy of Sciences

Publications

Morozov, M, Damjanovic, D., Setter, N., *The Nonlinearity and Subswitching Hysteresis in Hard and Soft PZT*, Journal of European Ceramic Society, 2005. **25:** p. 2483-2486.

Lomanova, N.A., Morozov, M.I., Ugolkov, V.L., Gusarov, V.V., *Properties of the Aurivillius Phases in the $Bi_4Ti_3O_{12} – BiFeO_3$ System*. Inorganic Materials, in press

Krzhizhanovskaya, M., Filatov, S., Gusarov, V. Paufler, P., Bubnova, R., Morozov, M., Meyer, D.C., *Aurivillius Phases in the $Bi_4Ti_3O_{12}/BiFeO_3$ System: Thermal Behaviour and Crystal Structure,* Z. Anorg. Allg. Chem. 2005. **631** (9): p. 1603-1608.

Morozov, M.I., Gusarov, V.V., *Synthesis of $A_{m-1}Bi_2M_mO_{3m+3}$ Compounds in the $Bi_4Ti_3O_{12} – BiFeO_3$ System*, Inorganic Materials, 2002. **38** (7): p.723-729

Morozov, M.I., Lomanova, N.A., Gusarov, V.V., *Specific Features of $BiFeO_3$ Formation in a Mixture of Bismuth (III) and Iron (III) Oxides*, Russian Journal of General Chemistry, 2003. **73** (11): p.1676-1680 (Engl. Transl.)

Morozov, M.I., Mezentseva, L.P., Gusarov, V.V., *Mechanism of Formation of $Bi_4Ti_3O_{12}$*, Russian Journal of General Chemistry, 2002. **72** (7): p.1038-1040 (Engl. Transl.)